The Role of MeCP2 Phosphorylation in the Development and Function of the Mouse Brain

By

Hongda Li

A dissertation submitted in partial fulfillment of

the requirements of the degree of

Doctor of Philosophy

(Genetics)

at the

UNIVERSITY OF WISCONSIN-MADISON

2013

Date of final oral examination: 08/16/13

The dissertation is approved by the following members of the Final Oral Committee:

Qiang Chang, Associate Professor, Laboratory of Genetics

Jerry Yin, Professor, Laboratory of Genetics

Xin Sun, Associate Professor, Laboratory of Genetics

Thomas Sutula, Professor, Department of Neurology,

John Svaren, Professor, Department of Comparative Biosciences

Abstract

DNA methylation-dependent epigenetic mechanisms underlie the development and function of the mammalian brain. The X-linked MeCP2 functions as a molecular linker between DNA methylation, chromatin remodeling and transcription regulation. Mutations in the human *MECP2* gene cause Rett syndrome.

The phosphorylations of MeCP2 at Serine 80 (S80) and Serine 421/424 (S421/S424) are dynamically regulated in opposite manners by neuronal activity. To elucidate the *in vivo* function of MeCP2 phosphorylation, we have generated knockin mice with serine to alanine mutations to abolish MeCP2 phosphorylation. We show here that mice that lack S421/S424 phosphorylation perform better in hippocampus-dependent learning and memory tests, present enhanced long-term potentiation at two synapses in the hippocampus, and show increased excitatory synaptogenesis. At the molecular level, the S421/S424 phosphor mutant MeCP2 protein binds more tightly to several MeCP2 target gene promoters and alters the expression of these genes. In contrast, loss of S80 phosphorylation in mice leads to increased anxiety and impaired hippocampus-dependent spatial memory. Our results supply the first genetic evidence that MeCP2 phosphorylations are necessary for modulating dynamic functions of the adult mouse brain.

Adult neurogenesis in the dentate gyrus occurs throughout the life and is important for the normal function of the adult hippocampus. Emerging evidence suggests the importance of DNA methylation-dependent regulation for adult neurogenesis. Surprisingly, we discovered that MeCP2 S421 phosphorylation is dynamically regulated in adult neural progenitor cells (aNPCs)

by cell cycle. And mice that lack S421/S424 phosphorylation present decreased aNPCs proliferation and increased neuronal differentiation *in vitro* and in *vivo*. S421/S424 phosphor mutant aNPCs exhibit reduced *Notch1* and *Dll1* expression and decreased Notch signaling. Restoring Notch signaling level in phosphor mutant aNPCs is sufficient to rescue neurogenesis phenotypes. On the other hand, loss of S80 phosphorylation leads to increased proliferation and decreased neuronal differentiation of aNPCs. Our results suggest that MeCP2 S80 and S421/S424 phosphorylations play opposite roles in regulating adult neurogenesis.

Taken together, we provide evidence from several aspects demonstrating the importance of MeCP2 S80 and S421/S424 phosphorylations for normal development and function of the nervous system.

Acknowledgments

First, I would like to thank my Ph.D advisor, Dr. Qiang Chang, for his constant help and support throughout my graduate school training. He was not only a good scientific leader who provided me the opportunity to work on interesting projects, but also a great friend who helped me a lot in and out of the lab. I also want to thank my committee members, Jerry Yin, Xin Sun, John Svaren and Tom Sutula, for their helpful insights and suggestions on my research projects.

Second, I would like to thank all the current and past members of the Chang lab. Dr. Xiaofen Zhong and Ronghui Li were wonderful labmates and friends, giving me great help both scientifically and personally. Dr. Emily Williams and Gene Ananiev taught me a lot about American culture and life. I want to thank Kevin Chau, Shruti Marwaha and Fei Yu, who provided great help maintaining the mouse colony. In addition, I appreciate the collaboration with Dr. Xinyu Zhao and Dr. Weixiang Guo. I want to acknowledge the help I got from Dr. Jing Zhang and Yangang Liu. Also, I want to thank all the undergraduates who had worked with me, Sasha Cai Lesher-Perez, Jim Liu, Mitul Kadakia, Jamie Masliah and Kaizhou Li.

Then, I would like to thank the fellowship programs in UW–Madison Stem Cell and Regenerative Medicine Center and the Waisman Center for supporting my graduate studies.

Finally, I want to thank my family and friends who have helped me in numerous ways during the past several years. Especially, I would like to acknowledge my parents for their endless love, support and understanding. I am grateful to all my friends including Xinjie Xu, Wei Shen, Shang Ma, Zhenxiao Luo, Zhen Zhang, Xiaohua Wang, Shun Feng, Yue Li et al, who added happiness into my life in Madison.

Table of Contents

Chapter 1: Introduction

DNA methylation and its role in brain development and plasticity

The brain is the most complex tissue of the body. A typical human cerebral cortex is estimated to contain 15–33 billion neurons, each connected by synapses to several thousand other neurons. Animals constantly receive external or internal stimuli and make the corresponding response. These experiences are then learned and memorized in the brain, a process that investigators have been trying to elucidate for decades. The prevailing hypothesis is that long-term memory is encoded by the altered synaptic strength in the neuronal circuits (Okano et al., 2000). However, the detailed mechanism remains elusive. Given that most of the cellular constituents are subject to molecular turnover except the DNA of postmitotic neurons, J.S. Griffith and H.R. Mahler first proposed the hypothesis in 1969 that "the physical basis of memory could lie in the enzyme modification of the DNA of the nerve cells" (Griffith and Mahler, 1969). However, it is until this decade that pharmacology and genetic studies have provided concrete evidence that epigenetic regulations, including DNA methylation and histone modifications, play critical roles in brain plasticity and memory formation.

Developmental biologist Conrad Hal Waddington coined the term "*epigenetics*" in 1940s, defined it as "the interactions of genes with their environment which bring the phenotype into being", and later extended his original definition as "an adaptive response can be fixed without waiting for the occurrence of a mutation" (Waddington, 1942). By this explanation, Waddington had foreseen two important characteristics of the epigenetic process: plasticity and long-term

action. Over the years, “epigenetics” was used to describe events that could not be explained by general genetic principles, such as paramutation in maize, position effect variegation in the fruit fly, and the imprinting of specific parental loci in mammals. Now, we understand that these phenomena are under similar “epigenetic” molecular mechanisms, in which heritable changes of gene expression or cellular phenotypes occur without changing the underlying DNA sequence (Goldberg et al., 2007). In a broad sense, epigenetic mechanisms provide an organism with the molecular means to promptly react to intrinsic and extrinsic cues with stable alterations in gene expression and cellular outcome.

Chromatin, the complex of DNA and its associated proteins, are the fundamental unit of a cell's epigenetic landscape. And much of the epigenetic research is focusing on the covalent and noncovalent modifications of DNA and histone proteins on the chromatin and the mechanisms that such modifications may alter overall chromatin structure. Specific amino-acid residues of histone N-terminal tails can be reversibly modified by various mechanisms, such as methylation, acetylation, phosphorylation, ubiquitination, and SUMOylation, with the list of modifications still growing (Kouzarides, 2007). Charge-altering modifications, such as acetylation and phosphorylation, can directly lead to changes in the physical properties of the chromatin structure. In addition, histone modifications can recruit specific binding partners, which serve as “readers” or “effectors” recognizing specific chromatin state and directing various downstream biological processes, including gene transcription, DNA repair, DNA replication, and higher-order chromatin structure regulation (Arita et al., 2012).

In contrast to the readily reversible histone modifications, DNA methylation has been generally considered as a highly stable epigenetic mark (Smith and Meissner, 2013). DNA

methylation is a biochemical process in which a methyl group is covalently added to the cytosine or adenine DNA nucleotides. Different from adenine methylation which exists primarily in bacteria as part of the restriction modification system, cytosine methylation is well conserved among most fungi, plant and animal organisms (Feng et al., 2010b). In mammals, cytosine methylation is primarily restricted to the symmetrical CpG context. Approximately 60%-80% of CpGs in the mammalian genome are generally methylated. Less than 10% of CpGs, largely unmethylated, are grouped in clusters which are termed CpG islands (Deaton and Bird, 2011). Generally, DNA methylation leads to silencing of gene transcription (Weber et al., 2007).

Three conserved enzymes, DNA methyltransferase 1 (DNMT1), DNMT3A and DNMT3B, are responsible for the deposition and maintenance of DNA methylation landscape of the mammalian genome (Okano et al., 1999). Maintenance methyltransferase DNMT1 add methyl groups to hemi-methylated DNA during DNA replication, whereas DNMT3A and DNMT3B are considered as *de novo* methyltransferase adding methyl groups to unmethylated DNA (Chen et al., 2003a).

During the very early embryonic development, all DNA methylation is erased and then reestablished at the time of implantation (Monk et al., 1987). Continuing with the embryogenesis, various cell type specific and tissue specific DNA methylation patterns are established at specific times (Kafri et al., 1992). DNA methylation plays critical roles in gene expression regulation and chromatin organization during embryonic development. Both DNMT1 and DNMT3B are highly expressed in embryonic cells, and knocking out either of the two genes leads to embryonic lethality (Li et al., 1992). Currently, how DNA methylation is initiated and how DNMTs are targeted to specific genomic locations remains unclear.

Once set up, the DNA methylation pattern in terminally differentiated cells is generally maintained. Correspondingly, the expression of DNA methyltransferases in somatic cells diminished greatly after embryonic development (Szyf et al., 1991). However, postmitotic neurons in the adult brain still hold substantial levels of DNMT1 and DNMT3a (Feng et al., 2005). The level of DNA methylation is also higher in adult brain than in other tissues (Tawa et al., 1990). More importantly, accumulating evidence indicates that DNA methylation can be dynamically altered in postmitotic neurons by neural activity or during behavioral training in response to external signals, suggesting possible roles of DNA methylation in adult brain plasticity.

The methylation dynamics of the brain-derived neurotrophic factor (*Bdnf*) gene in neurons has been extensively studied both *in vitro* and *in vivo*. The rodent *Bdnf* gene has nine exons, eight of which are promoter exons that alternatively splice onto the common coding exon to produce the *Bdnf* transcripts. (Aid et al., 2007). In primary neuronal culture, high potassium-induced neuronal depolarization leads to demethylation of *Bdnf* exon IV, correlated with an increase of *Bdnf* transcript upon neuronal activity (Chen et al., 2003b; Martinowich et al., 2003). Additionally, contextual fear conditioning was also found to alter DNA methylation patterns on same promoter (Lubin et al., 2008). Electroconvulsive treatment (ECT) to the dentate gyrus of the hippocampus demethylates the promoter of the *Bdnf* exon IX (Ma et al., 2009). Early life stress such as maltreatment or repeated maternal separation, however, increases the methylation level of *Bdnf* exon IX in prefrontal cortex (Roth et al., 2009). Collectively, the methylation of the *Bdnf* promoter exons is differentially regulated according to the types of upstream signals, together with the age and brain region. In addition to the *Bdnf* gene, the promoter methylation of

arginine vasopressin (AVP) and glucocorticoid receptor (GR) is also altered by early life stress, and such changes may persist into adulthood (Murgatroyd et al., 2009; Weaver et al., 2004). Recently, a genome-wide analysis of the CpG methylation landscape of the adult mouse dentate granule neurons indicates that about 1.4% of the CpGs measured show rapid de novo methylation or active demethylation after synchronized neuronal activation. And some modifications remained stable for at least 24 hours (Guo et al., 2011a).

The Sweatt's group performed a series of experiment to investigate the possible involvement of dynamic DNA methylation in learning and memory. They showed that contextual fear conditioning training is associated with rapid methylation and transcriptional silencing of the memory suppressor PP1 and demethylation and transcriptional activation of the synaptic plasticity gene *reelin* in the CA1 of hippocampus, and such methylation is reset to normal level 24 hours after fear conditioning task. Both the expression of *Dnmt3a* and *Dnmt3b* is upregulated in the adult hippocampus following contextual fear conditioning. Intra-hippocampal infusions of DNMT inhibitors right after the fear conditioning training blocks the memory formation (Miller and Sweatt, 2007). Anterior cingulate cortex (ACC) plays a critical role in remote memory for contextual fear conditioning (Frankland et al., 2004). Animals that received intra-ACC infusions of DNMT inhibitors 30 days after contextual fear conditioning training failed to display normal memory. Furthermore, contextual fear conditioning procedure induced persistent promoter hypermethylation of calcineurin (CaN), a memory suppressor, in the anterior cingulate cortex for at least 30 days, coupled with the long-term repression of the gene (Miller et al., 2010). These studies suggest that DNA methylation in the brain is essential for not only the initial memory formation but also the maintenance of those memories. Inhibition of DNMT activity also blocks

the induction of long term potentiation (LTP) at Schaffer collateral synapses (Levenson et al., 2006). Later, genetic study from the Fan lab showed that mice lacking both DNMT1 and DNMT3a in forebrain postmitotic neurons showed smaller cell sizes, reduced hippocampal LTP, impaired contextual fear conditioning memory as well as impaired spatial learning and memory (Feng et al., 2010a).

The importance of DNA methylation for brain function has been further demonstrated by its association with several neurological disorders, such as ICF syndrome and Rett syndrome. Dnmt3b mutations have been reported in 60% of ICF syndrome cases, characterized with chromosome instability, mental retardation, facial abnormalities and immune defects (Hansen et al., 1999). Rett syndrome, however, is generally caused by mutations in the *MECP2* gene, which encodes a protein specifically recognizing CpG methylation (Amir et al., 1999).

MeCP2 as the founding member of Methyl-CpG binding protein family

Two mechanisms have been proposed and demonstrated for DNA methylation-mediated transcriptional repression. First, the methylation of DNA itself physically impedes the binding of transcription factors to gene promoters. Second, and likely more importantly, the repression is mediated by proteins that specifically binds to methylated CpGs and alter chromatin structure, rendering it inaccessible to the transcription machinery.

In the late 1980's, Dr. Adrian Bird and colleagues established a reliable assay for biochemical isolation from mammalian cells of proteins that specifically recognize methylated DNA (Meehan

et al., 1989). The first such protein, methyl-CpG binding protein 2 (MeCP2) was purified and cloned in 1992 (Lewis et al., 1992). Subsequent deletion analyses defined an 85 amino acid region of MeCP2 both necessary and sufficient for methylated DNA binding, named methyl-CpG binding domain (MBD) (Nan et al., 1993). Additional members of the methyl-CpG binding protein family (MBD1, MBD2, MBD3 and MBD4) were soon identified through bioinformatic screening for MBD encoding genes from expressed sequence tag (EST) database (Hendrich and Bird, 1998). Orthologs of these proteins exist in all vertebrate species (Hendrich and Tweedie, 2003). Apart from MBD3, all of them bind to DNA probes with a single symmetrically methylated CpG *in vitro*, albeit with different affinities (Hendrich and Bird, 1998). In mammals, additional proteins carrying a MBD-like domain have been identified, including MBD5, MBD6, histone methylases SETDB1 and SETDB2. However, none of them show stable binding to methylated DNA *in vitro* or *in vivo* (Laget et al., 2010).

The MBD motif represents the only sequence feature found in common among all MBD family members. Co-crystal structure analysis of MBD domain and methylated DNA reveals that MBD domain interacts with methylated CpGs in the major groove, and this interaction is held by hydrogen bonds, salt bridges, and structured water molecules (Ho et al., 2008; Ohki et al., 2001). Outside the N-terminal MBD domain, MeCP2 also contains a central transcriptional repression domain (TRD), which is required for transcriptional repression through recruiting corepressors and chromatin remodeling complexes (Nan et al., 1998). Recently, three AT-hook-like domains has been discovered over a stretch of 250 amino acids in the central part of MeCP2 sequence, which bind to the minor groove of AT-rich DNA and may facilitate MeCP2 binding to DNA and nucleosome (Baker et al., 2013).

The *Mecp2* gene consists of 4 exons, which are alternatively spliced into *MECP2e1* and *MeCP2e2* isoforms that encode distinct proteins differing at the N-termini due to exclusion or inclusion of exon2 respectively (Mnatzakanian et al., 2004). *Mecp2e1* isoform contains 24 amino acids encoded by exon1 and lacks the 9 amino acid encoded by exon 2 for *Mecp2e2*. The e2 isoform was the first identified variant of MeCP2 and therefore better characterized, but the e1 isoform was later found to be more abundant in the brains of both human and mouse (Kriaucionis and Bird, 2004). Both MeCP2 isoforms are nuclear and colocalize with heavily methylated heterochromatic foci. No functional differences between the two MeCP2 isoforms have been reported yet. The fourth exon of *Mecp2* is the largest one and contains a long 3'-untranslated region, with several polyadenylation sites that enable the generation of multiple transcripts, which could be subject to tissue- and developmental-specific regulation (Pelka et al., 2005). While MeCP2 protein is widely expressed in various tissues, it is more abundant in the brain, and primarily in mature postmitotic neurons (Jung et al., 2003), but also detectable in astrocytes (Ballas et al., 2009) and microglia (Maezawa and Jin, 2010). During development, the level of MeCP2 protein relatively is low during embryogenesis and increases progressively with the postnatal brain development and neuronal maturation (Mullaney et al., 2004).

Similar to MeCP2, MBD1 also contains a domain in the C-terminus which is responsible for transcriptional repression. MBD4 contains a DNA glycosylase domain, which is involved in DNA repair. Most MBD proteins are ubiquitously expressed. MBD1 is more abundant in lung and liver. MBD2 is more highly expressed in the dorsal striatum in the brain, while MBD 4 is highly expressed in the immune system (Defossez and Stancheva, 2011).

Among all the MBD containing proteins, MeCP2 has been the most extensively studied, due

to its link with the neurodevelopmental disorder Rett syndrome.

Rett syndrome and other *MECP2* related disorders

Rett syndrome (RTT, MIM 312750) is a postnatal progressive neurodevelopmental disorder and the second most common causes of mental retardation in females. RTT was originally described by the Austrian pediatrician Andeas Rett in 1966 (Rett, 1966). However, it was 17 years later that Rett became worldwide recognized in the medical community when Hagberg at al. reported 35 cases of RTT in the English language (Hagberg et al., 1983). Patients with RTT appear to develop normally for the first 6-18 months of life, followed by a period of regression in language and motor skills. Affected individuals gradually lose purposeful hand use and develop repetitive stereotyped hand-wringing movements, accompanied by the deceleration of head growth, and general weight loss. As the syndrome progress, social withdrawal, irritability and self-abusive behavior become apparent, together with other autistic characteristics, such as unresponsiveness to social cues, expressionless face, and hypersensitivity to sound. Additional clinical features of RTT include ataxia, scoliosis, gait, seizure, anxiety, sleep disturbances and respiratory dysfunction. After the initial regression, most patients reach a pseudo-stationary stage and survive into adulthood. As patients grow older, they often develop Parkinson-like features, such as hypomimia, freezing and askinesia (Chahrour and Zoghbi, 2007).

As RTT occurs almost exclusively in females, early reports proposed that RTT is caused by an X-linked dominant mutation with lethality in hemizygous males. 99% of RTT cases are sporadic, which makes it challenging to map the disease locus by tradition linkage analysis. Exclusion mapping studies using rare RTT familial cases identified the Xq28 candidate region, and

subsequent sequencing of candidate genes revealed mutations of *MECP2* in RTT patients (Amir et al., 1999). Mutations in *MECP2* are found in more than 95-97% cases of classic RTT cases. Except for rare familial cases, mutations arise *de novo* in the paternal germline (Trappe et al., 2001) and usually involve a C to T transition at CpG dinucleotides (Wan et al., 1999), resulting in loss of function due to truncated, unstable or abnormal proteins. Although mutations are dispersed throughout the gene, eight missense and nonsense mutations within MBD and TRD domains (R106W, R133C, T158M, R168X, R255X, R270X, R294X and R306C) accounts for ~70% of all mutations, and C-terminal deletions account for another ~10%.

In addition to those individuals with classic or typical RTT, there are other atypical or variant RTT individuals who present some but not all RTT features (Zappella et al., 2001). 50-70% of these patients have mutations in *MECP2*. Mutations in the X-linked gene cyclin-dependent kinase-like 5 (*CDKL5*) were identified in the early seizure variant of RTT, which features onset of seizure before 5 month of life and lacks the clear period of regression typically seen in classic RTT (Grosso et al., 2007; Neul et al., 2010). Recent reports have identified mutations in *FOXG1* in individuals with the congenital variant of RTT (Neul et al., 2010).

Several genotype-phenotype correlation studies of RTT have been reported, but yielded conflicting results. However, the general conclusion is that patients with *MECP2* truncation mutations towards its C-terminal end have a phenotype that is less severe and less typical of classical Rett syndrome than patients with missense or N-terminal truncation mutations (Smeets et al., 2005). Non-random X-chromosome inactivation in the brain is another major source for the phenotypic variability in RTT patients. In female patients, only one of the two X-chromosomes is active in each cell and the choice of which X chromosome is active is usually

random, but occasionally skewed towards to one chromosome expressing either the wild-type or mutant *MECP2* allele. Extreme favorable skewing of X chromosome inactivation might account for the rare asymptomatic female carriers.

Males with classic Rett *MECP2* mutations usually suffer from severe neonatal encephalopathy and die within 1-2 years after birth. Mild *MECP2* mutations which would produce weak Rett phenotypes in females (C-terminal truncations and some missense mutations) can cause severe mental retardation associated with motor abnormalities in males (Budden et al., 2005). There are also examples of mutations that are only found in males with RTT phenotypes.

Interestingly, gain-of-function of MECP2 in human, typically through duplication or triplication of Xq28 that span the *MECP2* locus, is associated with a recently defined neurodevelopmental disorder *MECP2* duplication syndrome, which shares several clinically features with RTT syndrome (Friez et al., 2006). *MECP2* duplication syndrome is inherited in an X-linked manner with 100% penetrance in males with carrier mothers. Patients with *MECP2* duplication syndrome suffer from severe mental retardation, epileptic seizures, progressive spasticity, recurrent respiration infections, and often premature death. Other hallmark symptoms include autistic-like features, anxiety, stereotypic hand movement, and motor dysfunction (Ramocki et al., 2010).

Furthermore, mutations in *MECP2* not only result in RTT syndrome, but also cause a range of related neuropsychiatric disorders. *MECP2* mutations have been identified in patients diagnosed with Angelman syndrome (Ramocki et al., 2010), severe mental retardation (Klauck et al., 2002), Prader-Willi syndrome (Kleefstra et al., 2002). Milder mutations of *MECP2* may cause learning

disabilities, mild mental retardation and autism spectrum disorders (Carney et al., 2003). The full spectrum of phenotypes in *MECP2* disorders is far from being understood.

Modeling Rett syndrome in mice

To elucidate the mechanisms underlying RTT, several mouse models have been generated. In 2001, right after the discovery of *MECP2* mutations in Rett syndrome patient in 1999, *Mecp2* null mice, lacking either exon 3 or both exon 3 and 4, were made and showed severe neurological symptoms that mimic Rett syndrome (Chen et al., 2001; Guy et al., 2001). *Mecp2*-null males display no initial symptoms until 3-5 weeks of age, when they begin to develop hindlimb clasping, gait, hypoactivity, tremor, and irregular breathing, and ultimately die between 8-10 weeks. Mutant brains showed substantial reduction in both weight and neuronal cell size, but no obvious structural defects or signs of neurodegeneration. Heterozygous females mice also show behavioral symptoms, but with a later onset.

In addition to *Mecp2*-null mice, several mouse models harboring common Rett Mecp2 mutations have been made. Mice with a truncating mutation at amino acid 308 of MeCP2, similar to C-terminal deletions found in RTT patients, appear normal for about 6 weeks, then develop tremors, motor impairment, hypoactivity, stereotypic forelimb motions and finally die at around 15 month age (Shahbazian et al., 2002). The $Mecp2^{T158A}$ knockin mice also recapitulate a number of RTT-like symptoms, including late onset of hypoactivity, motor dysfunction, irregular breathing, and shorten lifespan. The T158A mutation, located at the C terminus of MBD domain, resulted in reduced MeCP2 protein stability (Goffin et al., 2012). The $MeCP2^{R306C}$ knockin mice

also develop phenotypes resembling that of Mecp2-null mice, including reduced brain weight, hindlimb clasp, tremor, locomotor deficit, and early death. Interestingly, the R306C mutation abolished the interaction between MeCP2 and the NcoR/SMRT co-repressor complexes (Lyst et al., 2013). More recently, two mouse models expressing either MeCP2^{R270X} or MeCP2^{G273X} have been generated. R270X is one of the common mutations found in Rett female patients. R270fs mutation in male patients causes severe neonatal encephalopathy and early death. However, male patients with an adjacent mutation G273fs develop RTT-like phenotypes and manage to survive for decades. Both of the *Mecp2*^{270X} and *Mecp2*^{G273X} mouse models show RTT-like symptoms. Interestingly, the G273X transgenic mice display significantly later onset and slower disease progression compared to R270X transgenic mice, resembling features of male RTT patients with G273fs and R270fs mutations, respectively. The authors proposed that the lack of an important AT-hook domain (amino acids 257–272) in R270X may cause the phenotype differences (Baker et al., 2013).

Mouse model for *MECP2* duplication syndrome has also been made. Two-fold overexpression of MeCP2 is achieved by make transgenic mice lines with bacterial artificial chromosome harboring the entire human *MECP2* locus (*MECP2*^{Tg}). *MECP2*^{Tg} mice developed normally until 20 weeks of age, when they became hypoactive and developed forepaw clasping, aggressiveness, kyphosis, seizures, and motor abnormalities, and died by 1 year of age (Collins et al., 2004). Of note, mice with MeCP2 overexpression in postmitotic neurons from the tau locus also recapitulated some aspects of *MECP2* duplication syndrome, including profound motor dysfunction characterized by tremors, gait ataxia and side to side swaying (Luikenhuis et al., 2004).

By taking advantage of the *Cre-loxP* recombination system, a variety of studies have been done to address the spatial and temporal requirement of MeCP2 in the brain. Brain-specific deletion of *Mecp2* at embryonic day 12 resulted in a phenotype almost identical to that of the null mutation, consistent with the notion that Rett syndrome is primarily a CNS disease with not much peripheral contribution (Chen et al., 2001). When *Mecp2* is deleted in forebrain postmitotic neurons, less severe neurological phenotypes, such as abnormal gait, increase anxiety and impaired social behavior, are observed with a later onset (Chen et al., 2001; Gemelli et al., 2006). Loss of MeCP2 from amygdala impairs normal anxiety behavior and amygdala-dependent learning and memory (Adachi et al., 2009). And removal of *Mecp2* from Sim1-expressing neurons in hypothalamus resulted in alterations in feeding behavior, aggression and stress response (Fyffe et al., 2008). In addition, loss of MeCP2 from dopaminergic neurons causes motor in coordination whereas loss from serotoninergic neurons leads to increased aggression (Samaco et al., 2009). Surprisingly, loss of MeCP2 from a subset of forebrain GABAergic neurons recapitulates many features of Rett syndrome, including stereotyped movement, impaired motor coordination, learning and memory deficit, severe respiratory dysrhythmias and premature lethality (Chao et al., 2010). Although MeCP2 expression in astrocytes is not as high as in neurons, mice with *Mecp2* deletion in astrocytes display some phenotypes shared with null *Mecp2* null mice, such as smaller body size, clasped hindlimb posture and irregular breathing, but their lifespan, locomotion and anxiety-related behavior were all normal (Lioy et al., 2011). Taken together, removal of MeCP2 from a subpopulation of cells in the brain usually reproduces some aspects of Rett syndrome, suggesting a wide range of requirement of MeCP2 in multiple brain regions and cell types.

The onset of symptoms in RTT patients as well as in mouse models occurs during postnatal development, coinciding with a period of intense synaptic refinement, suggesting the function of MeCP2 in the maturing nervous system is critical for establishing normal adult neurological function. This notion is supported by a study demonstrating that reactivation of MeCP2 in symptomatic adult *Mecp2*-deficient mice resulted in reversal of neurological symptoms and re-establishment of health (Guy et al., 2007). In a separate study, it was demonstrated that overexpression of MeCP2 in postmitotic neurons from *tau* locus was able to rescue the RTT phenotype in *Mecp2* null mice (Giacometti et al., 2007). Moreover, re-expression of *Mecp2* preferentially in astrocytes significantly improved locomotion and anxiety levels, restored respiratory abnormalities to a normal pattern, and greatly prolonged lifespan compared to globally null mice (Lioy et al., 2011). Interestingly, transplantation of wild type bone marrow into *Mecp2*-null mice markedly attenuated disease symptoms, suggesting a microglial contribution of RTT disease progression (Derecki et al., 2012).

On the other hand, inactivation of the *Mecp2* gene starting from adult stage (8-week old) in mice triggers the appearance of RTT-like phenotypes and death (Derecki et al., 2012). In a more recent study, Cheval H et al deleted *Mecp2* gene at three postnatal ages (3, 11 and 20 weeks after birth) to determine whether MeCP2 is required equally throughout life. *Mecp2* inactivation caused the appearance of RTT-like phenotypes and premature death independent of the age at inactivation. However, the disease progression rate is dramatically increased when *Mecp2* is deleted from mice at an older age, indicating an enhanced role for MeCP2 in the aging brain (Cheval et al., 2012).

The function of MeCP2 for learning memory and synaptic plasticity

Because of the early postnatal lethality of *Mecp2* null mice, early attempts to examine whether the loss of MeCP2 leads to deficits in learning and memory have been focused on the *Mecp2*^{308} model. *MeCP2*$^{308/y}$ mice displayed impaired hippocampus-dependent spatial memory in morris water maze test and contextual fear memory deficit in contextual fear conditioning test (Moretti et al., 2006). The recent reported *Mecp2* $^{T158A/y}$ mice also exhibit impaired context- and cue-dependent fear memory (Goffin et al., 2012). The other way to circumvent the lethality problem of *Mecp2* null mice is to use conditional knockout mice for behavioral tests. When MeCP2 was selectively deleted in from forebrain neurons, mice showed reduced cue-dependent fear memory in fear conditioning test (Gemelli et al., 2006). Mice lacking MeCP2 in GABAergic neurons presented impaired spatial memory in Morris water maze test (Chao et al., 2010). On the other hand, *MECP2*^{Tg} mice, with two-fold expression of MeCP2, displayed enhancement of contextual learning in fear conditioning test (Collins et al., 2004). Consistently, *tau-MeCP2* transgenic mice also show increased freezing responses in both context and cue fear conditioning tests (Na et al., 2012).

Long-term potentiation (LTP) and long-term depression (LTD) are forms of synaptic plasticity that are believed to underlie long-term memory formation. Impairments in LTP and LTD induction or maintenance have often been correlated with learning and memory. Schaffer-collateral LTP and LTD are significantly attenuated in symptomatic *Mecp2* null mice (Asaka et al., 2006). Impaired LTP is also reported in *Mecp2*$^{308/y}$ mice (Moretti et al., 2006). In contrast, LTP is enhanced with doubling of MeCP2 in *MECP2*^{Tg} mice (Collins et al., 2004). In addition, loss-of-MeCP2 function has been associated with reduced paired pulse facilitation and

faster excitatory postsynaptic response depression, measures of short-term synaptic plasticity (Asaka et al., 2006). Alternatively, gain-of-MeCP2 function has been shown to increase paired pulse response (Collins et al., 2004). In summary, these data suggest a bidirectional relationship between MeCP2 level and both long-term plasticity and some forms of short-term plasticity.

At the cellular level, hippocampal glutamatergic neurons that lack MeCP2 display a 46% reduction in synaptic response, whereas neurons with doubling of MeCP2 exhibit a 2-fold enhancement in synaptic response. These changes may primarily due to an altered number of glutamatergic synapses formed, as neurons from *Mecp2* null mice have an 40% reduction in VGLUT1-PSD95-positive puncta, whereas those from *MECP2*^{Tg} mice have a 60% increase in such puncta in comparison with wild type mice (Chao et al., 2007). These results reveal MeCP2 as an important factor in regulating glutamatergic synapse formation in postnatal development.

MeCP2 as a multifunctional protein

The ability of MeCP2 to bind to methylated DNA, together with its subcellular localization to pericentromeric heterochromatin, initially led researchers to propose MeCP2 as a global transcriptional repressor. Majority of the initial studies of MeCP2 function were attempted to elucidate its role in transcriptional repression. Corepressor Sin3A and histone deacetylases (HDACs) 1 and 2 were among the first identified MeCP2 interacting partners, through the binding to the TRD of MeCP2 (Jones et al., 1998; Nan et al., 1998). A more recent report revealed that MeCP2 interacts with the NCoR/SMRT co-repressor complex, including another histone deacetylase HDAC3 (Lyst et al., 2013). The involvement of HDACs in MeCP2

repression mechanism was further supported by the report that MeCP2-deficient brains show enhanced global histone acetylation level (Shahbazian et al., 2002; Skene et al., 2010). Additional MeCP2 interacting proteins include heterochromatin protein 1 (HP1), cSki corepressor, DNA methyltransferase DNMT1, the corepressor CoREST, histone methyltransferase Suv39H1, many of which have been implicated in transcription repression (Guy et al., 2011). Consistent with these findings, MeCP2 specially inhibits transcription from methylated promoters *in vitro* (Nan et al., 1997).

However, in a number of transcriptional profiling experiments aimed to identify misregulated genes in *Mecp2* deficient mice, only mild changes in gene expression were revealed (Tudor et al., 2002). One possible explanation is that critical disease-related alterations in gene expression might occur only in specific brain regions or neurons and, therefore, would be masked in analyses of the whole brain tissue. To circumvent this problem, Chahrour et al. analyzed gene expression in the hypothalamus of *MeCP2*-null, wild-type, and *MeCP2*^{Tg} mice. This approach revealed small but important changes in the expression of thousands of genes, many of which are affected in opposite ways with deletion or overexpression of MeCP2. Surprisingly, 85% of the misregulated genes in both mouse models were up-regulated in the transgenic hypothalami and down-regulated in the *Mecp2*-null hypothalami, suggesting that many of these genes are likely activated by MeCP2 (Chahrour et al., 2008). In favor of this notion, MeCP2 was found to associate with transcriptional activator CREB1, and co-occupancy of MeCP2 and CREB1 was detected at the promoter of *Sst*, a gene activated by MeCP2 (Chahrour et al., 2008).

Since RTT results from the loss of a transcriptional regulator, identifying the target genes of MeCP2 will not only provide insight into the mechanisms of disease pathogenesis but also help

developing effective treatments. Using candidate gene approach, several MeCP2 target genes have been identified and demonstrated to be involved in some aspects of RTT pathology. BDNF is a key signaling molecule in brain development and plasticity, and its protein level is significantly reduced in *MeCP2* null mice. Forebrain-specific deletion of *Bdnf* in *Mecp2* null mice resulted in earlier onset of locomotor dysfunction and reduced lifespan, while overexpression of *Bdnf* in *Mecp2* null mice improved locomotor function and extended their lifespan, suggesting the physiological significance of BDNF in RTT disease progression (Chang et al., 2006). Several studies have demonstrated that agonists of BNDF signaling partially rescue RTT-like features in MeCP2 null mice and extend their lifespan (Johnson et al., 2012; Schmid et al., 2012). Another example is *Crh*, a gene that modulates behavioral and physiologic responses to stress and anxiety. *Crh* levels, which are increased in the *MECP2*^{TG} mice but decreased in *Mecp2*-null mice, correlate with heightened and reduced anxiety-like behavior, respectively. In *MECP2*^{TG} animals, reducing the levels of *Crh* or its receptor *Crhr1* both suppressed anxiety-like behavior (Samaco et al., 2012).

To make the picture of MeCP2 function even more complicated and interesting, in a study aimed to identify for MeCP2 binding partners using co-immunoprecipitation coupled with mass spectrometry (MS), an RNA binding protein Y box-binding protein 1 (YB1) was identified (Young et al., 2005). The authors further demonstrated that MeCP2 interacts YB1 in a RNA-dependent manner and discovered several aberrant RNA splicing patterns in a *Mecp2* null mice.

Recent work from Adrain Bird's groups demonstrated that the MeCP2 protein is almost as abundant as the histone octamers in the mouse brain and MeCP2 is globally distributed across

entire mouse genome and this distribution tracks the density of 5-methylcytosine (Skene et al., 2010). In *Mecp2*-deficient brain, the levels of linker histone H1and histone H3 acetylation were elevated (Skene et al., 2010). There is also a report suggesting that MeCP2 competes with Histone H1 for binding to chromatin with methylated DNA *in vitro* (Nan et al., 1997*). In vivo*, MeCP2 and histone H1show similar mobility in the nucleus and share the same internucleosomal binding sites (Kumar et al., 2008; Misteli et al., 2000). These observations suggest that MeCP2 and histone H1 may share similar functions organizing chromatin structure in neurons, although the physiological significance of this interplay between MeCP2 and histone H1 awaits further investigation.

Like histones, MeCP2 is also subject to post-translational modifications, such as phosphorylation, which provides MeCP2 with functional plasticity upon stimuli.

Neuronal activity-induced MeCP2 phosphorylation

MeCP2 phosphorylation was initially discovered by the Greenberg group in 2003 (Chen et al., 2003b). Western blotting of neuronal lysates with antibodies to MeCP2 revealed that within minutes of membrane depolarization a previously unknown form of MeCP2 was present and migrated more slowly during SDS–polyacrylamide gel electrophoresis (SDS-PAGE). Alkaline phosphotase treatment of extracts from membrane-depolarized neurons caused the disappearance of this slow-migrating MeCP2 species, indicating it may be a result of phosphorylation. This phosphorylation site was later identified as serine 421 (S421) (Tao et al., 2009; Zhou et al., 2006). Mutating this serine into alanine *in vitro* abolishes the membrane depolarization-induced

slow-migrating MeCP2 species and interferes with neuronal activity induced *Bdnf* transcription. Later, an unbiased immunoprecipitation/mass spectrometry study revealed a much more complex picture of MeCP2 phosphorylation (Tao et al., 2009). 8 potential phosphorylation sites, including S421, were identified throughout the mouse MeCP2 protein. Among these, phosphorylation regulation at serine 80 (S80) was found to be opposite to that at S421. Specifically, S80 is phosphorylated in resting neurons but dephosphorylated in active neurons, whereas S421 is dephosphorylated in resting neurons but phosphorylated in active neurons. Most recently, three additional sites of neuronal activity-dependent MeCP2 phosphorylation were identified by phosphotryptic mapping (Ebert et al., 2013). Interestingly, phosphorylation of threonine 308 (T308) blocks the interaction of the repressor domain of MeCP2 with the nuclear receptor co-repressor (NCoR) complex.

So far, the most studied site of MeCP2 phosphorylation is S421. *In vitro* neuronal culture studies indicated that glutamate release at synapses and neurotrophin stimulation both trigger MeCP2 S421 phosphorylation (Zhou et al., 2006). Regardless of the type of stimuli, L-type voltage-sensitive calcium channels activation is required for S421 phosphorylation in neurons (Tao et al., 2009; Zhou et al., 2006). As for the kinases that directly phosphorylate S421, both CamKII and CamKIV have been implicated (Tao et al., 2009; Zhou et al., 2006), although no direct association has been established between MeCP2 and either kinase. *In vivo*, stimulus induced S421 phosphorylation has been reported in specific neuronal subtypes in various brain regions. Robust S421 phosphorylation can be detected in many neurons throughout the brain after kainic acid-induced seizure, a pathological form of synchronized neuronal activity (Tao et al., 2009; Zhou et al., 2006). Physiological light stimulation that regulates circadian behavior

triggers the phosphorylation of MeCP2 at S421 in neurons of the suprachiasmatic nucleus (SCN) (Zhou et al., 2006). In the hypothalamus, early life stress induces S421 phosphorylation specifically in neurons in the parvocellular division of the hypothalamic paraventricular nucleus (Murgatroyd et al., 2009). In the striatum, psychostimulants induce S421 phosphorylation selectively in GABAergic interneurons of the ventral structure of nucleus accumbens (Deng et al., 2010a), while cocaine has been shown to induce S421 phosphorylation in both the caudate putamen and the nucleus accumbens (Mao et al., 2011). To date, S421 phosphorylation has been observed only in neurons.

Besides S421, the other phosphorylation site that received some attention is S80. Different from S421, S80 is phosphorylated in resting neurons *in vitro* and *in vivo* (Tao et al., 2009). In cortical neurons, S80A mutation attenuated chromatin association affinity at candidate gene promoters and caused subtle gene expression changes (Tao et al., 2009). Furthermore, S80 phosphorylation has been observed in non-neuronal cells, can be directly phosphorylated by homeodomain-interacting protein kinase 2 (HIPK2), and may play a role in apoptosis (Bracaglia et al., 2009).

To elucidate the *in vivo* function of MeCP2, we have generated several Mecp2 knockin alleles with point mutations that either abolish or mimic MeCP2 phosphorylation. In this dissertation, I will not only present the phenotype characterization of these phosphor mutant mice but also provide some insight into the mechanisms how MeCP2 phosphorylation may modulate brain development and function.

Adult neurogenesis and its role in brain function

Adult mammalian brains were long believed to be postmitotic and with no capacity of generating new neurons. However, it is now generally accepted that new-born neurons and glia are continuously generated from neural stem cells (NSCs) in two regions of adult brains: the subgranular zone (SGZ) of the dentate gyrus (DG) of the hippocampus and the subventricular zone (SVZ) of the lateral ventricles (Eriksson et al., 1998; Kuhn et al., 1996; Lois and Alvarez-Buylla, 1994). Adult neurogenesis involves multiple processes that include proliferation, fate specification, differentiation, maturation, migration, and function integration of the newborn cells into the existing neuronal network (Gage, 2000).

In adult hippocampus, quiescent radial glia-like cells (RGLs) are considered neural stem cells. Once activated, RGLs can undergo either symmetric division expanding the RGL poll or asymmetric division to generate neurogenic or astrogliogenic progenitor cells while maintaining the RGL pool (Bonaguidi et al., 2011). Astroglial progenitor cells will give rise to astrocytes. Neural progenitor cells (NPCs) keep dividing and then generate neuroblasts and finally differentiate into glutamatergic granule cells of the dentate gyrus and integrate into the local neuronal network in the hippocampus (Encinas and Enikolopov, 2008). Similarly, quiescent neural stem cells give rise to transient amplifying cells via asymmetric division in SVZ. Transient amplifying cells further give rise to neuroblasts that migrate through the rostral migratory stream and differentiate into GABA- and dopamin-producing granule and periglomerular interneurons in the olfactory bulb (Alvarez-Buylla and Lim, 2004).

In the adult brain, hippocampus has been implicated in learning and memory, while the

olfactory bulb is involved in olfaction. Right after the initial discovery of adult neurogenesis in hippocampus, it was hypothesized that adult born neurons play roles in learning and memory. Although still under intensive debate, cumulative evidence generated over the years are supporting critical contributions of adult born neurons to hippocampus and olfactory bulb functions.

At the cellular level, matured newborn neurons exhibit hyperexcitability and enhanced synaptic plasticity in both hippocampus and olfactory bulb, which may give the newly integrated adult-born neurons unique properties in the memory storage process (Ge et al., 2007; Schmidt-Hieber et al., 2004). At the circuitry level, LTP induced by tetanic stimulation of the afferent medial perforant pathway is abolished in the slices from mice having received radiation to abrogate adult neurogenesis (Snyder et al., 2001). At the behavioral level, studies using irradiation or antimitotic drugs in rodents and more recently using genetically modified mice to eliminate hippocampus adult neurogenesis have provided convincing evidence that adult-born neurons are required for some (but not all) hippocampus-dependent memory, such as spatial-navigation learning, spatial pattern discrimination, trace fear conditioning, clearance of hippocampal memory trace (Deng et al., 2010b; Shors et al., 2001). Adult SVZ neurogenesis has been implicated in maintaining long-term integrity of the olfactory bulb, short-term and long-term olfactory memory (Lazarini and Lledo, 2011).

Adult Neurogenesis is dynamically regulated by a number of intrinsic as well as extrinsic factors. Given the significant similarity between embryonic and adult neurogenesis, it is not surprising that many intrinsic signaling pathways are conserved, including Notch, Shh, Wnts, and BMPs (Faigle and Song, 2013). Notch is a key regulator of NSCs/NPCs maintenance in both

embryonic and adult nervous system (Louvi and Artavanis-Tsakonas, 2006). Notch is required to maintain neural precursors in an undifferentiated self-renewing state, preventing premature neurogenesis (Artavanis-Tsakonas et al., 1999). Binding of the Notch receptor to a ligand on an adjacent cell triggers a series of proteolytic cleavages. As a result, the Notch intracellular domain (NICD) is released and enters the nucleus, activating downstream target genes. In the context of NSCs/NPCs, Notch activation leads to the transcription of *Hes* and *Hey* family genes (Bray and Bernard, 2010). In adult hippocampus, abrogation of Notch1 in neural progenitor cells promotes cell cycle exit and neuronal differentiation. Overexpression of intracellular domain of Notch1 (NICD), however, leads to proliferation and expansion of the neural stem/progenitor cells pool (Ables et al., 2010).

Epigenetic mechanisms, particularly DNA methylation, have emerged as an important link between external or internal stimuli (Zhao et al., 2003)and transcriptional control of gene expression in adult neural stem/progenitor cells.

Among the DNA methyltransferase, Dnmt3a is expressed in adult neural stem/progenitor cells and is required for neurogenesis (Wu et al., 2010). GADD45b, a protein previously implicated in DNA demethylation, is a neuronal activity-induced immediate early gene in mature hippocampal neurons (Barreto et al., 2007). Gadd45b knockout mice exhibit specific deficits in neural activity-induced proliferation of neural progenitors and dendritic growth of newborn neurons in the adult hippocampus (Ma et al., 2009).

Among MBD family proteins, the role of MBD1 in adult neurogenesis has been extensively studied. MBD1 knockout mice develop normally, but have reduced hippocampal neurogenesis

and impaired spatial learning (Zhao et al., 2003). MBD1 promotes neuronal differentiation by binding to FGF2 promoter and repress its expression (Li et al., 2008). Moreover, recent study indicated that MBD1 facilitate adult neurogenesis via Numbl, a Notch pathway modulator, through repression of a microRNA *miR-184* (Liu et al., 2010).

MeCP2 is another MBD protein that is involved in regulating adult neurogenesis. MeCP2 is important for maintaining neuronal identity in neural progenitor cells though the suppression of GFAP expression (Kohyama et al., 2008). Newborn neurons in the DG of MeCP2 deficient mice exhibit deficits in neuronal maturation and spine formation (Smrt et al., 2007). A recent study also suggests MeCP2, in cooperation with Sox2, represses expression of *miR-137*, a microRNA that promotes adult NPC proliferation and inhibits neuronal differentiation (Szulwach et al., 2010).

In this dissertation, we provide evidence that MeCP2 S80 and S421phosphorylation may function as a pair of balancing forces in regulating adult neurogenesis. Loss of S421 phosphorylation and loss of S80 phosphorylation result in opposite changes in the proliferation and neuronal differentiation of adult NPCs.

Chapter 2: Loss of Activity-Induced Phosphorylation of MeCP2 Enhances Synaptogenesis, LTP, and Spatial Memory

This chapter has been published as:

Li H, Zhong X, Chau KF, Williams EC, Chang Q (2011) Loss of activity-induced phosphorylation of MeCP2 enhances synaptogenesis, LTP and spatial memory. *Nat Neurosci* 14:1001–1008.

Summary

DNA methylation-dependent epigenetic mechanisms underlie the development and function of the mammalian brain. MeCP2 expresses highly in neurons, and functions as a molecular linker between DNA methylation, chromatin remodeling and transcription regulation. Previous *in vitro* studies showed neuronal activity-induced phosphorylation (NAIP) of MeCP2 precedes its release from the *Bdnf* promoter and the ensuing *Bdnf* transcription. However, the *in vivo* function of this phosphorylation event remains elusive. We generated knockin mice that lack NAIP of MeCP2, and show here the *Mecp2* phospho-mutant mice perform better in hippocampus-dependent memory tests, present enhanced LTP at two synapses in the hippocampus, and show increased excitatory synaptogenesis. At the molecular level, the phospho-mutant MeCP2 protein binds more tightly to several MeCP2 target gene promoters and alters the expression of these genes. Our results supply the first genetic evidence that NAIP of MeCP2 is required in modulating dynamic functions of the adult mouse brain.

Introduction

The genetic and epigenetic mechanisms underlying the development, maintenance, and function of the mammalian nervous system have been extensively studied over the years. To understand what functional role DNA methylation-dependent epigenetic mechanisms may play in any of these biological processes, it is important to study how DNA methylation and the recognition of DNA methylation by the methyl-DNA binding domain containing proteins (MBDs) may be dynamically regulated in neuronal nuclei in response to extracellular signals. While there is pharmacological (Miller et al., 2010; Miller and Sweatt, 2007) and genetic (Feng et al., 2010a) evidence that dynamic DNA methylation is required for learning and memory, relatively little is known about how binding to methylated DNA by the MBDs may be dynamically regulated to support normal brain functions.

As the founding member of the MBD gene family, *Mecp2* (methyl-CpG binding protein 2) encodes a protein that specifically binds to methylated DNA and represses transcription (Lewis et al., 1992; Nan et al., 1997). Earlier studies show that MeCP2 interacts with the transcriptional repressor mSin3A and histone deacetylases (Jones et al., 1998), suggesting it may function as a molecular linker between DNA methylation, chromatin remodeling and subsequent gene silencing (Bird and Wolffe, 1999). However, recent studies also demonstrate that MeCP2 may activate transcription of some genes, while repress transcription of others (Chahrour et al., 2008; Yasui et al., 2007). Mutations in the X-linked human *MECP2* gene cause Rett syndrome (RTT) (Amir et al., 1999), an autism spectrum neurodevelopmental disorder that predominantly affects females (Hagberg, 1985). At an estimated prevalence of 1 in 10,000-15,000 girls, RTT is the second most common X-linked mental retardation in females.

To better understand the functions of MeCP2 and help reveal the molecular mechanism of RTT, it is important to study how MeCP2 dynamically regulates neuronal gene transcription in response to diverse extracellular stimuli, and to reveal the physiological significance of such regulation. The most common extracellular stimulus in the brain is neuronal activity. Two earlier *in vitro* studies in rat neurons have shown that neuronal activity-induced phosphorylation (NAIP) at serine 421 (S421) precedes the release of MeCP2 from the neuronal specific promoter of the brain-derived neurotrophic factor (*Bdnf*) gene and the subsequent expression of BDNF (Chen et al., 2003b; Zhou et al., 2006). Recently, a more detailed analysis of the mouse brain by mass spectrometry has identified NAIP at two serines, S421 and S424 of the MeCP2 protein (Tao et al., 2009). Moreover, both sensory inputs and psychostimulants have been shown to induce phosphorylation of MeCP2 at S421 in the intact mouse brain (Deng et al., 2010a; Zhou et al., 2006). Collectively, these studies raise the possibility that NAIP of MeCP2 may serve as a molecular switch on the chromatin for dynamically modulating neuronal functions. To reveal what *in vivo* function requires NAIP of MeCP2, we have generated knockin mice that carry point mutations in the endogenous *Mecp2* gene locus to abolish phosphorylation at both S421 and S424. We show here that phosphorylation at S421 can be induced by depolarization, high frequency electrical stimulation, and behavioral training in the hippocampus of wild type mice; and that the $Mecp2^{S421A;S424A/y}$ mice lack phosphorylation at S421 in the brain at both the baseline level and after seizure. We further demonstrate that the $Mecp2^{S421A;S424A/y}$ mice perform better in two hippocampus-dependent learning and memory tests than their wild type littermates, present enhanced long-term potentiation at both the Schaffer collateral-CA1 synapses and the mossy fiber-CA3 synapses, have increased excitatory synaptogenesis, and show corresponding gene expression changes that are consistent with these phenotypes. Finally, to take advantage of the

consistency of the anti-flag antibody so that we may better quantify the promoter occupancy of the phospho-mutant MeCP2 protein, we generated two novel *Mecp2* knockin alleles: the *Mecp2*$^{S421A;S424A\text{-}flag/y}$ mice expressing the MeCP2$^{S421A;S424A}$-flag protein from the endogenous *Mecp2* locus and the *Mecp2*$^{WT\text{-}flag/y}$ mice expressing the MeCP2-flag protein from the endogenous *Mecp2* locus. We show that the MeCP2$^{S421A;S424A}$-flag protein binds more tightly to known MeCP2 target gene promoters than does the MeCP2-flag protein, indicating the phospho-dead form of MeCP2 may function as a hypermorph. Our findings provide the first genetic evidence that neuronal activity-induced MeCP2 phosphorylation is required for the development, maintenance, and function of the adult mouse brain. These results may be relevant for understanding RTT disease mechanisms. Moreover, these results add to the emerging picture of epigenetic regulation of nervous system function, which include not only changes in DNA methylation itself, but also a critical role for stimulus-dependent phosphorylation of a methyl-DNA binding protein.

Results

Loss of NAIP of MeCP2 in *Mecp2*$^{S421A;S424A/y}$ mice

To compare the level of S421 phosphorylation in the silent hippocampus with that in the active hippocampus, we treated freshly prepared hippocampal slices with either tetradotoxin (TTX, to suppress neuronal activity) or potassium chloride (KCl, to depolarize neurons), and performed double immunostaining with a phospho-S421 (p-S421) specific antibody and a NeuN antibody (a neuronal marker). The intensity of p-S421 signal was dramatically higher in the KCl-treated slices than in the TTX-treated slices (**Fig. 1a,e**), indicating the induction of S421 phosphorylation by depolarization. As a control, the intensity of NeuN signal was the same in KCl- and TTX-treated slices (**Fig. 1a**). We next tested whether phosphorylation of S421 may be induced by more physiologically relevant stimuli. High frequency electrical stimulation (HFS) is commonly used to induce long-term potentiation (LTP) in hippocampal slices. Using the same p-S421 specific antibody, we detected more than 100% increase in the intensity of p-S421 signal after HFS in acute hippocampal slices, as compared to its level in slices under baseline electrical stimulation (**Fig. 1b,e**). Again NeuN immunoreactivity was similar in slices receiving either baseline stimulation or HFS (**Fig. 1b**). Finally, we tested whether phosphorylation of S421 may be induced by behavioral trainings, such as contextual fear conditioning and Morris water maze. In the contextual fear training experiment, we compared p-S421 immunoreactivity in hippocampal sections from mice that received shock immediately after being put into the box (immediate shock control) and mice that received shock two minutes

after being put into the box (context trained), and found a 59% increase of p-S421 signal in the context trained mice over the immediate shock control (**Fig. 1c,e**). In the Morris water maze training experiment, we compared p-S421 immunoreactivity in hippocampal sections from mice that received the hidden platform version of Morris water maze (WM) training (WM trained) and mice that swam the same amount of time in the same tank with no platform (yoked/swimming control), and found a 88% increase of p-S421 signal in the hippocampus of WM trained mice over the yoked/swimming control (**Fig. 1d,e**). In addition to co-staining with NeuN (**Fig. 1c,d**), we performed immunostaining against total MeCP2 on the adjacent sections, and detected no difference in total MeCP2 expression between the context trained group and the immediate shock control, and between the WM trained group and the yoked/swimming control (**Supplementary Fig. 1**). Taken together, our data suggest that increased neuronal activity level, induced by artificial depolarization, physiologically relevant electrical stimulation, or behavioral training, can lead to phosphorylation of S421 on the MeCP2 protein in the mouse hippocampus.

Recently, a detailed mass spectrometry analysis (Tao et al., 2009) identifies two serines in MeCP2 (S421 and S424), whose phosphorylation is induced by neuronal activity in the mouse brain. Yet the same study finds NAIP of MeCP2 only at S421, but not S424, in the rat brain. To completely abolish NAIP of MeCP2, we generated mice that encode serine to alanine (S to A) mutations at both the 421th and the 424th amino acids in the endogenous *Mecp2* gene (Tao et al., 2009). The *Mecp2*$^{S421A;S424A/y}$ mice showed none of the RTT phenotypes observed in the *Mecp2* null mice (i.e. small brain or hindlimb clasping), bred normally, and had a normal lifespan (Tao et al., 2009). On brain sections prepared from the *Mecp2*$^{S421A;S424A/y}$ mice, the temporal and spatial expression patterns of the MeCP2$^{S421A;S424A}$ protein were indistinguishable from those of

the wild type MeCP2 protein in the wild type mice (data not shown). As an example, MeCP2$^{S421A;S424A}$ immunoreactivity (**Fig. 2a**) in the pyramidal neurons (co-stained by NeuN, **Fig. 2b**) of the CA1 region (marked by arrowheads in **Fig. 2a**–**h**) in the adult hippocampus is shown to be indistinguishable from MeCP2 immunoreactivity in the wild type (**Fig. 2c,d**). Moreover, the sub-cellular localization of the MeCP2$^{S421A;S424A}$ protein in cortical neurons (**Supplementary Fig. 2a**–**d**) was also identical to that of the wild type MeCP2 protein (**Supplementary Fig. 2e**–**h**). In brain lysates prepared from the *Mecp2*$^{S421A;S424A/y}$ mice, the MeCP2$^{S421A;S424A}$ protein was expressed at the same level as that of the MeCP2 protein in wild type mice both under normal condition and after seizure (**Fig. 2i**). We next examined the phosphorylation status of S421 in the *Mecp2*$^{S421A;S424A/y}$ and control mice. Consistent with our expectation, while phosphorylation at S421 was present at baseline (**Fig. 2g,i**) and greatly induced by seizure in the wild type brain (**Fig. 2i**), it was completely abolished in the *Mecp2*$^{S421A;S424A/y}$ mice both at baseline (**Fig.2e,i**) and after seizure (**Fig. 2i**). By RT-PCR based sequencing of the expressed *Mecp2*$^{S421A;S424A}$ RNA transcript, we have previously shown that S424 has been changed to A424 (Tao et al., 2009). Since the mutation to alanine is a proven way to abolish serine phosphorylation, A424 cannot be phosphorylated under any conditions in the *Mecp2*$^{S421A;S424A/y}$ mice. Taken together, these results suggest that the S421A;S424A double mutation specifically abolished NAIP of MeCP2, without changing the expression level, expression pattern and intracellular localization of the mutant protein.

Enhanced hippocampal memory in *Mecp2*$^{S421A;S424A/y}$ mice

To reveal the physiological relevance of neuronal activity-induced MeCP2 phosphorylation, we performed a series of behavioral analyses of the *Mecp2*$^{S421A;S424A/y}$ mice. To eliminate potential influence of different genetic backgrounds on animal behavior, we backcrossed the *Mecp2*$^{S421A;S424A}$ mice with the C57BL/6 mice for a minimum of 10 generations. As an initial screen for phenotypes covering anxiety, exploratory activity, motor coordination, and learning and memory, we compared the *Mecp2*$^{S421A;S424A/y}$ mice to their wild type littermates in the open field test, the rotarod test, and the fear conditioning test. In the open field test, the *Mecp2*$^{S421A;S424A/y}$ mice showed a similar level of anxiety, as measured by the percentages of distance traveled in the middle (13.3±0.9% vs. 14.0±1.6%, p=0.7) and the corners (39.5±1.1% vs. 38.6±1.6%, p=0.6) of the field, as their wild type littermates (**Supplementary Fig. 4a**,**b**); and the same amount of exploratory activity, as measured by the total distance traveled, as their wild type littermates (**Supplementary Fig. 4c**). To confirm these results, we performed another widely used anxiety test--the elevated plus maze--with another cohort of *Mecp2*$^{S421A;S424A/y}$ mice and their wild type littermates, and observed similar levels of exploratory activity and anxiety in the *Mecp2*$^{S421A;S424A/y}$ mice and their wild type littermates (**Supplementary Fig. 4d**–**f**). In a test for motor coordination, the *Mecp2*$^{S421A;S424A/y}$ mice fell off the rotating rod slightly quicker than their wild type littermate (**Supplementary Fig. 4g**). However, the difference was not statistically significant (p=0.30).

After the first two screening tests yielded no difference, we observed a strong phenotype in the last test of the screening--the fear conditioning test. In this classic Pavlovian conditioning preparation aimed at studying fear learning and memory (illustrated in **Fig. 3a**), the *Mecp2*$^{S421A;S424A/y}$ mice froze more than their wild type littermates (**Fig. 3c**) in the context test,

while they froze the same as the wild type littermates (**Fig. 3c**) in the cue test. It is widely believed that the context test is dependent of the function of both the hippocampus and the amygdala, while the cue test is only dependent of the function of the amygdala. Thus the combination of results from the context test and the cue test strongly suggests a difference in hippocampus function between the *Mecp2*$^{S421A;S424A/y}$ and the wild type mice. To confirm the context test results, we performed context-only training (no tone played during training, as illustrated in **Fig. 3b**) and testing with a fresh cohort of *Mecp2*$^{S421A;S424A/y}$ mice and their wild type littermates. The *Mecp2*$^{S421A;S424A/y}$ mice again froze more than the wild type (**Fig. 3d**) in the context test. In both training paradigms, no significant difference in baseline freezing (pre-shock during training sessions, and pre-tone in the cue test sessions) was observed between the *Mecp2*$^{S421A;S424A/y}$ mice and their wild type littermates (**Fig. 3c**–**d**). To further confirm the involvement of the hippocampus in an independent assay, we performed the Morris water maze test (as illustrated in **Fig. 4a**), a well-established hippocampus-dependent spatial learning and memory test, on yet another cohort of *Mecp2*$^{S421A;S424A/y}$ mice and their wild type littermates. The hidden platform version of the water maze test was used in this experiment. Both the *Mecp2*$^{S421A;S424A/y}$ mice and their wild type littermates swam at the same speed during training and testing (**Fig. 4b**). Throughout the training period, both genotypes of mice learned the location of the hidden platform equally well, as indicated by the persistent decrease in time needed to find and climb onto the platform (**Fig. 4c**). In the probe trials, while both the *Mecp2*$^{S421A;S424A/y}$ and the wild type mice remembered where the hidden platform was placed during training by spending significantly more time in the target quadrant than the other quadrants (indicating that both genotypes remembered the location of the platform), the *Mecp2*$^{S421A;S424A/y}$ mice spent significantly more time than the wild type littermates in the target quadrant (**Fig. 4d**), which

clearly demonstrated that the *Mecp2*$^{S421A;S424A/y}$ mice had better spatial memory than their wild type littermates. Taken together, these results strongly suggest the *Mecp2*$^{S421A;S424A/y}$ mice have altered hippocampal function.

Enhanced LTP and synaptogenesis in *Mecp2*$^{S421A;S424A/y}$ mice

Since our behavioral analysis identified the hippocampus as one brain region whose function was altered by abolishing activity-induced MeCP2 phosphorylation, we decided to study synaptic physiology in the hippocampus of the *Mecp2*$^{S421A;S424A/y}$ mice. In this series of experiments, we focused our analysis on two well-characterized synapses, the Schaffer collateral-CA1 synapse and the mossy fiber-CA3 synapse. In both cases, we first examined basal synaptic transmission in the *Mecp2*$^{S421A;S424A/y}$ mice and their wild type littermates. By using extracellular field potential recording, we examined the input-output curve and paired-pulse facilitation (PPF, a form of presynaptic short term plasticity). The input-output curves showed no significant difference (**Supplementary Fig. 5**) between the *Mecp2*$^{S421A;S424A/y}$ mice and their wild type littermates. Similarly, no difference was detected in paired-pulse facilitation (administered at six interstimulus intervals of 25, 50, 100, 200, 300, 400 and 500ms) between the *Mecp2*$^{S421A;S424A/y}$ mice and their wild type littermates (**Supplementary Figs. 6** and **7**). In addition, we examined frequency facilitation at the mossy fiber-CA3 synapse, and detected no difference between the *Mecp2*$^{S421A;S424A/y}$ mice and their wild type littermates (**Supplementary Fig. 8**). Taken together, these results suggest abolishing NAIP at S421 and S424 of the MeCP2 protein does not alter basal synaptic transmission or presynaptic short term plasticity at either the

Schaffer collateral-CA1 synapses or the mossy fiber-CA3 synapses in the hippocampus.

We next examined the long term potentiation (LTP) at both the Schaffer collateral-CA1 synapse and the mossy fiber-CA3 synapses in the *Mecp2*$^{S421A;S424A/y}$ mice. In hippocampal slices prepared from both the *Mecp2*$^{S421A;S424A/y}$ mice and their wild type littermates, LTP was readily induced by two trains of 100 Hz stimulation for 1s with an intertetanus interval of 20 s in the Schaffer collateral-CA1 synapse and lasted for 3 hours (**Fig. 5a**,**b**). At the mossy fiber-CA3 synapse, LTP was induced in both genotypes by two trains of 100 Hz stimulation for 1s with an intertetanus interval of 20 s in the presence of 50 μM D-AP5 and lasted for more than 60 minutes (**Fig. 6a**,**b**). Analysis by two-way ANOVA with repeated measures revealed significantly stronger LTP in *Mecp2*$^{S421A;S424A/y}$ mice than in their wild type littermates at both the Schaffer collateral-CA1 synapse (**Fig. 5c**) and the mossy fiber-CA3 synapse (**Fig. 6c**). At the Schaffer collateral-CA1 synapse, the late phase of the LTP was affected, since the average LTP magnitudes during the last 20 minutes of recordings were significantly different between the two genotypes (**Fig. 5d**). These results were consistent with the enhanced hippocampus-dependent learning and memory in these mice revealed by the fear conditioning test and the Morris water maze.

We next examined whether there were any changes at the cellular level that may underlie the altered synaptic physiology and behavioral output of the hippocampus in the *Mecp2*$^{S421A;S424A/y}$ mice. Primary hippocampal and cortical neurons were isolated from postnatal day 0–1 *Mecp2*$^{S421A;S424A/y}$ and wild type littermate pups, and cultured separately for 21 days *in vitro* (DIV). Triple immunostaining of VGLUT1 (excitatory presynaptic marker), PSD95 (postsynaptic marker), and MAP2 (dendritic marker) was performed to examine the development

of excitatory synapses (**Fig. 7a**). Quantification of the densities of VGLUT1 puncta, PSD95 puncta, and co-localized VGLUT1/PSD95 puncta was performed along MAP2 labeled neurites (**Fig. 7b,d**). In the hippocampal culture, our analysis revealed a 45% increase in the number of VGLUT1 puncta (p=0.00003), a 28% increase in the number of PSD95 puncta (p=0.005), and a 152% increase in the number of co-localized VGLUT1/PSD95 puncta (p=0.000002) in *Mecp2*$^{S421A;S424A/y}$ neurons, compared to those in the wild type neurons (**Fig. 7c**). In the cortical culture, similar analysis revealed a 99% increase in the number of VGLUT1 puncta (p=0.00002), a 37% increase in the number of PSD95 puncta (p=0.002), and a 84% increase in the number of co-localized VGLUT1/PSD95 puncta (p=0.045) in *Mecp2*$^{S421A;S424A/y}$ neurons, compared to those in the wild type neurons (**Fig. 7e**). Since co-localized VGLUT1/PSD95 puncta likely represent functional excitatory synapses, our results strongly suggest an increase in excitatory synaptogenesis in both the hippocampal and cortical neurons from the *Mecp2*$^{S421A;S424A/y}$ mice. These results are consistent with the enhanced hippocampal LTP and the enhanced learning and memory phenotypes observed in these mice.

Altered gene expression in *Mecp2*$^{S421A;S424A/y}$ hippocampus

Given the well-established role of MeCP2 in modulating gene transcription (Chahrour et al., 2008; Nan et al., 1997), we suspected potential gene transcription changes may underline the cellular, synaptic, and behavioral phenotypes observed in the *Mecp2*$^{S421A;S424A/y}$ mice. To reveal what gene transcription changes are caused by the loss of NAIP of MeCP2 in these mice, we first examined known MeCP2 target genes with established neuronal functions. *Bdnf* is such a gene

(Chen et al., 2003b; Martinowich et al., 2003). We microdissected the hippocampus from the *Mecp2*$^{S421A;S424A/y}$ mice (n=14) and their wild type littermates (n=14), extracted RNA, performed realtime PCR, and detected an increase in *Bdnf* transcript covering its protein coding region (Bdnf CDS) in the *Mecp2*$^{S421A;S424A/y}$ hippocampus (**Fig. 8a**). In addition, we found an increase in *Bdnf* transcript covering its neuronal specific promoter (Exon IV, Bdnf E4) in the *Mecp2*$^{S421A;S424A/y}$ hippocampus (**Fig. 8a**). The increase in *Bdnf* transcription is consistent with the observed phenotypes of enhanced hippocampal LTP and hippocampus-dependent learning and memory in the *Mecp2*$^{S421A;S424A/y}$ mice.

Recognizing that the phenotypes of the better contextual fear memory, the enhanced hippocampal LTP, the increased excitatory synaptogenesis, and the increase in *Bdnf* transcription in the *Mecp2*$^{S421A;S424A/y}$ mice are similar to those observed in transgenic mice overexpressing *Mecp2* (*Mecp2*^{Tg}) (Chahrour et al., 2008; Chao et al., 2007; Collins et al., 2004), we examined the expression of three additional genes whose levels were changed in the *Mecp2*^{Tg} mice (Chahrour et al., 2008). These included myocyte enhancer factor 2 (*Mef2c*), bone morphogenetic protein 4 (*Bmp4*), and metabotropic glutamate receptor 1 (*Grm1*), all of which are important for the development and function of the nervous system. Moreover, MeCP2 has been shown to directly bind to the promoter of *Mef2c* and repress its transcription (Chahrour et al., 2008). We found increased expression of *Bmp4* and decreased expression of *Mef2c* and *Grm1* (**Fig. 8a**) in the *Mecp2*$^{S421A;S424A/y}$ hippocampus. The expression change of each of the three genes in the *Mecp2*$^{S421A;S424A/y}$ mice was very similar to that in the *Mecp2*^{Tg} mice. However, it is not immediately clear how expression changes in *Bmp4*, *Mef2c* and *Grm1* may help explain the observed phenotypes in the *Mecp2*$^{S421A;S424A/y}$ mice.

Altered promoter association by the phospho-mutant MeCP2

As a first step to understand how the loss of phosphorylation may alter gene transcription, we examined the ability of the phospho-dead form of MeCP2 to bind to gene promoters. To better quantify the promoter occupancy of the phospho-dead MeCP2 protein, we generated two novel *Mecp2* knockin alleles: the *Mecp2*$^{S421A;S424A\text{-}flag/y}$ mice expressing the MeCP2$^{S421A;S424A}$-flag protein from the endogenous *Mecp2* locus and the *Mecp2*$^{WT\text{-}flag/y}$ mice expressing the MeCP2-flag protein from the endogenous *Mecp2* locus. These unique mouse lines allowed us to take advantage of a very reliable anti-flag antibody to conduct chromatin immunoprecipitation (ChIP) experiments. Western blot analysis confirmed that both the MeCP2$^{S421A;S424A}$-flag protein and the MeCP2-flag protein were expressed at the same level as the MeCP2 protein (data not shown). Behavioral testing confirmed that the *Mecp2*$^{S421A;S424A\text{-}flag/y}$ mice had enhanced hippocampus-dependent learning and memory (**Supplementary Fig. 3i**) similar to that observed in the *Mecp2*$^{S421A;S424A/y}$ mice, while the *Mecp2*$^{WT\text{-}flag/y}$ mice performed similar to the *Mecp2*$^{+/y}$ mice (data not shown). These data suggest that the *Mecp2*$^{S421A;S424A\text{-}flag/y}$ mice are functionally indistinguishable from the *Mecp2*$^{S421A;S424A/y}$ mice, and that the *Mecp2*$^{WT\text{-}flag/y}$ mice are functionally indistinguishable the *Mecp2*$^{+/y}$ mice.

Because the transcriptional changes detected in Fig. 8a were from the *in vivo* hippocampus, we reasoned it would be the most appropriate to use hippocampi from the *Mecp2*$^{S421A;S424A\text{-}flag/y}$ and the *Mecp2*$^{WT\text{-}flag/y}$ mice for ChIP analysis to examine promoter occupancy of the phospho-mutant form and the wild type form of MeCP2. Results from this experiment revealed increased

promoter occupancy by the MeCP2$^{S421A;S424A}$-flag protein, as compared with that by the MeCP2-flag protein, on the promoters of *Bdnf*, *Bmp4*, *Mef2c*, and *Grm1* (**Fig. 8b**). Thus, the loss of phosphorylation appears to enhance the binding of MeCP2 to its target gene promoters. Because MeCP2 has been shown to be capable of activating the transcription of some genes and repressing the transcription of other genes at the same time (Chahrour et al., 2008; Yasui et al., 2007), it is possible that the increased promoter occupancy of the phospho-mutant form of MeCP2 may lead to opposite transcriptional outcomes in the phospho-mutant hippocampus. More detailed studies in the future will help reveal the mechanisms of such regulations.

Discussion

NAIP of MeCP2 has been hypothesized to be a potential mechanism for dynamically regulating its binding to methylated DNA and thus its ability to coordinate neuronal gene transcription (Chen et al., 2003b; Tao et al., 2009; Zhou et al., 2006). Yet it is not clear what, if any, function requires such phosphorylation in the *in vivo* brain. We generated the *Mecp2*$^{S421A;S424A}$ knockin mice to abolish NAIP of MeCP2, and provide here the first genetic evidence that NAIP of MeCP2 is involved in regulating several important functions in the *in vivo* brain, including promoter occupancy, gene transcription, excitatory synaptogenesis, LTP, and learning and memory.

The wide range of phenotypes observed in the *Mecp2*$^{S421A;S424A/y}$ mice spans the molecular, cellular, synaptic, and animal behavioral levels. Although it is not easy to establish causal links across all levels, the phenotypes observed in *Mecp2*$^{S421A;S424A/y}$ mice, including the increased *Bdnf* expression, the increased excitatory synaptogenesis, the enhanced hippocampal LTP, and the enhanced hippocampus-dependent learning and memory, are very consistent with each other. Moreover, the *Mecp2*$^{S421A;S424A/y}$ mice and the *Mecp2*^{Tg} mice (Chahrour et al., 2008; Chao et al., 2007; Collins et al., 2004) showed remarkable phenotypic similarities across the levels of promoter occupancy, gene expression, excitatory synaptogenesis, synaptic physiology, and animal behavior (**Supplementary Fig. 10**), raising the possibility that these two mouse models may share some common underlying mechanisms . While these two mouse models appear to converge on the same molecular event--increased promoter occupancy, they achieve it through different means. In the *Mecp2* phospho-mutant mice, the expression level of the phospho-mutant protein is not altered. Yet the loss of NAIP makes it bind more tightly to gene

promoters. In the *Mecp2*^{Tg} mice, the increase in MeCP2 protein level resulted in enhanced binding of MeCP2 at the promoters of its target genes. Together, these studies highlight the need in precisely regulating the ability of MeCP2 to bind to gene promoters.

Previously, Zhou *et al.*(Zhou et al., 2006) showed that, using a lentivirus-based approach to simultaneously knockdown endogenous MeCP2 and express exogenous MeCP2^{S421A} in cultured neurons, loss of phosphorylation at S421 led to reduced *Bdnf* transcription. Several factors may have contributed to the apparent discrepancy between this publication and our current findings. First, we abolished potential phosphorylation at both S421 and S424 by mutating both serines to alanines, while Zhou *et al.* only mutated S421. Second, our results came from the adult hippocampus of living mice, while results in Zhou *et al.* came from cultured neurons that were isolated from embryonic rat brain. Thus, not only our *in vivo* system is different from their *in vitro* system, but also the age and species of the animals used in the two studies are significantly different. Third, it is also possible that the efficiencies of knocking down the endogenous wild type MeCP2 and the viral infection may not have been 100% in Zhou *el al*, which may have resulted in either the presence of both the wild type MeCP2 and the mutant MeCP2^{S421A} in the same neuron or the mixture of wild type and mutant neurons in the same culture. Nonetheless, our finding of the elevated *Bdnf* level *in vivo* is consistent with the enhanced LTP and better spatial memory in the *Mecp2*$^{S421A;S424A/y}$ mice, which, interestingly, were also observed in the *Mecp2*^{Tg} mice.

Several important questions remain unanswered, and await more extensive studies in the future. First, the precise synaptic mechanisms linking MeCP2 phosphorylation with hippocampal LTPs remain elusive. Since it is widely believed that pre-synaptic changes

underlie CA3 LTP and post-synaptic changes underlie CA1 LTP, the loss of MeCP2 phosphorylation appears to cause both pre- and post-synaptic changes. This is possible because activity-induced MeCP2 phosphorylation could happen in both pre- and post-synaptic neurons. Second, although our data of enhanced CA1 LTP in the *Mecp2*$^{S421A;S424A/y}$ mice at late time points (160-180 minutes after LTP induction) are consistent with a change in the transcription-dependent phase of LTP (late or L-LTP), no unequivocal conclusion can be drawn because no transcription inhibitors were included in our experiment. We also note that while CA1 LTP in the *Mecp2*$^{S421A;S424A/y}$ mice appears to be enhanced at early time points after LTP induction, it is not clear how MeCP2 phosphorylation may be involved in transcription-independent regulation of synaptic plasticity. Finally, because we focused our attention on revealing the functional relevance of activity-induced MeCP2 phosphorylation *in vivo*, the gene transcription and promoter occupancy analysis included here was limited to a few candidate genes. However, given that MeCP2 is capable of binding to a single methylated CpG pair[4] and is widely distributed across the genome (Skene et al., 2010), it is highly likely that altered MeCP2$^{S421A;S424A}$ occupancy may happen at other genomic loci, and that additional gene expression changes may exist and also underlie the cellular, synaptic, and behavioral phenotypes observed in the *Mecp2*$^{S421A;S424A/y}$ mice. To fully understand the molecular mechanisms underlying these phenotypes, it is important to study in the future, where the MeCP2$^{S421A;S424A}$ protein binds the DNA across the genome, whether and how the loss of phosphorylation may affect its association with other chromatin remodeling complexes, and ultimately how neuronal gene transcription is altered by the loss of phosphorylation

Figures

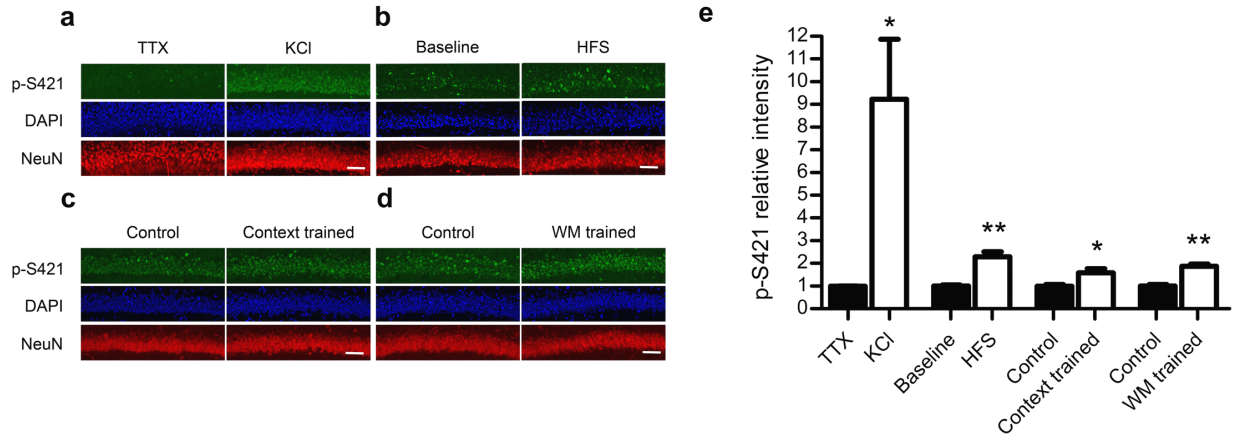

Figure 1 Phosphorylation at serine 421 induced by depolarization, high frequency stimulation and behavioral trainings. **(a–d)** Representative confocal microscope images of co-staining of DAPI (labeling all cell nuclei), NeuN (labeling all neuronal nuclei), and p-S421 in the CA1 region of hippocampal slices treated with 1 μM TTX or 50 mM KCl for one hour (a), receiving baseline stimulation or high frequency stimulation (HFS, 100 Hz, 1 s, twice with 20 s interval) (b), from mice that received shock immediately after being put into the box (immediate shock control) and mice that received shock two minutes after being put into the box (context trained) (c), or from mice that received the hidden platform version of Morris water maze (WM) training (WM trained) and mice that swam the same amount of time in the same tank with no platform (yoked/swimming control) (d). Scale bars=20 μm. **(e)** Quantification of relative p-S421 intensity in the depolarization experiment (n=4 for each group), high frequency stimulation experiment (n=4 for each group), the contextual fear training experiment (n=5 for each group), and the Morris water maze training experiment (n=3 for each group). Data are presented as mean ±s.e.m. *$P < 0.05$. **$P < 0.01$

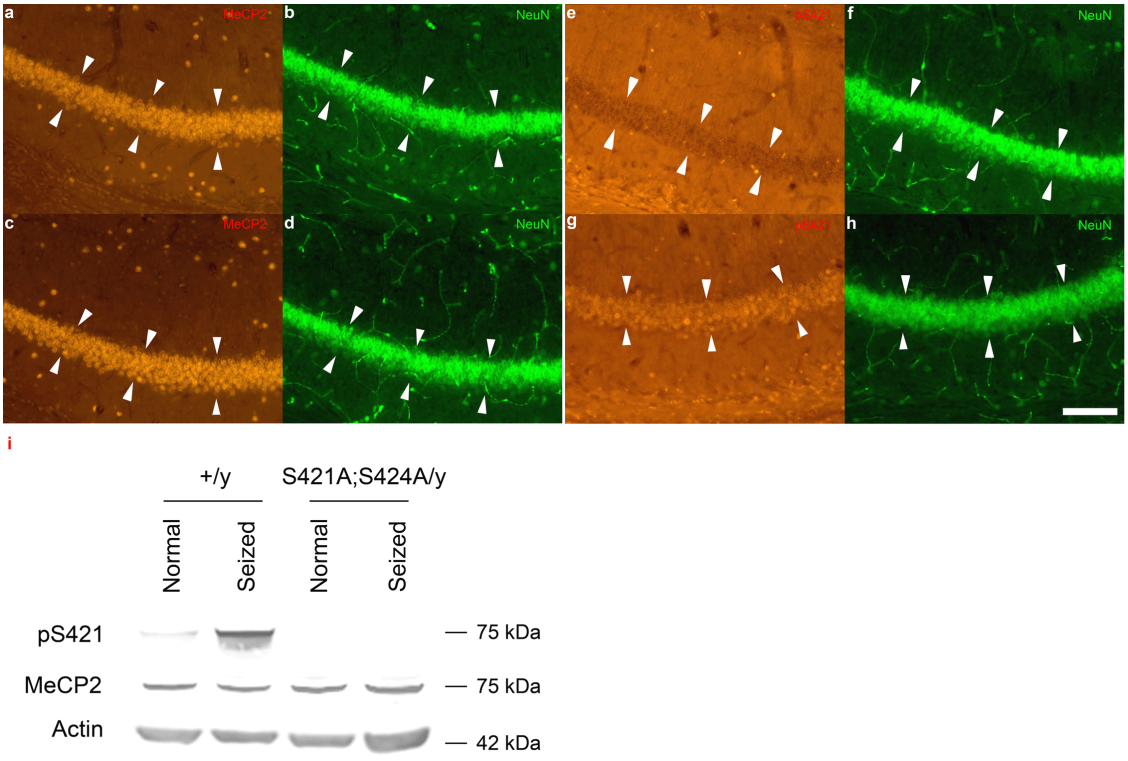

Figure 2 Loss of NAIP at serine 421 (S421) in the *Mecp2*$^{S421A;S424A/y}$ mice. Representative images of the CA1 region of the hippocampus from the *Mecp2*$^{S421A;S424A/y}$ mice **(a, b, e, f)** and their wild type littermates **(c, d, g, h)** co-stained with MeCP2 (a, c) and NeuN (b, d) or p-S421 (e, g) and NeuN (f, h). a and b, c and d, e and f, g and h are the red and green channels of the same images. Arrowheads in a–h mark the pyramidal cell layer in the CA1. Scale bar=100 μm. Scale bar in h applies to a–h. **(i)** Western blot analysis was performed to compare the expression levels of p-S421 (top panel), MeCP2 (middle panel), and beta-actin (bottom panel) in the brains of the wild type (left two lanes) and *Mecp2*$^{S421A;S424A/y}$ mice (right two lanes) under normal condition and after seizure. Shown here are partial blots covering the region around the expected molecular weights of the proteins of interest. Full length blots are shown in Supplementary Figure 3.

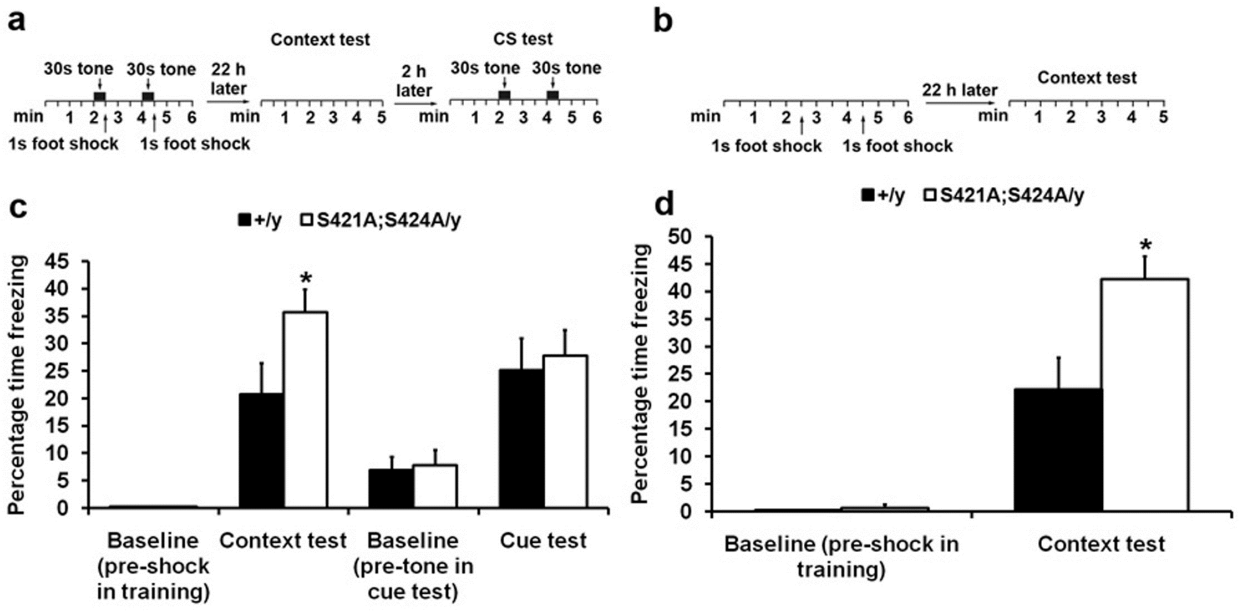

Figure 3 Enhanced contextual fear memory in the *Mecp2*$^{S421A;S424A/y}$ mice. **(a)** Schematic drawing of the design of training paradigm I (tone paired with shock) and the ensuing context test and cue test. **(b)** Schematic drawing of the design of training paradigm II (shock only) and the ensuing context test. **(c)** The contextual memory and the cue memory were measured by the percentage of time the mice spent freezing 22 and 24 hours, respectively, after training. Because none of the wild type and mutant mice froze pre-shock in training sessions in training paradigm I, those bars are 0s. n=10 in each genotype. Bar graph shows mean ±s.e.m. **(d)** The contextual memory was measure by the percentage of time the mice spent freezing 22 hours after training. Because none of the wild type mice froze pre-shock in training sessions in training paradigm II, that bar is 0. n=5 in each genotype. Bar graph shows mean± s.e.m. *P < 0.05.

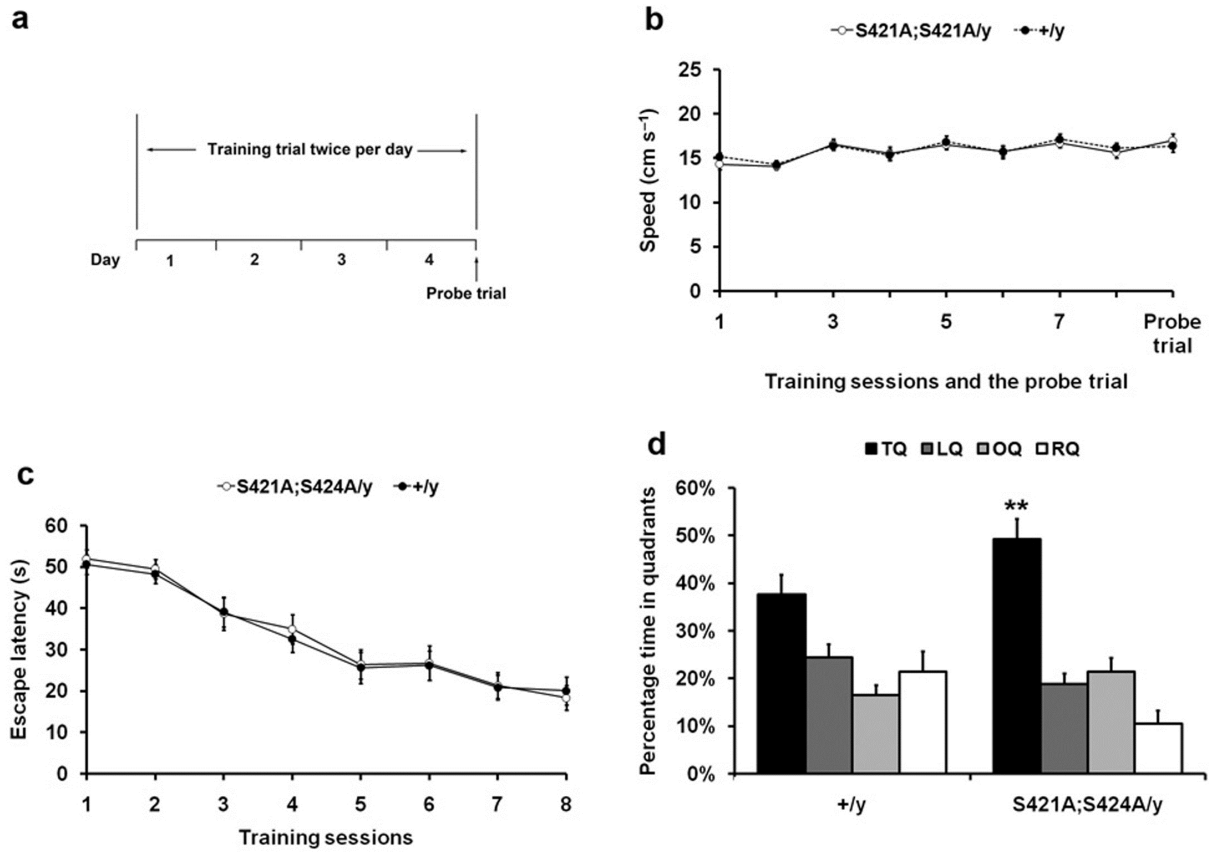

Figure 4 Enhanced spatial memory in the *Mecp2*$^{S421A;S424A/y}$ mice. **(a)** Schematic drawing of the Morris water maze test design. **(b)** Swimming speeds of the wild type and the *Mecp2*$^{S421A;S424A/y}$ mice measured during the training sessions and probe trials. **(c)** Escape latency (time to find the hidden platform) plotted against the 8 training sessions over 4 days. **(d)** Percentage of time spent in the target quadrant (TQ), the quadrant left to the TQ (LQ), the quadrant opposite to the TQ (OQ), and the quadrant right to the TQ (RQ) during the probe trial. n=20 in each genotype. Bar graph shows mean ±s.e.m. Statistical analysis was performed as the following. First, a two way repeated measures ANOVA (One Factor Repetition) was performed, which revealed a statistically significant interaction between genotype and quadrant

($F(3,114)=3.77$, $p=0.013$). Subsequently, a Tukey-HSD *post hoc* test was performed on that interaction to complete the pairwise comparison of the percentage of time spent by each genotype in each quadrant, which revealed that both the wild type and the *Mecp2*$^{S421A;S424A/y}$ mice spent significantly more time in the target quadrant (in which a hidden platform was placed during the training sessions) than the other quadrants during the probe trial; and that most importantly, the *Mecp2*$^{S421A;S424A/y}$ mice spent significantly more time in the target quadrant than their wild type littermates did (49% vs. 37%, $p = 0.012$). **$P < 0.01$.

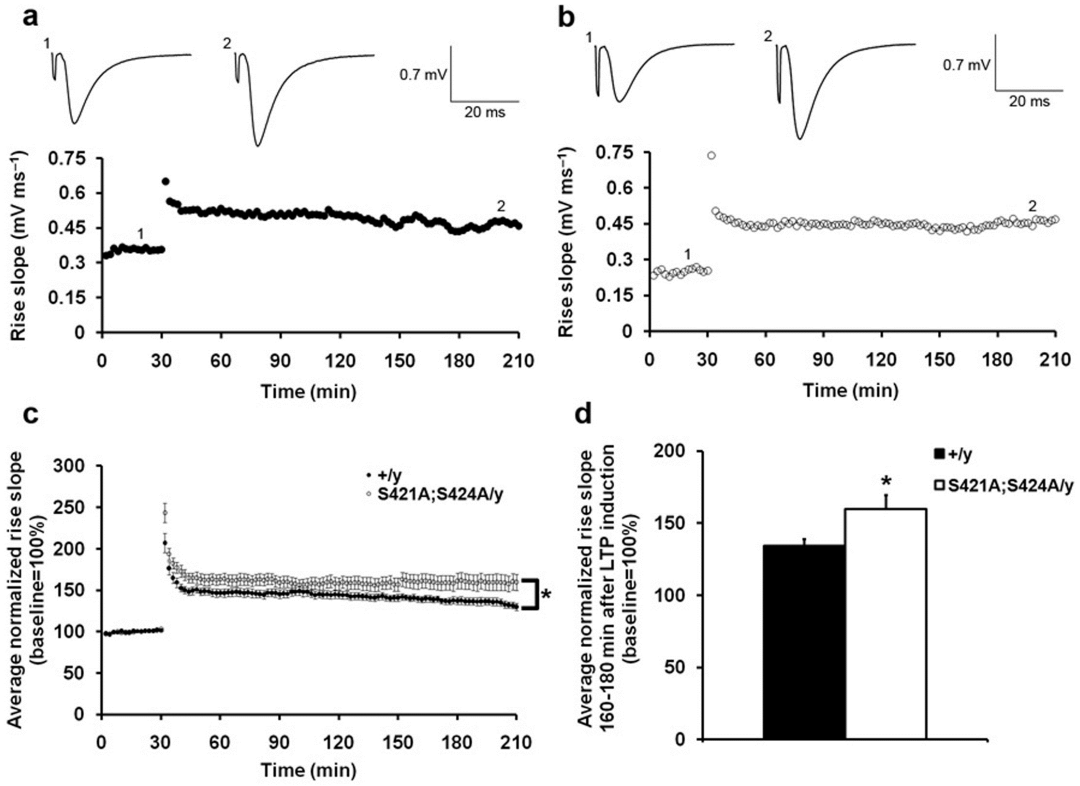

Figure 5 Enhanced Schaffer collateral-CA1 LTP in the *Mecp2*$^{S421A;S424A/y}$ mice. **(a,b)** Representative recording of field EPSP (fEPSP) rise slope in wild type (a) and the *Mecp2*$^{S421A;S424A/y}$ (b) slices. Sample traces in each genotype represent before (1) and 160 minutes after (2) the tetanic stimulation (100 Hz, 1 s, twice with 20 s interval). **(c)** Average normalized (against baseline) fEPSP rise slope in the wild type (closed circle) and the *Mecp2*$^{S421A;S424A/y}$ (open circle) slices. Error bars represent s.e.m. Statistical analysis was done using two-way ANOVA with repeated measure. $F(1,30)=4.67$, $p=0.04$. **(d)** Average normalized (against baseline) fEPSP rise slope 160-180 minutes after the LTP induction in the wild type and the *Mecp2*$^{S421A;S424A/y}$ slices. Bar graph shows mean ± s.e.m. 16 slices from 14 *Mecp2*$^{S421A;S424A/y}$ mice and 16 slices from 15 wild type littermates were included in (c) and (d). *$P < 0.05$.

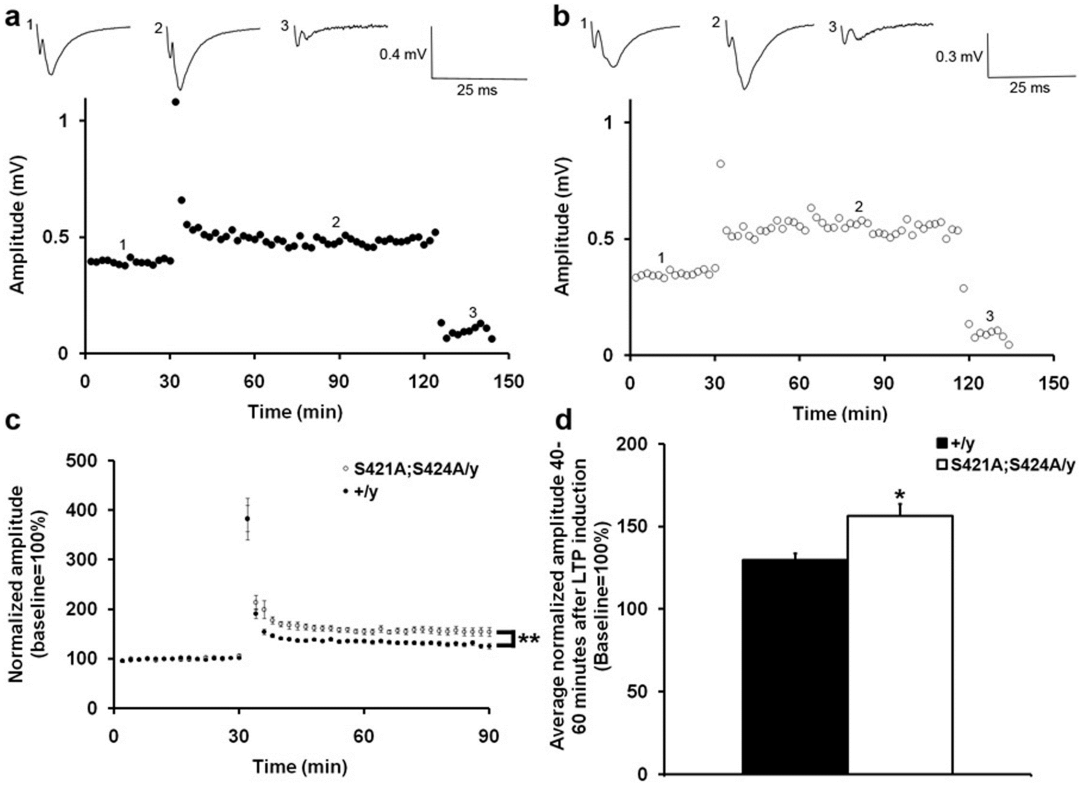

Figure 6 Enhanced mossy fiber-CA3 LTP in the *Mecp2*$^{S421A;S424A/y}$ mice. **(a,b)** Representative recording of field EPSP (fEPSP) amplitudes in wild type (a) and the *Mecp2*$^{S421A;S424A/y}$ (b) slices. Sample traces in each genotype represent before (1) and 40 minutes after (2) the tetanic stimulation (100 Hz, 1 s, twice with 20 s interval), and after the application of DCG-IV (3). **(c)** Average normalized (against baseline) amplitudes in the wild type (closed circle) and the *Mecp2*$^{S421A;S424A/y}$ (open circle) slices. Error bars represent s.e.m. Statistical analysis was done using two-way ANOVA with repeated measure. $F(1,32)= 11.203$, $p=0.002$. **(d)** Average normalized (against baseline) amplitudes 40-60 minutes after the LTP induction in the wild type and the *Mecp2*$^{S421A;S424A/y}$ slices. Bar graph shows mean±s.e.m. 18 slices from 12 *Mecp2*$^{S421A;S424A/y}$ mice and 16 slices from 11 wild type littermates were included in (c) and (d). *P <0.05. **P <0.01.

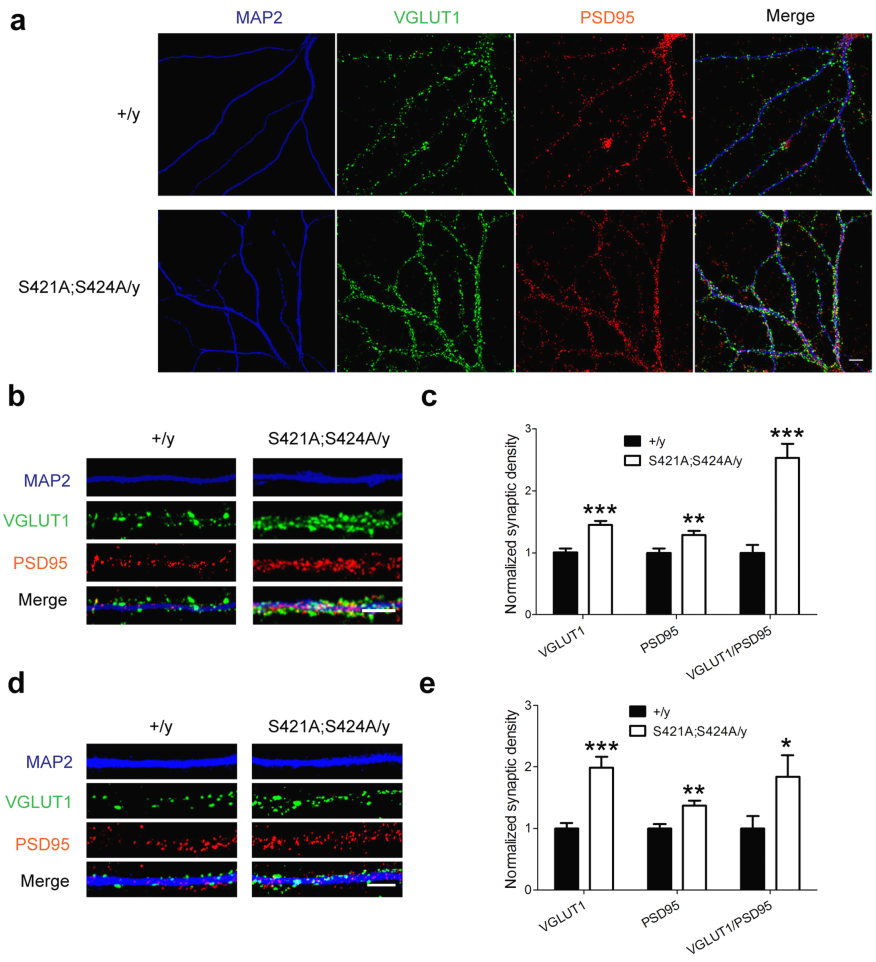

Figure 7 Increased excitatory synaptogenesis in the *Mecp2*$^{S421A;S424A/y}$ mice. **(a)** Representative confocal microscope images of cultured hippocampal neurons (21 DIV) from either the *Mecp2*$^{S421A;S424A/y}$ mice or their wild type littermates co-stained with anti-VGLUT1, anti-PSD95, and anti-MAP2 antibodies. Scale bars=10 μm. Representative images of neurites from both genotypes that were analyzed in the hippocampal culture **(b)** and the cortical culture **(d).** Quantification of the densities (number of puncta per μm) of VGLUT1 puncta, PSD95 puncta, and co-localized VGLT1/PSD95 puncta in the hippocampal culture **(c)** and the cortical culture **(e)**. Numbers from the *Mecp2*$^{S421A;S424A/y}$ neurons were normalized against those from the wild type neurons. *P<0.05. **P<0.01. ***P < 0.001.

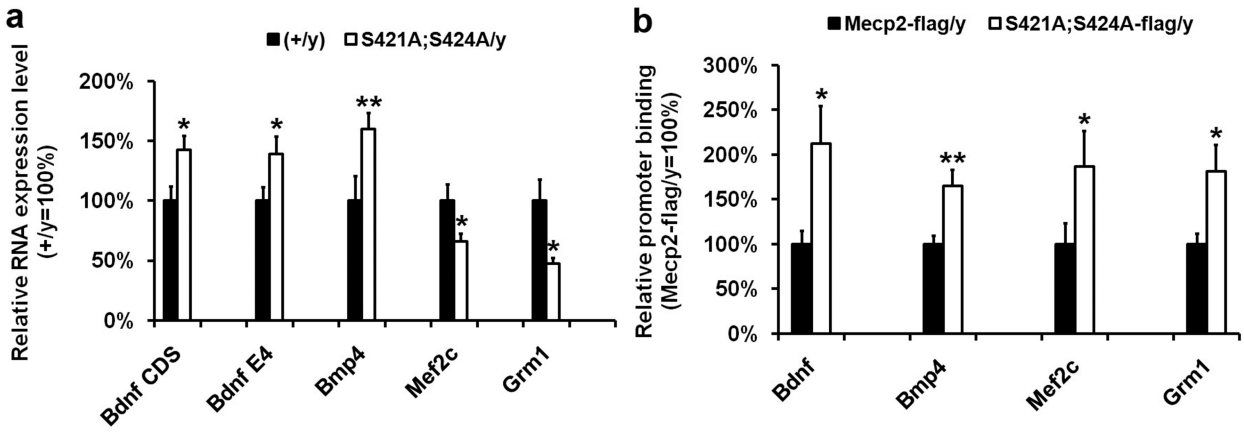

Figure 8 Altered expression of MeCP2 target genes in the hippocampus of the *Mecp2*$^{S421A;S424A/y}$ mice and increased promoter binding by the MeCP2$^{S421A;S424A}$-flag protein. **(a)** Relative expression levels of *Bdnf* CDS, *Bdnf* E4, *Bmp4*, *Mef2c*, and *Grm1* in the adult hippocampus of the wild type (closed bar) and the *Mecp2*$^{S421A;S424A/y}$ mice (open bar). n=14 in each genotype for *Bdnf* CDS, *Bdnf* E4. n=8 in each genotype for *Bmp4*, *Mef2c*, and *Grm1*. p=0.02 for *Bdnf* CDS. p=0.04 for *Bdnf* E4. p=0.01 for *Bmp4*. p=0.05 for *Mef2c*. p=0.02 for *Grm1*. **(b)** Relative binding of the MeCP2-flag and MeCP2$^{S421A;S424A}$-flag protein to the promoters of *Bdnf* (exon IV), *Bmp4*, *Mef2c*, and *Grm1* in the adult hippocampus of the *Mecp2*$^{WT\text{-}flag/y}$ mice (closed bar) and the *Mecp2*$^{S421A;S424A\text{-}flag/y}$ mice (open bar), respectively. n=6 in each genotype. p=0.03 for *Bdnf*. p=0.01 for *Bmp4*. p=0.05 for *Mef2c*. p=0.04 for *Grm1*. *P <0.05. **P< 0.01.

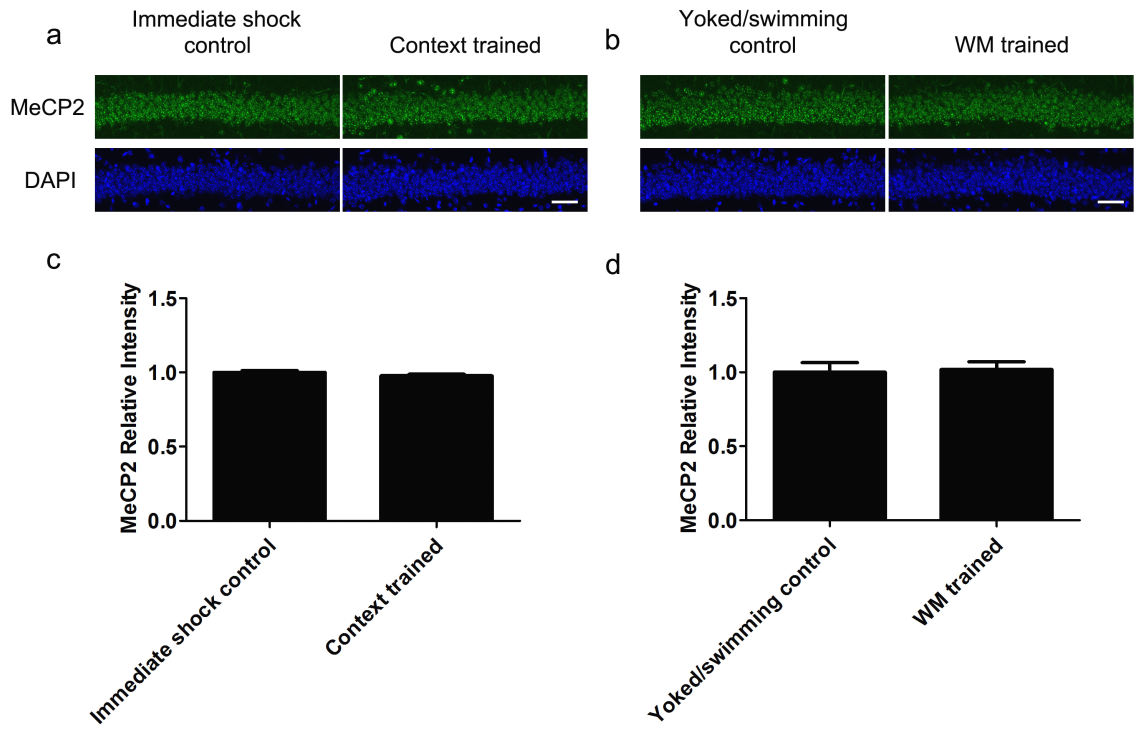

Supplementary Figure 1 Total MeCP2 level is unchanged after behavioral training. **(a-b)** Representative confocal microscope images of the CA1 region of hippocampal sections from mice that received shock immediately after being put into the box (immediate shock control) and mice that received shock two minutes after being put into the box (context trained) (a), or from mice that received the hidden platform version of Morris water maze (WM) training (WM trained) and mice that swam the same amount of time in the same tank with no platform (yoked/swimming control) (b) stained with total MeCP2 antibody and DAPI. Scale bars=20μm. **(c-d)** Quantification of MeCP2 immunoreactivity in hippocampus sections of mice in the contextual fear training experiment (c), and the Morris water maze training experiment (d).

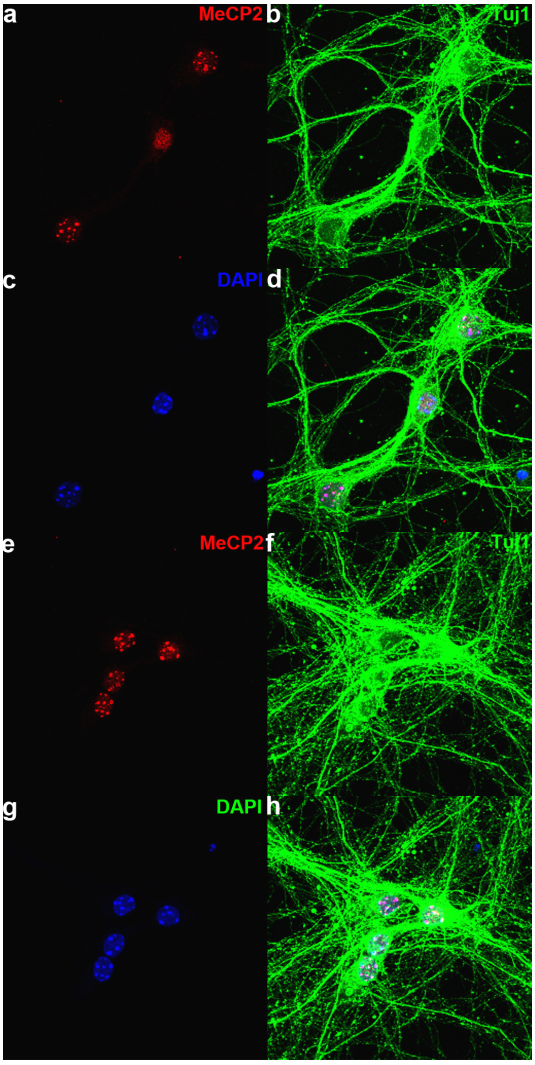

Supplementary Figure 2 Subcellular localization of MeCP2$^{S421A;S424A}$ protein in cortical neurons. Representative confocal microscopy images of primary culture of cortical neurons isolated from the wild type **(a-d)** and the *Mecp2*$^{S421A;S424A/y}$ **(e-h)** mice. (a, e) MeCP2 immunoreactivity. (b, f) Tuj1 (beta III tubulin) immunoreactivity. (c, g) DAPI staining. (d, h) Overlay of all three channels to demonstrate co-localization of MeCP2 immunoactivity with DAPI strong spots in neuronal nuclei (cell bodies and neuritis are positive for beta III tubulin). Note the magenta color caused by co-localized red and blue colors. Scale bar=25μm. Scale bar in h applies to a-h.

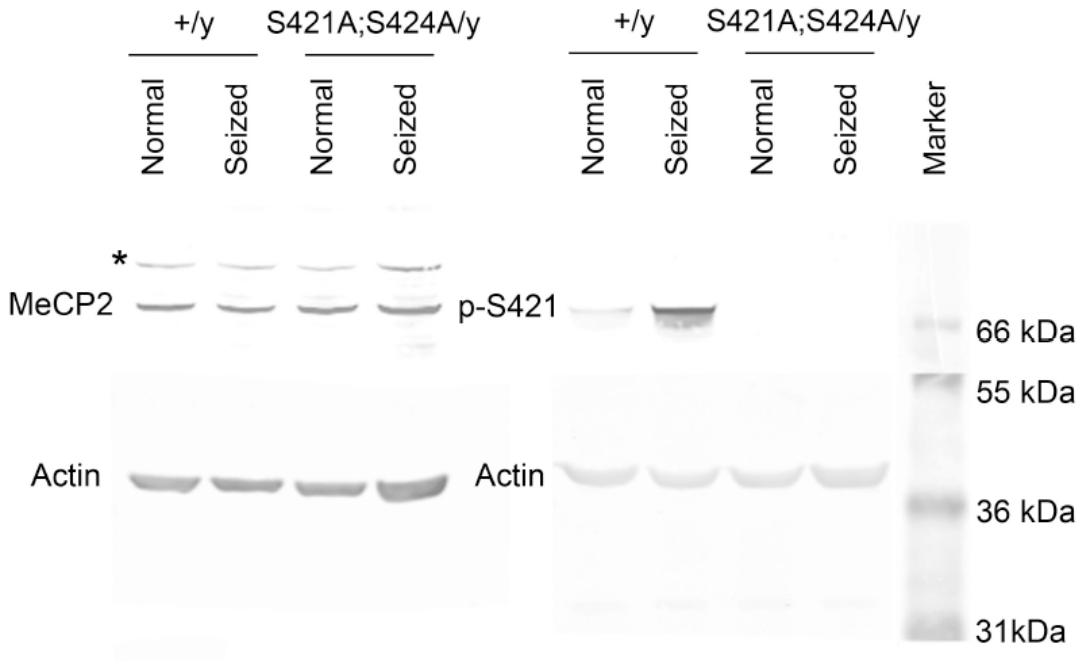

Supplementary Figure 3. Full length Western blots of those shown in Figure 2iare shown in Supplementary Figure 3. Note that for both the blot on the left and the blot on the right, the membrane was cut at 55 kDa so that the bottom half of the membrane was blotted with the anti-β actin antibody and the top half the membrane was blotted with either the anti-MeCP2 antibody or anti-pS421 antibody. * indicates a non-specific band detected by the anti-MeCP2 antibody.

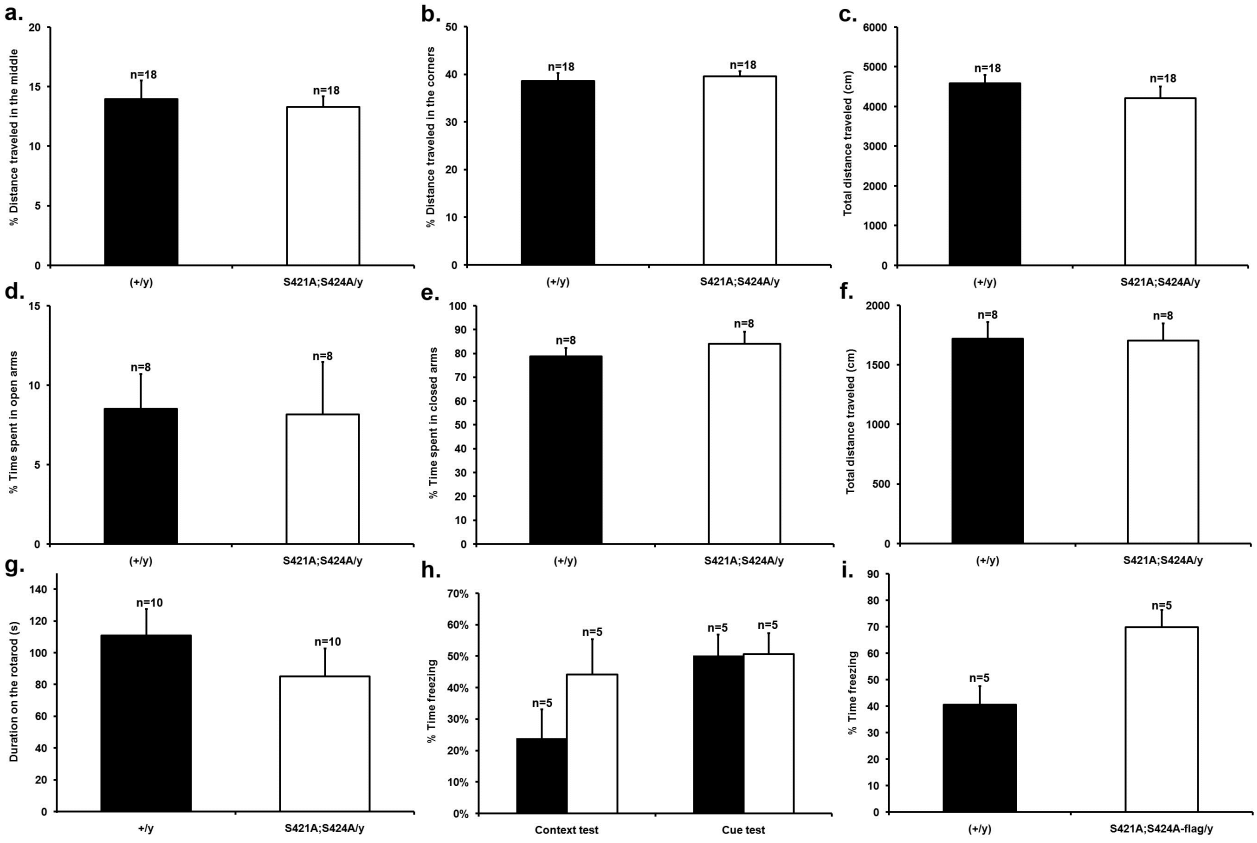

Supplementary Figure 4 Additional behavioral tests on the *Mecp2*$^{S421A;S424A/y}$ mice and the *Mecp2*$^{S421A;S424A\text{-}flag/y}$ mice. The *Mecp2*$^{S421A;S424A/y}$ mice showed the same level of anxiety as their wild type littermates in the open field arena test **(a-c)**, as measured by the percentages of distance traveled in the middle of the field (a) and the corners of the field (b). The total distance traveled was the same between the two genotypes (c). 18 mice from each genotype were tested. p=0.7 in (a). p=0.6 in (b). p=0.3 in (c). The *Mecp2*$^{S421A;S424A/y}$ mice showed the same level of anxiety as their wild type littermates in the elevated plus maze test **(d-f)**, as measured by the percentages of time spent in the open arms (d) and closed arms (e). The total distance traveled was the same between the two genotypes (f). 8 mice from each genotype were tested. p=0.9 in (e). p=0.4 in (e). p=0.9 in (f). The *Mecp2*$^{S421A;S424A/y}$ mice performed as well as their wild

type littermates in the rotarod test, as measured by the amount of time they were able to hang onto the rotating rod **(g)**. n=10 in each genotype. p=0.3 (g). When the shock intensity was doubled in the fear conditioning training (training paradigm I as illustrated in Figure 3a), no difference was observed between the *Mecp2*$^{S421A;S424A/y}$ mice and their wild type littermates in the amount of time spent freezing in the cue test **(h).** However, the percentage of time spent freezing doubled in both the *Mecp2*$^{S421A;S424A/y}$ mice and their wild type littermates during the cue test (~50% h with ~25% in Figure 3c). In contrast, the difference between the genotypes and the amount of time spent freezing in the context test remained similar to when a lower shock intensity was used in the training session (44% in *Mecp2*$^{S421A;S424A/y}$ v.s. 24% in wild type in h, as compared with 36% in *Mecp2*$^{S421A;S424A/y}$ v.s. 21% in wild type in Figure 3c). The *Mecp2*$^{S421A;S424A\text{-}flag/y}$ mice froze significantly more than their wild type littermates (70%±7% v.s. 41%±7%, p=0.02) in the context test (training paradigm II as illustrated in Figure 3b) **(i)**. Note that both genotypes showed higher freezing than those in Figure 3d. This is most likely due to the fact that the *Mecp2*$^{S421A;S424A\text{-}flag/y}$ mice and their wild type littermates were still in a mixed genetic background.

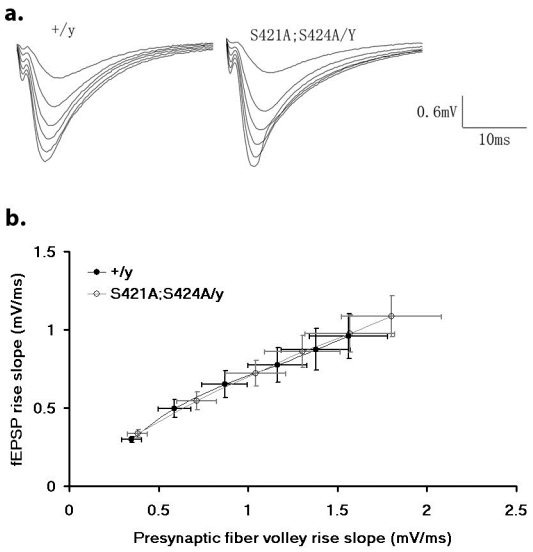

Supplementary Figure 5 Unchanged input-output properties at the Schaffer collateral-CA1 synapse in the *Mecp2*$^{S421A;S424A/y}$ mice. The first stimulation intensity was adjusted to evoke 30% of the maximum postsynaptic response. Each of the subsequent stimulation intensities was higher than the previous step by 0.5 mV. (a) Sample traces and averages of all recordings (b) from the wild type and *Mecp2*$^{S421A;S424A/y}$ slices showing fEPSP steps in response to increasing intensities of the presynaptic fiber volleys. Sample traces shown are averages of 6 sweeps of recordings. 16 slices from 13 wild type mice and 16 slices from 15 *Mecp2*$^{S421A;S424A/y}$ mice were included in the analysis. Two-way ANOVA with repeated measures was performed for statistical analysis. No significant genotype effect was found for either the presynaptic fiber volley ($p=0.55$) or the fEPSP ($p=0.51$).

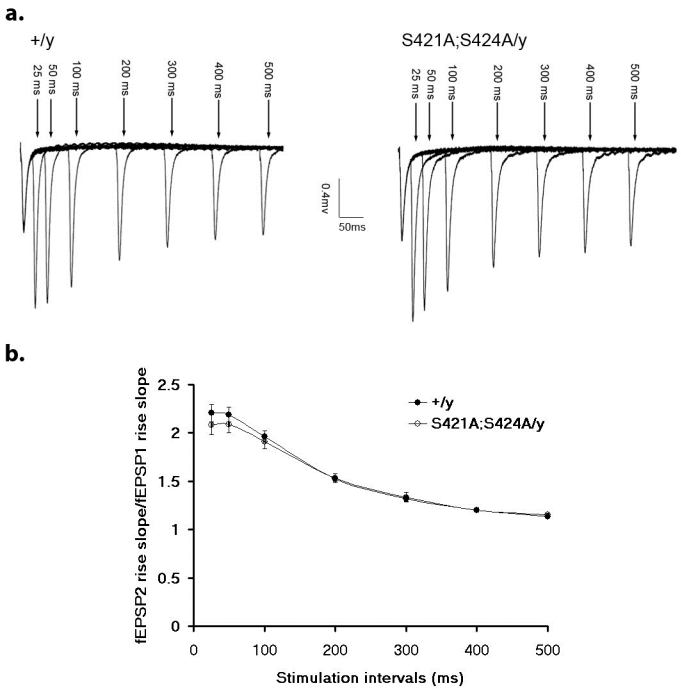

Supplementary Figure 6 Unchanged paired-pulse facilitation at the Schaffer collateral-CA1synapse in the *Mecp2*$^{S421A;S424A/y}$ mice. (a) Sample traces from the wild type and *Mecp2*$^{S421A;S424A/y}$ slices showing identical levels of potentiation of the second fEPSP at different stimulation intervals for the paired presynaptic stimulation. (b) Average fEPSP rise slope 2/fEPSP rise slope 1 ratios at different stimulation intervals in the wild type and *Mecp2*$^{S421A;S424A/y}$ slices. Sample traces shown are averages of 6 sweeps of recordings. 24 slices from 20 wild type mice and 22 slices from 18 *Mecp2*$^{S421A;S424A/y}$ mice were included in the analysis. Two-way ANOVA with repeated measures was performed for statistical analysis. For genotype effect across all stimulation intervals, $F(1,264)=0.29$, $p=0.60$. For interaction between stimulation interval and genotype, $F(6,264)=1.11$, $p=0.36$. Subsequent *post hoc* tests for the genotype effect at each stimulation interval also revealed no significant difference ($p=0.38$ at 25ms, $p=0.39$ at 50ms, $p=0.52$ at 100ms, $p=0.89$ at 200ms, $p=0.80$ at 300ms, $p=0.99$ at 400ms, $p=0.39$ at 500ms).

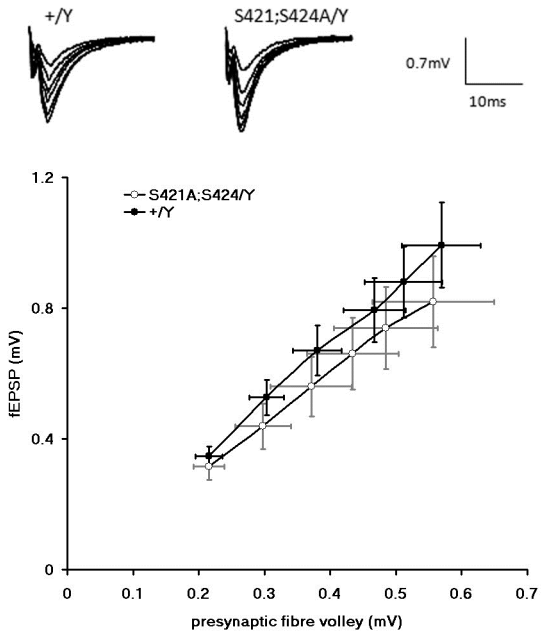

Supplementary Figure 7 Unchanged input-output properties at the mossy fiber-CA3 synapse in the *Mecp2*$^{S421A;S424A/y}$ mice. The first stimulation intensity was adjusted to evoke 30% of the maximum postsynaptic response. Each of the subsequent stimulation intensities was higher than the previous step by 0.5 mV. Sample traces (top) and averages of all recordings (bottom) from the wild type and *Mecp2*$^{S421A;S424A/y}$ slices showing fEPSP steps in response to increasing intensities of the presynaptic fiber volleys. Sample traces shown are averages of 6 sweeps of recordings. 8 slices from 6 wild type mice and 7 slices from 6 *Mecp2*$^{S421A;S424A/y}$ mice were included in the analysis. Two-way ANOVA with repeated measures was performed for statistical analysis. No significant genotype effect was found for either the presynaptic fiber volley ($p=0.84$) or the fEPSP ($p=0.38$).

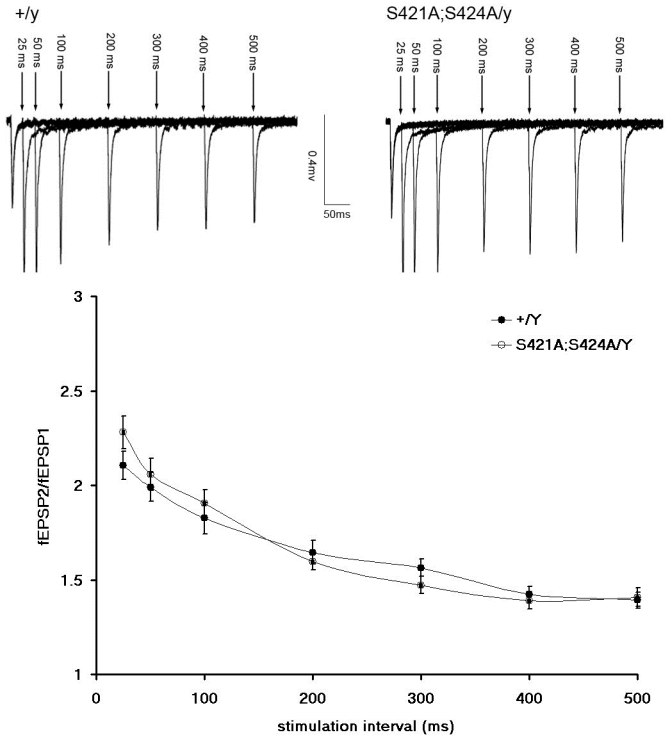

Supplementary Figure 8 Unchanged paired-pulse facilitation at the mossy fiber-CA3 synapse in the *Mecp2*$^{S421A;S424A/y}$ mice. Top: sample traces from the wild type and *Mecp2*$^{S421A;S424A/y}$ slices showing identical levels of potentiation of the second fEPSP at different stimulation intervals for the paired presynaptic stimulation. Bottom: average fEPSP2/fEPSP1 ratios at different stimulation intervals in the wild type and *Mecp2*$^{S421A;S424A/y}$ slices. Sample traces shown are averages of 6 sweeps of recordings. 10 slices from 6 mice in both genotypes were included in the analysis. Two-way ANOVA with repeated measures was performed for statistical analysis. For genotype effect across all stimulation intervals, $F(1,18)=0.097$, $p=0.76$. For interaction between stimulation interval and genotype, $F(6,108)=3.045$, $p=0.009$. However, subsequent *post hoc* tests for the genotype effect at each stimulation interval revealed no significant difference ($p=0.06$ at 25ms, $p=0.46$ at 50ms, $p=0.38$ at 100ms, $p=0.58$ at 200ms, $p=0.32$ at 300ms, $p=0.70$ at 400ms, $p=0.86$ at 500ms).

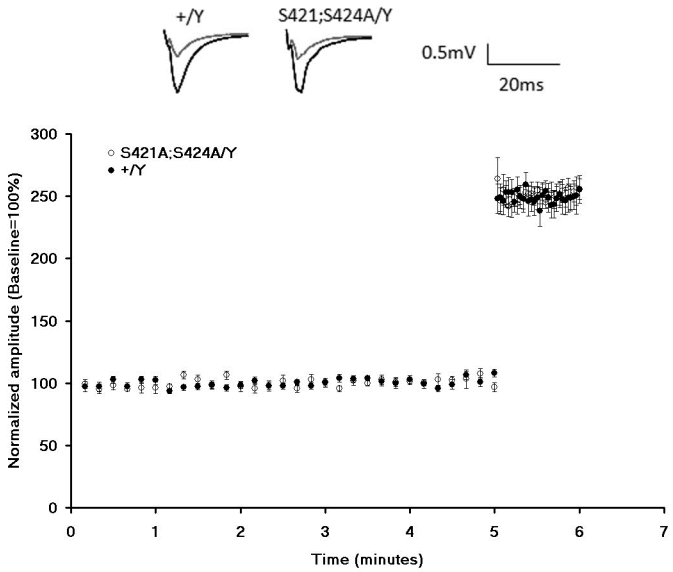

Supplementary Figure 9 Unchanged frequency facilitation at the mossy fiber-CA3 synapse in the *Mecp2*$^{S421A;S424A/y}$ mice. Top: sample traces from the wild type and *Mecp2*$^{S421A;S424A/y}$ slices showing identical levels of frequency facilitation achieved by increasing the stimulation rate from 0.1Hz to 0.5Hz. Bottom: Average responses to different stimulation rates were plotted over time. Stimulation rate was maintained at baseline (0.1Hz) for 5 minutes, before changing to 0.5Hz. 10 slices from 6 mice in both genotypes were included in the analysis. p=0.887.

	Mecp2 deficiency	*Mecp2*^{Tg}	*Mecp2*$^{S421A;S424A}$
MeCP2 aberration	loss of function	overexpression	Ser to Ala
life span	8-10 weeks	30% 1 year, 70% normal	normal
hindlimb clasping	Yes	Yes	No
learning and memory	impaired	enhanced	enhanced
LTP	reduced	enhanced	enhanced
synaptogenesis	reduced	increased	increased
Bndf expression	reduced	increased	increased

Supplementary Figure 10: Phenotype comparison of *Mecp2*$^{S421A;S424A/y}$ mice with *Mecp2* deficient mice and *Mecp2*^{TG} mice.

Materials and Methods:

Mouse genotyping

Two PCR genotyping assays were developed. Primers for the first assay were 5'-TCACAAGTTAACAGTGCCAGCTGC-3' (forward) and 5'-ACCCCCTTGGGACTGAAGTTACAGA-3' (reverse). A ~100 bp band in this assay represents the wild type *Mecp2* allele. A ~200 bp band in this assay represents the *Mecp2*$^{S421A;S424A}$ allele. Primers for the second assay were 5'-CGAGGAGGCGCACTGGAAGCA-3' (forward) and 5'-ACCTGACTGTGCTTGTCGGTAAG (reverse). A 413 bp band in this assay represents the *Mecp2*$^{S421A;S424A}$ allele.

Immunostaining and Western blot analyses of S421 phosphorylation

Anti-MeCP2 (Abcam), anti-phospho-S421 (custom made by Covance), anti-S100b (SWANT), anti-NeuN (Santa Cruz), and anti-actin (Sigma) were used. For immunostaining, 10-12 weeks old mice were transcardially perfused with normal saline solution followed by 4% paraformaldehyde (PFA). Brains were dissected, post-fixed in 4% PFA, cryoprotected in 30% sucrose, embedded and frozen in Tissue Tek. Serial coronal sections were cut at 40 μm throughout the brain, and stained with appropriate primary and secondary antibodies. For Western blot, brains were quickly dissected out from 10-12 weeks old mice and homogenized in RIPA buffer containing both the protease inhibitor cocktail (Roche) and the protein phosphatase inhibitor cocktail (Roche). Lysate was run on 10% NuPAGE Bis-Tris gel (Invitrogen), and transferred to Protran BA 85 nitrocellulose membranes (Whatman). The membrane was

incubated with appropriate primary and IR dye-conjugated secondary antibodies (Thermo Scientific), and scanned by the Odyssey infrared imaging system.

Mouse behavioral tests

10-12 weeks old mice were used in all tests. All protocols were approved by the Institutional Animal Care and Use Committee at University of Wisconsin-Madison.

Open field arena: Each mouse was placed in the center of a transparent plastic chamber (41 x 41 x 30 cm) and allowed to explore freely for 15 min, while an overhead computer-controlled camera monitored its activity. Automated data analysis was done using LimeLight2 (Coulbourn Instruments, Whitehall, PA, USA).

Elevated Plus-Maze: Each mouse was placed in the center of the maze, consisting four perpendicular arms (Two enclosed by 20 cm walls; the other two open) elevated 40 cm above ground, and allowed explore freely for 10 min, while an overhead computer-controlled camera monitored its behavior. The percentage of time each mouse spent in the open arms and the closed arms was measured using the LimeLight2 software.

Rotarod test: Mice were placed onto a horizontal rotating rod, with the rotation speed accelerating from 2 rpm to 20 rpm over 5 min. A test lasted from the time the mouse was placed on the rod until it fell off or until 5 min had elapsed.

Fear conditioning test: In training paradigm I, mice were placed into a shock chamber and allowed to explore for 2 min. Then, a white noise tone (87 dB) sounded for 30 sec (conditional stimulus or “CS”). During the last 1.5 sec of the tone, mice received a mild footshock (0.5 mA)

(unconditioned stimulus or “US”). 2 min later, the same tone-footshock (CS-US) combination was delivered again. 1 min after the end of the second CS-US, mice were returned to their home cages. The context test was performed 22 hr after the training. During the test, mice were placed back into the same training chamber, and monitored by an overhead camera in the chamber for 5 min. 2 hr after the context test, the cue test was performed, in which colored plexiglass inserts were placed into the training chamber to hide the shock grid and to change the "context" of the chamber. Mice were then placed in the chamber and monitored by the overhead camera for 6 min, during which two CS (spaced the same way as in the training session) were given. In training paradigm II, everything stayed the same except that no tones (CS) were given. Only the context test was administered on the mice trained in training paradigm II. All events in the fear conditioning test were programmed and data recorded through the FreezeFrame2 and FreezeView software from (Actimetrics Software, Wilmette, IL, USA).

Morris water maze: Mice were trained to locate a hidden platform (1 cm below the surface of the water) in a circular pool (1.20 m in diameter) of opaque water using distal visual cues. Mice were given 2 blocks of 4 training trials a day for 4 consecutive days. During a training trial, each mouse was released into the pool from 1 of 4 starting positions in a random order. The location of the hidden platform remained constant throughout training. Time to find the platform was measured in each trial. If a mouse did not find the platform within 60 sec, it was gently guided by hand onto the platform and allowed to remain there for 10 sec. After 4 days, the probe test was performed with no platform. Each mouse was allowed to search the platform for 60 sec, while an overhead camera recorded its movement. Time spent searching in each quadrant by a mouse was used to characterize its search behavior.

Electrophysiology

8-12 weeks old mice were anesthetized and killed by decapitation. 400 μm transverse hippocampal slices were prepared using a Vibratome Tissue Chopper. Slices were recovered in oxygenated ACSF at room temperature for at least 1 hr. The ACSF contained (in mM): 124 NaCl, 2.5 KCl, 1.25 NaH_2PO_4, 26 $NaHCO_3$, 1.2 $MgCl_2$, 2.5 $CaCl_2$, and 15 glucose. All recordings were performed at 30 ± 1 °C in a submerged chamber (Warner instruments, Hamden, CT) continuously superfused with oxygenated ACSF. Schaffer collateral-CA1 synaptic responses and mossy fiber-CA3 synaptic responses were recorded as extracellular field potentials (fEPSPs) from the CA1 stratum radiatum and the CA3 stratum lucidum area, respectively. Unless otherwise-mentioned, test stimuli were delivered at a frequency of 0.05 Hz. The stimulus intensity was set to produce 25-30% of the maximum response in all the experiments. Paired-pulse facilitation (PPF) was performed at 25, 50, 100, 200, 300, 400, and 500 ms interstimulus intervals. Frequency facilitation was investigated by increasing the stimulation rate from 0.1 Hz to 0.5 Hz. LTP was induced by two trains of 100 Hz stimulation lasting 1 s with a 20 s intertetanus interval. No bicuculline was applied during any recording. For CA3 LTP induction, tetanus was delivered in the presence of 50 mM D-(2)-2-amino-5-phosphonopentanoic acid (D-APV) to prevent contamination of the NMDA-dependent pathway converging on CA3 neurons. Mossy fiber synaptic responses were identified by large PPF and frequency facilitation. Experiments were included for data analysis only if DCG-IV caused a greater than 75% reduction in the synaptic response. For Schaffer collateral-CA1 recordings, fEPSP rise slope was calculated as the slope of the rising phase 20-80% of the peak response. For CA3 recordings, the amplitude of individual synaptic

response was measured after subtraction of the response that remained in the presence of DCG-IV. Data were acquired and analyzed with pClamp10.2 software (Axon Instruments, Sunnyvale, CA). Signals were filtered at 2 Hz and sampled at 10 kHz by Digidata 1440A (Axon Instruments, Sunnyvale, CA). Traces were averaged for every 2 min interval.

Immunohistological analysis of excitatory synaptogenesis in cultured hippocampal and cortical neurons.

Dissociated hippocampi and cortical neurons were isolated from postnatal day 0 or day 1 *Mecp2*$^{S421A;S424A/y}$ and *Mecp2*$^{+/y}$ pups, and plated at a density of 1 x 10^4/cm^2 on poly-L-lysine (Sigma# P2636) coated coverslips. Culture medium was Neurobasal (Invitrogen #21103-049) containing 2% B27 (Invitrogen #12587-010), 1% N2 (invitrogen#17502-048), and 0.5 mM GlutaMax (Invitrogen#35050-061). Cultured hippocampal and cortical neurons were fixed at DIV (days in vitro) 21 with 4% PFA and 4% sucrose in PBS, washed with PBS, permeabilized with Tritonx-100 in PBS, blocked with 10% Normal Donkey Serum in PBS (all at room temperature), and incubated at 4 ºC overnight with mouse anti-MAP2 (Millipore#05-346, 1:300), rabbit anti-PSD95 (Cell Signaling#2507, 1:200) and goat anti-VGLUT1 (Santa Cruz#sc-13320, 1:200) antibodies in PBS containing 10% normal donkey serum. The next day, after being washed in PBS, the coverslips were incubated with secondary antibodies, including AffiniPure F(ab´)$_2$ Fragment donkey IgG(H+L) conjugated with DyLight-488 (anti-goat),-549 (anti-rabbit), -649 (anti-mouse) respectively (1:200, Jackson immunoResearch Laboratories). Coverslips were then washed in PBS and stained with DAPI before being mounted on glass slides with FLUOROMOUNT G (SouthernBiotech#0100-01).

Image analysis

Images in Figures. 1 and 7 were captured on a Nikon A1RSI confocal microscope. For each experimental series, all the images were acquired with identical settings for laser power, photomultiplier gain and offset. Z-stacks were collapsed in a maximum projection and analyzed with NIH ImageJ software. For quantification of MeCP2 pS421 level in CA1, all the images were quantified using a single threshold value, which is determined by the background level of the control sections in each experiment. MeCP2 pS421 level was measured as the average MeCP2 p421 intensity in the CA1 neuronal nucleus, which is identified by NeuN immunoreactivity. For pre- and post-synaptic puncta quantification of the primary neuronal cell culture, only primary dendritic branches were included in the analysis. VGLUT1 and PSD95 images were thresholded using constant settings for each experiment, and converted to binary images. Thresholds were chosen such that all recognizable punctate structures were included into the analysis. VGLUT1 and PSD95 puncta were identified by the "partial analysis" function in ImageJ, with the minimal size 0.2 μm^2 for VGLUT1 and 0.1 μm^2 for PSD95. VGLUT1 puncta with overlap or directly adjacent PSD95 puncta were scored as colocalized VGLUT1/PSD-95 puncta. Puncta density was measured as the puncta number per μm of dendritic branch.

RNA extraction, reverse transcription, and real time PCR

Total RNA from mouse hippocampus was isolated using SV Total RNA Isolation System (Promega). cDNA was made using qScript^{TM} cDNA SuperMix (Quanta Bioscience). Real-time PCR was performed on an iQ5 Real-Time PCR machine using iQ SYBR Green

Supermix (Bio-Rad). Fold change was calculated with the $2^{-\text{delta Ct}}$ method after normalization to *Gapdh*. Primers were: 5'-AATGGGAAGCTTGTCATCAACG-3' (Gapdh-F), 5'-GAAGACACCAGTAGACTCCACGACATA-3' (Gapdh-R), 5'-CGCCATGCAATTTCCACTATCAATAATTTAAC-3'(Bdnf E4-F), 5'-CTTTTTCAGTCACTACTTGTCAAAGTAAAC-3' (Bdnf E4-R), 5'-GACCATCCTTTTCCTTACTATGG-3' (Bndf CDS-F), 5'-CCATTCACGCTCTCCAGAGTC-3' (Bdnf CDS-R), 5'-CATCACGAAGAACATCTGGAG-3' (Bmp4-F), 5'-CGAGGAGATCACCTCATTCTC-3' (Bmp4-R), 5'-CAACAACATATGGTACTGAGTAC-3' (Mef2c-F), 5'-CATGTTATGTAGGTGCTGCTGC-3' (Mef2c-R), 5'-ACAGAAGGGAATTACGGCGAGA-3' (Grm1-F), 5'-ATCAAAGCTCTTCTCGCCAGCA-3' (Grm1-R).

Chromatin immunoprecipitation and gene promoter specific real time PCR

Hippocampi were dissected from 9-12 weeks old mice, diced into small pieces and crosslinked in 0.5% formaldehyde, washed with ice-cold PBS, sonicated with Misonix Sonicator 3000 in lysis buffer (1% SDS, 10 mM EDTA, 20 mM Tris-HCl, pH 8.1, Roche protease inhibitor cocktail), and cleared by centrifugation to generate sheared chromatin. Dynabeads (Invitrogen) were pre-washed with PBS/BSA (0.5% BSA in PBS) and incubated with anti-FLAG antibody (Sigma) to form the beads/antibody complex. For immunoprecipitation, sheared chromatin was diluted in dilution buffer (0.01% SDS, 1.1% Triton X-100, 1.2 mM EDTA, 16.7 mM Tris-HCl, pH 8.1, 167 mM NaCl) and incubated with beads/antibody complex overnight on a Nutator at 4 ºC.

The next day, the beads/antibody/chromatin complex were washed with washing buffer (50 mM Hepes, pH 7.6, 1 mM EDTA, 0.7% DOC, 1% NP-40, 0.5 M LiCl) and TBS. The immunoprecipitated chromatin was then eluted from the beads in elution buffer (1% SDS, 10 mM EDTA, 20 mM Tris-HCl, pH 8.1), and reverse-crosslinked. Sheared chromatin not incubated with beads/antibody complex was processed the same way to generate input DNA. Both ChIP DNA and input DNA were treated with RNase A (Thermo Scientific) and proteinase K (Promega), purified by ethanol precipitation, and dissolved in water (Promega). 20 ng of ChIP DNA and input DNA was used for each quantitative real-time PCR. Real-time PCR was performed on an iQ5 Real-Time PCR machine using iQ SYBR Green Supermix (Bio-Rad). The ChIP DNA level was normalized to the input DNA level using the $2^{-\text{delta Ct}}$ method. Relative promoter occupancy was calculated by setting the MeCP2-flag binding level as 100%. Primers were: 5'-TTCTGTGTGCGTGAATTTGC-3' (Bdnf E4-F),
5'-TGGGTGGGAGTCCACGAG-3' (Bdnf E4-R),
5'-TACAGTAGCATTGTGGGTTC-3' (Mef2c-F),
5'-AGGAGGGATTAATCATGCTC-3' (Mef2c-R),
5'-CTCTAGTGTTTTCATGTGAC-3' (Grm1-F),
5'-GGAGTAGCCAAATGTAGAGT-3' (Grm1-R),
5'-TGAAGCTGATAGTTCCTTCC-3' (Bmp4-F),
5'-GCTAGCTGGGAGGTGGAATG-3' (Bmp4-R).

Statistical analysis

For Morris water maze data, two way ANOVA with repeated measures was performed to reveal any significant interaction between genotype and quadrant, which was followed by a Tukey-HSD

post hoc test to complete the pairwise comparison of the percentage of time spent by each genotype in each quadrant. For LTP and basic synaptic transmission data, two-way ANOVA with repeated measures was performed. For the rest of the data, the Student's t-test was performed. Statistical significance was determined at $p < 0.05$.

Chapter 3: Cell cycle-linked MeCP2 phosphorylation regulates adult neurogenesis through the Notch signaling pathway

This chapter is based on the manuscript titled “Cell cycle-linked MeCP2 phosphorylation regulates adult neurogenesis through the Notch signaling pathway” by Hongda Li, Xiaofen Zhong, Kevin Fongching Chau, Nicholas J. Santistevan, Weixiang Guo, Guangyao Kong, Xuekun Li, Mitul Kadakia1, Jamie Masliah, Peng Jin, Jing Zhang, Xinyu Zhao, and Qiang Chang.

The manuscript is under review at Nature Neuroscience.

Summary

Neuronal activity-induced MeCP2 phosphorylation in postmitotic neurons is required for the normal development and function of the mammalian brain. Yet it is not known whether other signals may induce MeCP2 phosphorylation in other cell types, and what functions MeCP2 phosphorylation may have in those contexts. Here we show that cell cycle-linked MeCP2 phosphorylation regulates the balance between proliferation and differentiation in neural progenitor cells through the Notch signaling pathway.

Introduction

In the adult mammalian brain, continuously neurogenesis occurs in two regions: the subgranular zone (SGZ) of the dentate gyrus (DG) of the hippocampus and the subventricular zone (SVZ) of the lateral ventricles (Eriksson et al., 1998; Kuhn et al., 1996; Lois and Alvarez-Buylla, 1994). Adult-born granule cells in the dentate gyrus integrate into the local neuronal network in the hippocampus and contribute to neural plasticity and learning and memory (Encinas and Enikolopov, 2008). In SVZ, new born cells finally differentiate into interneurons, migrate to the olfactory bulb, and contribute to olfactory function(Alvarez-Buylla and Lim, 2004).

Adult Neurogenesis is dynamically regulated by a number of intrinsic as well as extrinsic factors. Epigenetic mechanisms, practically DNA methylation, have emerged as in important link between external or internal stimuli and transcriptional control of gene expression in adult neural stem/progenitor cells. DNA methyltransferase 3A (DNMT3A) deficient mice exhibit impaired neuronal differentiation (Wu et al., 2010). GADD45b, a protein previously implicated in DNA demethylation, is a neuronal activity-induced immediate early gene in mature hippocampal neurons (Barreto et al., 2007). *Gadd45b* knockout mice exhibit specific deficits in neural activity-induced proliferation of neural progenitors and dendritic growth of newborn neurons in the adult hippocampus (Ma et al., 2009). Loss of Methyl-CpG-binding domain protein 1 (MBD1) leads to increased adult neural progenitor cell proliferation and decreased neuronal and glial differentiation (Liu et al., 2010; Zhao et al., 2003).

Methyl-CpG binding protein 2 (MeCP2) is an important reader and interpreter of DNA methylation across the genome (Jaenisch and Bird, 2003). Mutations in *MECP2* have been

identified as the cause of Rett syndrome (RTT) (Amir et al., 1999), a severe neurodevelopmental disorder (Hagberg, 1985). In postmitotic neurons, depolarization induced Ca^{2+} influx through voltage-gated calcium channels (VGCCs) has been shown to trigger phosphorylation of MeCP2 at serine 421 (S421) (Chen et al., 2003b; Zhou et al., 2006), which is required for regulating synaptogenesis, dendritic morphology, synaptic homeostasis, long-term potentiation and spatial memory in the adult mouse brain (Cohen et al., 2011; Li et al., 2011; Zhong et al., 2012).

Here, we report that MeCP2 S421 phosphorylation exists in adult neural progenitor cells (aNPCs) and is regulated by cell cycle. Moreover, preventing S421 phosphorylation with serine to alanine mutation decreases aNPCs proliferation and increases neuronal differentiation *in vitro* and in *vivo*. Phosphor mutant aNPCs exhibit reduced *Notch1* and *Dll1* expression and Notch signaling. More importantly, restoring Notch signaling level in phosphor mutant aNPCs is sufficient to rescue the neurogenesis phenotypes. Our results provide another example that external and internal signals access MeCP2 through phosphorylation to generate adaptive functional outputs, which is important for the normal development and function of the mammalian nervous system.

Results

Phosphorylation of MeCP2 Ser421 is regulated by cell cycle in aNPCs

The activity-dependent Ser421 phosphorylation in neurons is induced by calcium influx through L-type voltage-gated voltage-gated calcium channels (VGCC), and following activation of Ca2+/calmodulin-dependent protein kinase (CaMK) (Tao et al., 2009; Zhou et al., 2006), a neuronal specific mechanism which does not exist in the proliferating adult neural stem/progenitor cells to our knowledge. To assess the possible existence of MeCP2 S421 phosphorylation in aNPCs, we isolated adult proliferating neural progenitor cells from the dentate gyrus (DG) of both wild type (WT) and *Mecp2*$^{S421A;S424A/y}$ phosphor-mutant hippocampus (**Supplementary Fig. 1a**). The cultured WT and phosphor-mutant aNPCs proliferate normally, and express aNPC marker Nestin and MCM2 (**Supplementary Fig. 1b**). The total MeCP2 level is indistinguishable in WT and phosphor-mutant aNPCs (**Fig. 1a**), consistent with previous report that loss of S421 phosphorylation does not influence the basal protein level of MeCP2 (Li et al., 2011). Interestingly, we discovered that S421 was phosphorylated (**Fig. 1a**) inWT aNPC and this phosphorylation was abolished in phosphor-mutant aNPCs (**Fig. 1a**).

To elucidate how S421 phosphorylation is regulated in aNPCs, we first reason that growth factors might be the driving force maintaining S421 phosphorylation in the proliferating aNPC. Withdrawing growth factors in the growth media led to concurrent decrease of phosphorylation of S421 (**Fig. 1b-c**) and absence of G2/M phase cells (**Supplementary Fig. 1c**) in WT aNPCs. To investigate whether S421 phosphorylation is linked to cell cycle, we arrested WT aNPCs at

the G2/M phase with nocodazole (**Supplementary Fig. 1d**) or colchicine and observed a dramatic increase in the level of phospho-S421 (**Fig. 1d**,f and **Supplementary Fig. 1e**). Fluorescence-activated cell sorting (FACS) analysis also confirms the presence of MeCP2 S421 phosphorylation in phospho-Histone H3 positive M phase aNPCs (data not shown). Using a series of pharmacological reagents, we excluded the involvement of VGCCs, CaMKK and CaMKII in regulating S421 phosphorylation in aNPCs (**Supplementary Fig. 1f**), because selective inhibitors of VGCCs, CaMKK or CaMKII failed to block cell cycle-linked S421 phosphorylation in these cells, indicating aNPCs utilize a different kinase system for S421 phosphorylation than the neurons do. Cell cycle dependent kinases (CDKs) are a family of serine/threonine kinases that are important for cell cycle regulation. Applying roscovitine, a CDK inhibitor, to pre-synchronized aNPCs effectively blocks nocodazole-induced S421 phosphorylation, suggesting that cell cycle dependent kinases (CDKs) were required for S421 phosphorylation in aNPCs (**Fig. 1e-f**).

Altered proliferation and differentiation of MeCP2 phosphor-mutant aNPC *in vitro* and *in vivo*

To reveal the functional significance of S421 phosphorylation in aNPCs, we examined proliferation and differentiation in early passage WT and phosphor-mutant aNPCs. After pulse-labeling the cells with BrdU for 8 hours, we observe significantly fewer BrdU-labeled cells in phosphor-mutant aNPCs (**Fig. 2a-b**) than those in the WT aNPCs, indicating a reduced proliferation potential of phosphor-mutant aNPCs. Moreover, upon differentiation,

significantly more Tuj1 positive cells were detected in phosphor-mutant aNPCs (**Fig. 2c-d**), suggesting increased potential in neural differentiation. In contrast, no difference in glial differentiation was observed between the WT and phosphor-mutant aNPCs (**Fig. 2e-f**). Consistent with the stereological counting data (**Fig. 2a-f**), the expression levels of *Tuj1* and *NeuroD1*, two neuronal genes, were significantly higher in differentiated phosphor-mutant aNPCs than in WT aNPCs; while the expression levels of *GFAP*, a glial gene, remained unchanged in these cells (**Fig. 2g**). In addition, when aNPCs were isolated from the forebrain of adult WT and the *Mecp2*$^{S421A;S424A/y}$ mice, the phosphor-mutant aNPCs also demonstrated increased neural differentiation as determined by the percentage of Tuj1 positive cells, *Tuj1* transcription and NeuroD promoter driven luciferase expression (**Supplementary Fig. 2a-c**)

To validate our observations on *in vitro* cultured aNPCs, we first performed BrdU labeling (**Fig. 3a-b**) to mark all the proliferating aNPCs in the subgranular zone of the hippocampus in adult mice, and conducted stereological counting on sections throughout the hippocampus to compare the numbers of BrdU labeled cells in the hippocampus between 9 pairs of *Mecp2*$^{S421A;S424A/y}$ and WT littermates (within each pair, the mutant and WT came from the same litter; the 9 pairs came from 9 different litters). In each pair, fewer BrdU labeled cells (on average 11% less than WT) were found in the *Mecp2*$^{S421A;S424A/y}$ hippocampus than in the WT littermate (**Fig. 3c**, p=0.003). Consistent with the BrdU labeling results, fewer Ki67 (a proliferation marker) stained cells (on average 35% less than WT) were found in the *Mecp2*$^{S421A;S424A/y}$ hippocampus than in the WT littermates in stereological analysis from 6 additional pairs of mice (**Fig. 3d**, p=0.03). In addition to aNPC proliferation, we also examined the cell fates of these adult-born cells 4 weeks after they were born (as illustrated in **Fig. 3e**). In

the study, dividing aNPCs in the hippocampus of 8-9 weeks old *Mecp2*$^{S421A;S424A/y}$ mice (n=9) and their WT littermates (n=8) were first labeled by BrdU and given 4 weeks to differentiate. Sections throughout the hippocampus were triple labeled with an anti-BrdU antibody (to mark adult-born cells), an anti-NeuN antibody (to mark neurons), and an anti-S100beta antibody (to mark glial cells). Under a confocal microscope, cells were identified as new neurons if they were positive for both BrdU and NeuN (**Fig. 3f**, indicated by arrows), as new glial cells if they were positive for both BrdU and S100beta (**Fig. 3f**, indicated by an arrowhead), or as undifferentiated if they were only positive for BrdU. All BrdU positive cells in the subgranular zone from all stained sections were included in the analysis. Our results showed that a higher proportion of the dividing aNPCs in the hippocampus of the *Mecp2*$^{S421A;S424A/y}$ mice differentiated into neurons (**Fig. 3g**, p=0.04) at the expense of undifferentiated cells (**Fig. 3g**, p=0.02). The percentage of glial cells differentiated from the newborn cells in the adult hippocampus did not change significantly in the *Mecp2*$^{S421A;S424A/y}$ mice when compared with the WT littermates (**Fig. 3g**, p=0.66). Taken together, our *in vitro* and *in vivo* observations consistently identify a critical role of S421 phosphorylation in regulating aNPC proliferation and differentiation.

Reduced Notch signaling in MeCP2 phosphor-mutant aNPCs and phenotypic rescue by NICD overexpression

To elucidate the underlying molecular mechanism, we performed transcription profiling of aNPCs using the Neurogenesis and Neural Stem Cells PCR Array. Among the significant transcription changes in phosphor-mutant aNPCs, several belonged to the well-studied Notch

signaling pathway (**Supplementary Fig. 3a**). In adult hippocampus, Notch signaling is required for the expansion and cell-renewal of neural stem/progenitor cells (Louvi and Artavanis-Tsakonas, 2006). Abrogation of Notch1, a Notch signaling receptor, in neural progenitor cells promotes cell cycle exit for neuronal differentiation (Ables et al., 2010). Overexpression of intracellular domain of Notch1 (NICD), however, leads to proliferation and expansion of the neural stem/progenitor cells pool (Ables et al., 2010).

To first confirm the misregulation of Notch signaling in phosphor-mutant aNPCs, we expanded our analysis to examine RNA levels of additional components of the Notch pathway, and found consistent decrease in the ligand (*Dll1* and *Jag2*), receptor (*Notch1*) and several target genes (*Hes3*, *Hes5*, *Hey1*, and *Heyl*) of this pathway in phosphor-mutant aNPCs (**Fig. 4a,g** and **Supplementary Fig. 3b**). In addition, Western blot results confirmed the significant decrease in DLL1 protein level in phosphor-mutant aNPCs (**Fig. 4b-c**). To determine whether the transcriptional change in *Dll1* and *Notch1* was a direct effect of altered promoter occupancy by the phosphor-mutant MeCP2 protein, we conducted chromatin immunoprecipitation (ChIP) experiment and found increased binding of the phosphor-mutant protein at the promoters of both *Dll1* and *Notch1* (**Fig. 4d**). Consistent with the idea that decreased Notch signaling in phosphor-mutant aNPC may underlie the observed changes in aNPC proliferation/differentiation, treatment of WT aNPCs with a Notch inhibitor led to decreased proliferation and increased neural differentiation similar to those observed in phosphor-mutant aNPCs (**Supplementary Fig. 3c**).

Because NICD serves as the link between ligand/receptor interaction on the cell membrane and target gene activation in the nucleus (Bray and Bernard, 2010) and NICD level was lower in

the phosphor-mutant aNPCs (**Fig. 4e-f**), we attempted to rescue the proliferation/differentiation phenotypes by overexpressing NICD in these cells. GFP- or NICD-expressing lentiviruses were produced and used to infect either WT or phosphor-mutant aNPCs. While the NICD level in GFP-lentivirus-infected phosphor-mutant aNPCs remained much lower than that in GFP-lentivirus-infected WT aNPCs, the NICD level was similar between NICD-lentivirus-infected phosphor-mutant aNPCs and GFP-lentivirus-infected WT aNPCs (**Supplementary Fig. 3e**). Furthermore, overexpression of NICD, but not overexpression of GFP, was sufficient to reverse the reduced transcription of Notch signaling target genes in the phosphor-mutant aNPCs (**Fig.5a)**. Finally, the key phenotypes of reduced proliferation and increased neural differentiation in phosphor-mutant aNPCs were both rescued by the overexpression of NICD, as determined by comparing the number of BrdU labeled aNPCs (**Fig. 5b-c**), the number of Tuj1 positive cells (**Fig. 5d-e**) and the expression level of *Tuj1* and *NeuroD1* RNA (**Fig. 5f**) upon induction of differentiation in WT and phosphor-mutant aNPCs infected with either NICD- or GFP-lentiviruses.

Discussion

Neuronal activity induced phosphorylation of MeCP2 is required for normal brain development and function (Cohen et al., 2011; Li et al., 2011). Our study provides the first evidence that S421 phosphorylation is present in a proliferating cell type and plays a key role in regulating the proliferation and neuronal differentiation of aNPCs. We show that S421 phosphorylation is maintained through the proliferation of aNPCs and specifically enriched in cells in the G2/M phase of cell cycle in a CDK dependent manner. Our results suggest a positive feedback loop among aNPCs proliferation, S421 phosphorylation and Notch signaling in regulating adult neurogenesis (**Supplementary Fig. 4**). Cell cycle-linked MeCP2 S421 phosphorylation maintains Notch signaling function in the proliferating aNPCs. Activation of Notch signaling promotes aNPCs proliferation and inhibits neuronal differentiation. In phosphor-mutant aNPCs, loss of S421 phosphorylation leads to down-regulation of Notch signaling pathway through repression of Dll1 and Notch1 expression, resulting in decreased proliferation and increased neuronal differentiation of aNPCs. Although the direct kinase remains elusive, our results strongly suggest that the pathways and kinases upstream of S421 phosphorylation in aNPCs are distinct from those previously identified in postmitotic neurons. Thus, S421 phosphorylation appears to be a general regulatory switch accessible to diverse stimuli acting through distinct signaling pathways with important functional outcomes in different cell types.

Phosphor-mutant mice exhibit reduced aNPC proliferation and increased neuronal differentiation in adult hippocampus, and cultured aNPC from phosphor-mutant mice recapitulate these phenotypes *in vitro*. MeCP2 S421 phosphorylation is maintained through aNPC cell cycle intrinsically, and regulates Notch signaling possibility through altered promoter

binding of MeCP2 to *Dll1* and *Notch1*. This evidence suggests a cell-autonomous mechanism for the proliferation and increased neuronal differentiation phenotypes in phosphor-mutant aNPCs. However, we also cannot rule out the possibility of non-cell autonomous contributions. The process of adult neurogenesis is dynamically modulated by many environmental stimuli, local niche signals and diverse internal cues (Faigle and Song, 2013). Gadd45b is an example of epigenetic regulator that links activity-induced changes of DNA methylation in mature neurons to modulation of neurogenesis in the adult SGZ (Ma et al., 2009). It is possible that neuronal activity-induced MeCP2 phosphorylation employs a similar mechanism in regulating adult neurogenesis. Because both cell cycle-linked MeCP2 phosphorylation in aNPCs and the neuronal activity-induced MeCP2 phosphorylation in postmitotic neurons are abolished in phosphor-mutant mice. *Bdnf* and *Bmp4* were misregulated in the hippocampus of phosphor-mutant mice, both of which are important modulators for adult neurogenesis (Bath et al., 2012; Lim et al., 2000; Waterhouse et al., 2012). To distinguish the cell-autonomous and non-cell autonomous contributions of MeCP2 S421 phosphorylation in adult neurogenesis, neural stem/progenitor cells specific knockin mice need to be generated. On the other hand, it is also interesting to generate neuronal specific knockin mice to examine the role of neuronal MeCP2 phosphorylation in modulating adult neurogenesis.

It was demonstrated in earlier reports that loss of MeCP2 S421 phosphorylation in mice led to increased dendritic complexity, enhanced synaptogenesis, LTP, and spatial memory, and impaired synaptic homeostasis (Cohen et al., 2011; Li et al., 2011; Zhong et al., 2012). However, it is difficult to assess whether the altered adult neurogenesis in phosphor-mutant mice have contribution to these phenotypes. Again, generating neural stem/progenitor cells specific knockin

mice would provide evidence for the functional significance of aNPC MeCP2 phosphorylation in synaptic plasticity and learning and memory.

SVZ is the other niche of adult neurogenesis, and adult-born neurons from SVZ contribute to olfactory bulb functions. Phosphor-mutant aNPCs isolated from the forebrain, in which SVZ becomes the dominant aNPCs source, also present more potential for neuronal differentiation. Further investigation will be done to determine whether phosphor-mutant mice exhibit altered SVZ neurogenesis and olfactory bulb function.

Earlier mass spectrometry study indicated that both S421 and S424 phosphorylations of MeCP2 were induced by neuronal activity (Tao et al., 2009). Due to the lack of a good phospho-specific antibody for S424, the regulation and function of S424 phosphorylation is not well studied so far. It will be interesting to examine the existence of S424 phosphorylation in the context of aNPCs using mass spectrometry, or in the future when good phospho-specific antibodies for S424 become available. The MeCP2 sequence from S421 to S424, when S421 is phosphorylated, actually matches the consensus phosphorylation site of Casein kinase 1 (pS/T-X-X-S/T), raising the possibility that S421 phosphorylation leads to the following S424 phosphorylation by Casein kinase 1. Thus, the adult neurogenesis phenotypes we observed in *Mecp2*$^{S421A;S424A/y}$ mice could be the result of loss of phosphorylation from both sites.

Figures

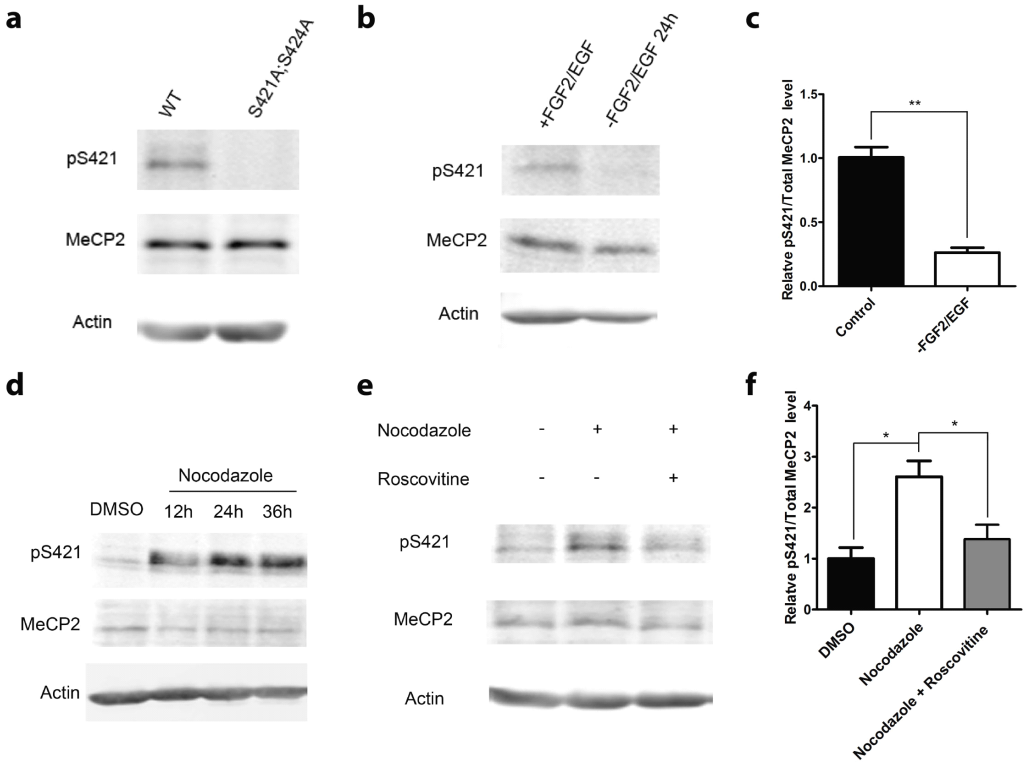

Figure 1: Phosphorylation of MeCP2 Ser421 is regulated by cell cycle in aNPCs.

(a) Western blot analysis of MeCP2 Ser421 phosphorylation in WT and phosphor-mutant aNPCs. (b, c) Western blot analysis and quantification of the relative MeCP2 Ser421 phosphorylation level in WT aNPCs under normal proliferating condition and FGF2/EGF withdrawal for 24 hours. (n=3 in each group) (d) Western blot analysis reveals that MeCP2 Ser421 phosphorylation is induced by synchronizing aNPCs with nocodazole (150ng/ml). (e,f) Western blot analysis and quantification of the relative MeCP2 Ser421 phosphorylation level in aNPCs under conditions: 1) DMSO, 2) 36 hours of nocodazole treatment, 3) 24 hours of roscovitine (25 μM) treatment after pre-synchronization of the cells by nocodazole for 12 hours. (n=3 in each group) The bar graph shows the mean ± s.e.m * $p<0.05$ ** $p<0.01$

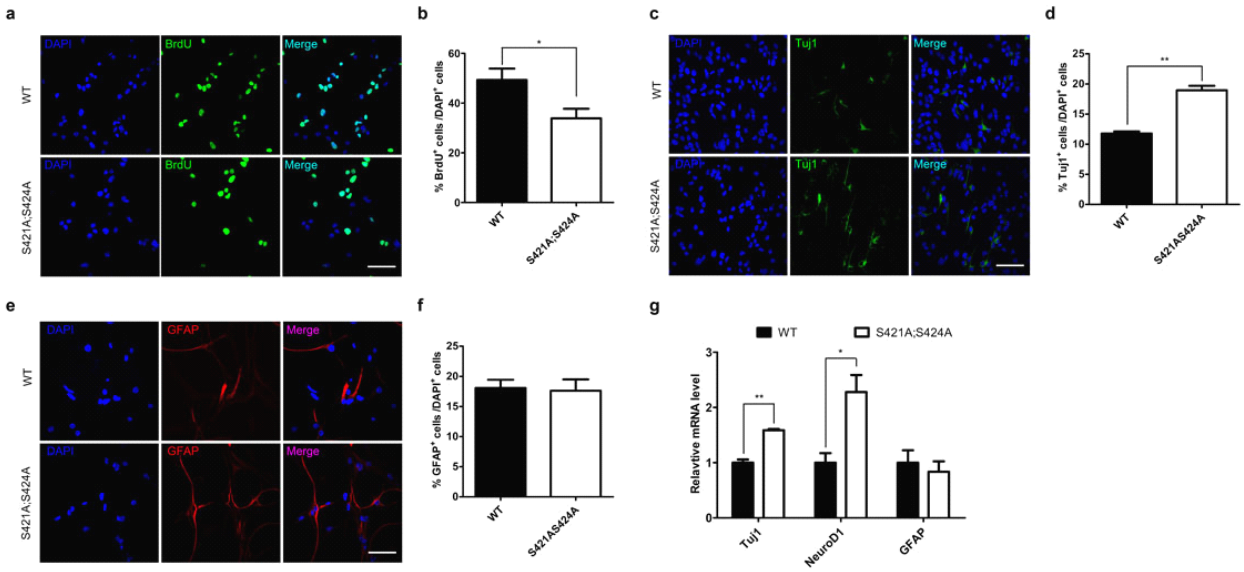

Figure 2: aNPCs isolated from DG of phosphor-mutant mice exhibit altered proliferation and neuronal differentiation

(a) Representative images of aNPCs isolated from wild type and phosphor-mutant mice with BrdU pulse labeling, followed by immunocytochemistry analysis (b) Quantification of the percentage of BrdU-labeled cells in wild type and phosphor-mutant aNPCs. (n=3 in each group) (c) Representative immunocytochemistry images of Tuj1+ neurons differentiated from wild type and phosphor-mutant aNPCs (d) Quantification of the percentage of Tuj1+ cells in wild type and phosphor-mutant aNPCs under differentiation condition. (n=3 in each group) (e) Representative immunocytochemistry images of GFAP+ astrocyte differentiated from wild type and phosphor-mutant aNPCs (f) Quantification of the percentage of GFAP+ cells in wild type and phosphor-mutant aNPCs under differentiation condition. (n=3 in each group) (g) Relative mRNA level of neuronal marker (Tuj1 and NeuroD1) and astrocyte marker (GFAP) in wild type and phosphor-mutant aNPCs under differentiation condition, assayed by RT-qPCR. (n=3 in each group) Scale bar:50 μm. The bar graph shows the mean ± s.e.m * $p<0.05$ ** $p<0.01$

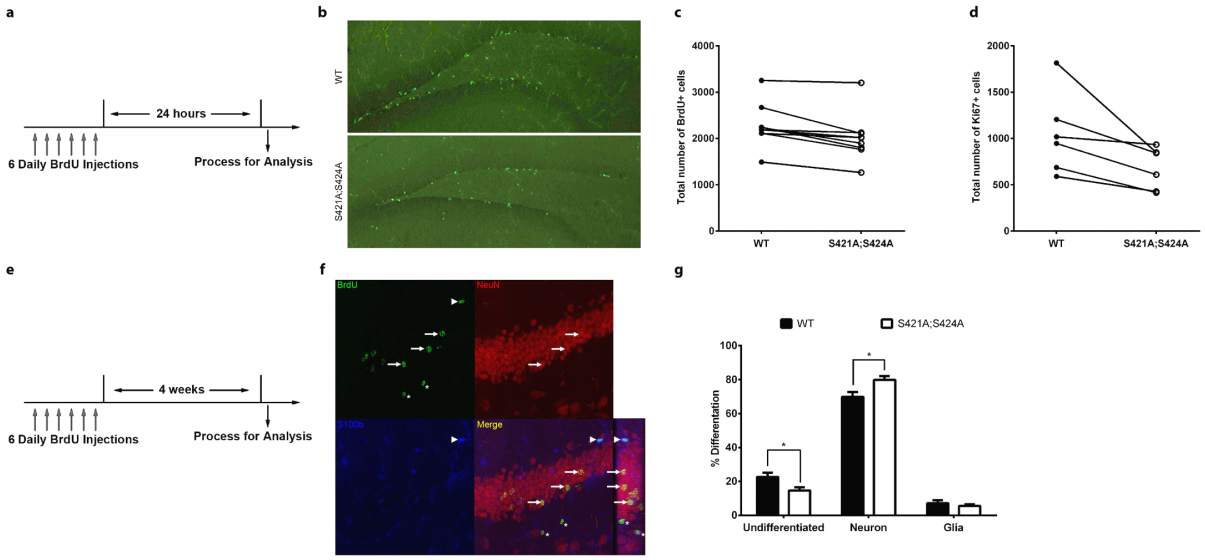

Figure 3: Altered aNPC proliferation and differentiation in DG of *Mecp2*$^{S421A;S424A/y}$ mice (a) Schematic drawing of the design of the BrdU labeling experiment. (b) Representative images of coronal sections from the wild type and the *Mecp2*$^{S421A;S424A/y}$ brains stained for BrdU immunoreactivity. (c) Quantification of BrdU+ cells obtained through stereological counting from 9 pairs of wild type and *Mecp2*$^{S421A;S424A/y}$ mice. Each pair is linked by a line. Paired Student's t-test was performed. p=0.003. (d) Quantification of the total number of Ki67+ cells obtained through stereological counting from 6 pairs of wild type and *Mecp2*$^{S421A;S424A/y}$ mice. Each pair is linked by a line. Paired Student's t-test was performed. p=0.03. (e) Schematic drawing of the design of BrdU pulse/chase experiment to examine the differentiation profile of the adult-born hippocampal cells. (f) Representative confocal microscopy images to demonstrate how each cell type is identified. Three adult-born neurons (co-stained by BrdU and NeuN) are marked by arrows. One adult-born glial cell (co-stained by BrdU and S100b) is marked by an arrowhead. Two undifferentiated cells (stained by BrdU only) are marked by asterisks. (g) Quantification of proportions of the three cell fate choices made by the dividing neural stem cells

in the adult hippocampus of wild type and *Mecp2*$^{S421A;S424A/y}$ mice. For the undifferentiated, p=0.02. For neuron, p=0.04. For glia, p=0.66.

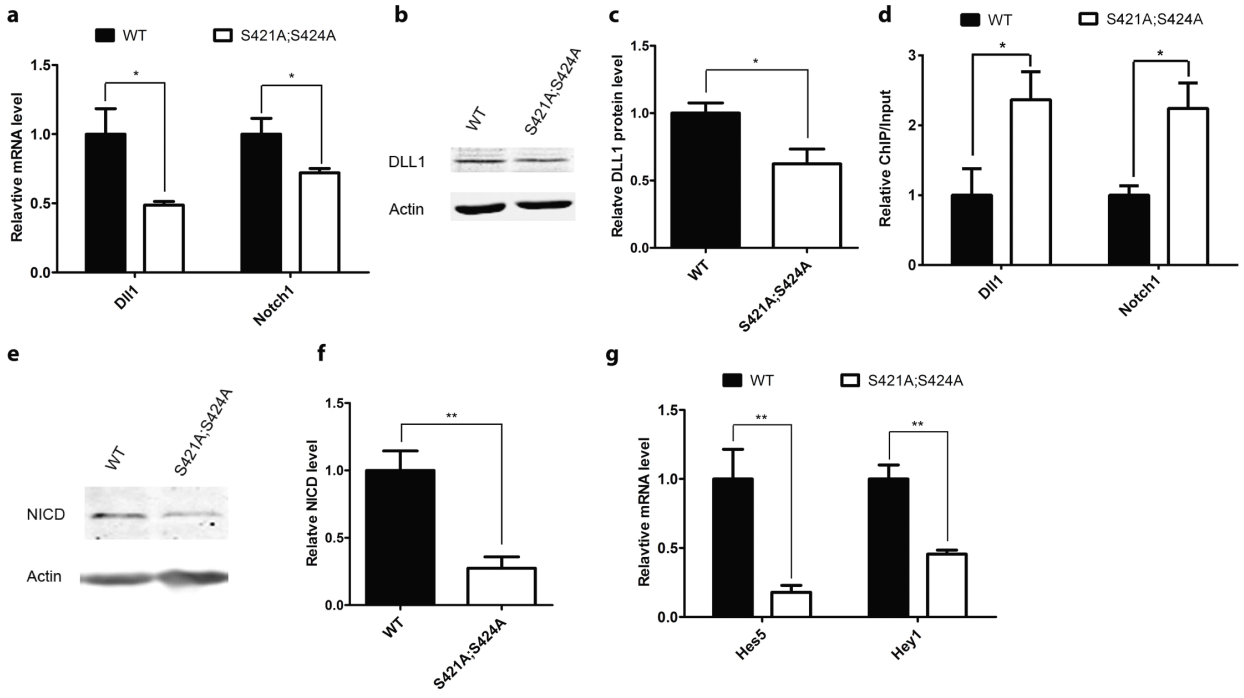

Figure 4: Reduced Notch signaling in phosphor-mutant aNPCs

(a) RT-qPCR analysis of the relative mRNA level of *Dll1* and *Notch1* in wild type and phosphor-mutant aNPCs. (n=5 in each group for *Dll1*, n=8 in each group for *Notch1*) (b,c) Western blot analysis and quantification of the relative protein level of DLL1 in wild type and phosphor-mutant aNPCs. (n=4 in each group) (d) ChIP-qPCR analysis of the chromatin occupation of MeCP2 on *Dll1* and *Notch1* promoters. (n=4 in each group) (e, f) Western blot analysis and quantification of NICD level in wild type and phosphor-mutant aNPCs (n=5 in each group) (g) RT-qPCR analysis of the relative mRNA level of Notch target gene *Hes5* and *Hey1* in wild type and phosphor-mutant aNPCs. (n=5 in each group)

The bar graph shows the mean ± s.e.m * $p<0.05$ ** $p<0.01$

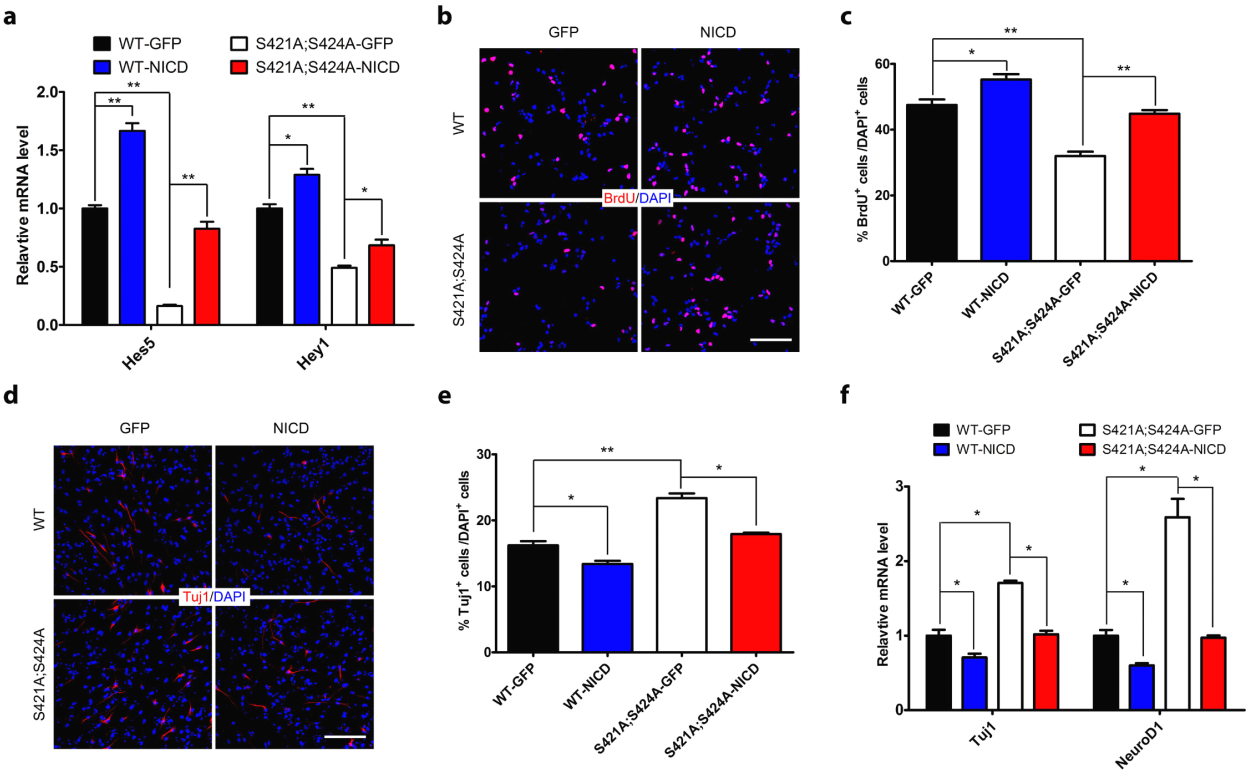

Figure 5: Overexpression of NICD rescues the phenotypes of phosphor-mutant aNPCs (a) RT-qPCR analysis of the relative mRNA level of *Hes5* and *Hey1* in wild type and phosphor-mutant aNPCs infected with GFP or NICD letivirus. (n=3 in each group) (b, c) Representative images and quantification of BrdU-labeled cells in wild type and phosphor-mutant aNPCs infected with GFP or NICD letivirus, followed by BrdU pulse labeling. (n=3 in each group) (d, e) Representative images and quantification of Tuj1+ neurons differentiated from wild type and phosphor-mutant aNPCs infected with GFP or NICD letivirus. (n=3 in each group) (f) Relative mRNA level of neuronal marker (Tuj1 and NeuroD1) and astrocyte marker (GFAP) in wild type and phosphor-mutant aNPCs, which are infected with GFP or NICD letivirus and then cultured in differentiation condition. (n=3 in each group) Scale bar:50 μm. The bar graph shows the mean ± s.e.m * $p<0.05$ ** $p<0.01$

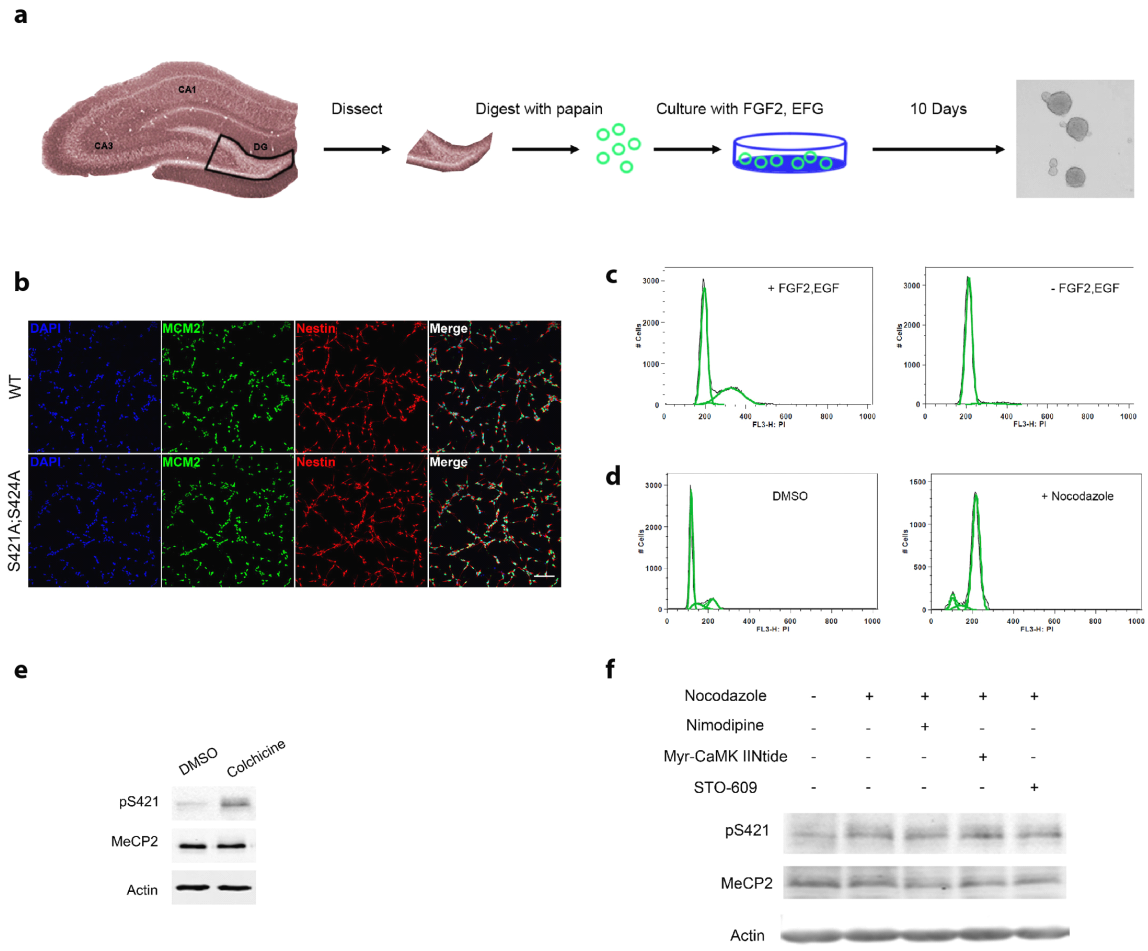

Supplementary Figure 1: MeCP2 Ser421 phosphorylation regulation in aNPCs.

(a) Schematic drawing showing the isolation of aNPCs from the dentate gyrus for culture. (b) Immunocytochemistry analysis of aNPCs isolated from WT and phosphor-mutant mice for neural stem cell marker MCM2 (green) and Nestin (red). Scale bars: 50 µm. (c,d) Cell cylce analysis of DNA content of aNPCs under normal condition, FGF2/EGF withdrawal, treated with DMSO, or treated with nocodazole. (e) Western blot analysis of MeCP2 Ser421 phosphorylation level in aNPCs treated with DMSO or colchicine (1µg/µl)) (f) Western blot analysis of MeCP2 Ser421 phosphorylation level in aNPCs treated with DMSO, nocodazole or nocodazole coupled with Nimodipine (5µM), Myr-CaMK IINtide (5µM), or STO-609 (1.5µM).

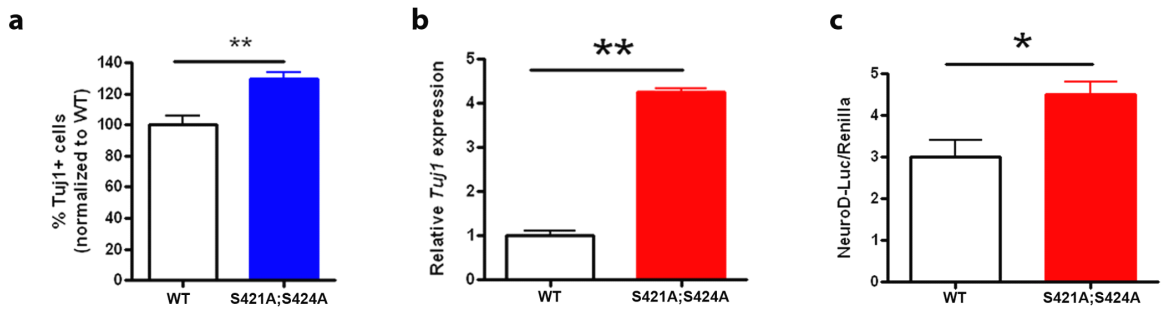

Supplementary Figure 2: Altered neural differentiation of MeCP2 phosphor-mutant aNPC isolated from adult subventricular zone.

aNPCs isolated from the adult subventricular zone of WT and phosphor-mutant mice exhibit increased neuronal differentiation, assayed by stereology counting of Tuj1+ cells (a), RT-qPCR analysis of *Tuj1* RNA level (b), and NeuroD1 promoter-driven luciferase reporter level (c). The bar graph shows the mean ± s.e.m * $p<0.05$ ** $p<0.01$.

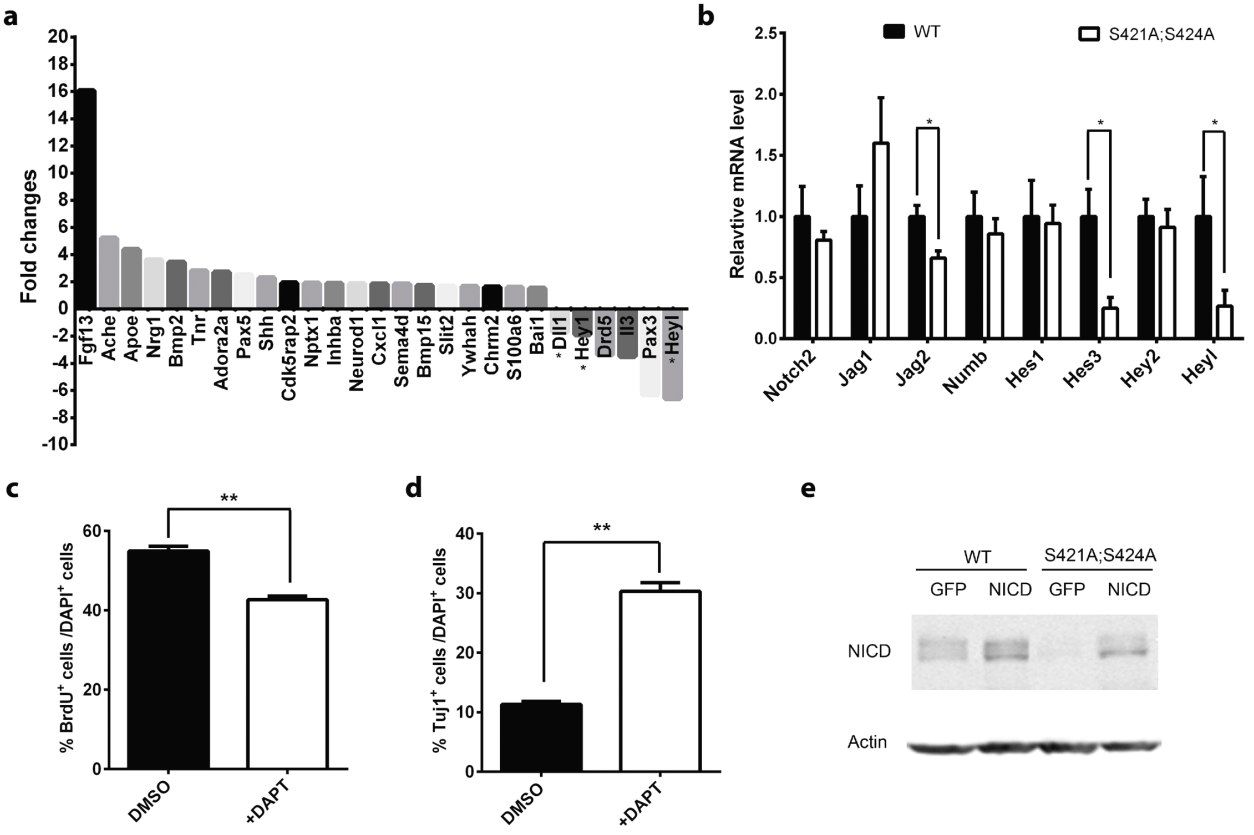

Supplementary Figure 3: Decreased Notch signaling in phosphor-mutant aNPCs

(a) The genes with larger than 1.5 fold changes from Neurogenesis and Neural Stem Cells PCR Array of WT and phosphor-mutant aNPCs (Normalized to WT, n=3 in each group). Notch pathway related genes are marked with an asterisk. (b) RT-qPCR analysis of the relative mRNA level of other Notch pathway related genes in WT and phosphor-mutant aNPCs (n=5 in each group). (c) Quantification of the percentage of BrdU-labeled cells in aNPCs treated with DMSO or DAPT (5μM), followed by BrdU pulse labeling. (d) Quantification of the percentage of Tuj1+ neurons differentiated from WT and phosphor-mutant aNPCs treated with DMSO or DAPT. (e) Western blot analysis confirms the overexpression of NICD in WT and phosphor-mutant aNPCs infected with NICD-letivirus. The bar graph shows the mean ± s.e.m * $p<0.05$ ** $p<0.01$.

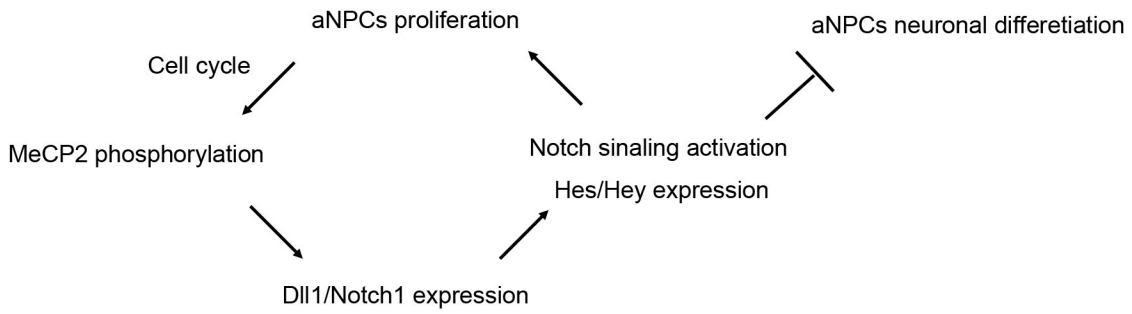

Supplementary Figure 4: Putative model for the function of MeCP2 S421 phosphorylation in aNPCs.

Materials and methods

Animals

All the experiments were performed using male mice. *Mecp2*$^{S421A;S424A/y}$ mice have been backcrossed to C57BL/6 background for more than 10 generations. Mice were housed in 12hr light (6am-6pm)/12 hr dark (6pm-6am) cycle. Mice were housed <5 mice/cage. All protocols were approved by the Institutional Animal Care and Use Committee at University of Wisconsin-Madison.

DNA construct

The cDNA of the intracellular domain of mouse Notch1 (NICD) was subcloned to lentivirus expression vector. Expression of NICD is driven by EF-1 Alpha (EF1α) promoter (pEF1α vector is a gift from Dr. Su-chun Zhang's lab).

Antibodies and drugs

The following primary antibodies were used: Anti-MeCP2 (Cell Signaling, 3456), Anti-MeCP2 (Abcam, ab50005), Anti phospho-S421 (custom made by Covance), anti-β-Actin (Sigma-Aldrich, a5441), anti-DLL1(Abcam, Ab84620), anti-NICD(Cell Signaling, 4147), anti-phospho-Histone H3 (Ser10)(Cell Signalling,3377), anti-Histone H3 (Active Motif, 39163), anti-S100b (SWANT), anti-NeuN (Millipore, MAB377), anti-BrdU (Accurate Chemical & Scientific, H7786), anti-Ki67 (Dako, M7248), anti-Tuj1 (Progema, G7121), anti-GFAP (Dako, Z0334), anti-Nestin (Aves labs, NES), anti-MCM2 (Santa Cruz, sc-9839). DyLight 680/800 conjugated secondary antibodies (Thermo Fisher Scientific) were used for Western blot. Alexa Fluor conjugated

secondary antibodies (Invitrogen) were used for immunofluorescence staining.

The following drugs were used: DAPT(Sigma-Aldrich), nocodazole (Sigma-Aldrich), colchicine (Sigma-Aldrich), roscovitine (Calbiochem), nimodipine (Sigma-Aldrich), Myr-CaMK IINtide (Calbiochem), STO-609 (Tocris)

In vivo proliferation of aNPCs in the adult hippocampus

Tissue processing and in vivo cell proliferation analysis were performed as previously described (Smrt et al., 2007; Zhao et al., 2003). Briefly, BrdU was dissolved in normal saline solution at a concentration of 10mg/ml, and filter sterilized. 8-9 weeks old mice received daily BrdU injections at the dose of 50mg/Kg body weight for 6 consecutive days, and were sacrificed for analysis 24 hours after the last (the 6th) BrdU injection. Stereological counting of the total number of BrdU or Ki67 labeled cells was performed under a Carl Zeiss Axioplan 2 Imaging microscope and the MBF Bioscience Stereo Investigator 8 software, using every 6th serial sections throughout the hippocampus.

In vivo differentiation of aNPCs in the adult hippocampus

Tissue processing and in vivo cell differentiation analysis were performed as previously described (Smrt et al., 2007; Zhao et al., 2003). Briefly, BrdU was dissolved in normal saline solution at a concentration of 10mg/ml, and filter sterilized. 8-9 weeks old mice received daily BrdU injections at the dose of 50mg/Kg body weight for 6 consecutive days, and were sacrificed for analysis 28 days after the last (the 6th) BrdU injection. Every 6th of the serial sections throughout the hippocampus were co-stained with an anti-BrdU antibody (to mark adult-born

cells), an anti-NeuN antibody (to mark neurons), and an anti-S100beta antibody (to mark glial cells). Quantification was done using a confocal microscope (Nikon Eclipse E600, with Nikon EZ-C1 3.50 software) to first look for immunoreactivity of BrdU, and then switch to the other channels to check whether a given BrdU positive cell was also labeled by NeuN or S100beta. Cells were identified as neurons if they were positive for both BrdU and NeuN, as glial cells if they were positive for both BrdU and S100beta, or as undifferentiated if they were only positive for BrdU. All BrdU positive cells in the subgranular zone from all stained sections were included in the analysis. Percentage of each cell fate in each mouse was determined by dividing the number of cells from each cell fate by the total number of BrdU positive cells from the hippocampus of that mouse.

Immunohistochemistry

10-12 weeks old mice were transcardially perfused with normal saline solution followed by 4% paraformaldehyde (PFA). Brains were carefully dissected out, post-fixed in 4% paraformaldehyde, cryoprotected in 30% sucrose, embedded and frozen in Tissue Tek. Serial coronal sections were cut at 40μm throughout the brain, and stained with appropriate primary and secondary antibodies.

Isolation and culture of adult NPCs

aNPCs used in this study were isolated from the DG of 6 to 8-week-old male *Mecp2*$^{S421A;S424A/y}$ mice and wild-type (WT) littermate controls based on published methods (Guo et al., 2012). Briefly, DG was microdissected from 400 μm coronal sections of forebrain. After enzymatic digestion using MACS Neural Tissue Dissociation kit (Miltenyi Biotech), DMEM/F-12

(Invitrogen) containing 10% FBS (Invitrogen) were added into each sample for stopping digestion. After filtering through a 70-μm cell strainer (BD Biosciences) and washing with DMEM/F-12, the single-cell suspension was collected and cultured with proliferation medium: Neurobasal medium (Invitrogen) containing 20 ng/ml basic fibroblast growth factor (FGF-2, Waisman Biomanufacturing), 20 ng/ml epidermal growth factor (EGF, Peprotech), B27 supplement (Invitrogen), Penicillin Streptomycin (Invitrogen), and L-glutamine(Invitrogen) in a 5% CO2 incubator at 37ºC. Half of the medium was replaced every two days.

Proliferation and differentiation assays of adult NPCs

Proliferation and differentiation of aNPCs were analyzed using published method (Guo et al., 2011b). Only early passage cells (between passage 4 and 10) and the same passage numbers of wild type and *Mecp2*$^{S421A;S424A/y}$ cells were used for the assay. For each experiment, stereological counting (Stereo Investigator, MBF Bioscience) of immunofluorescence positive cells from duplicated wells were analyzed, and results were averaged as one data point (n = 1). At least 3 independent experiments (n = 3) were performed and used for statistical analyses for each analysis.

In cell proliferation assay, we dissociated aNPCs with 0.05% Trypsin-EDTA (Invitrogen) for no longer than 1 min, stopped the digest with Trypsin inhibitor (Sigma-Aldrich) and finally plated the cells on poly-L-lysine/laminin-coated cover slips at a density of 100,000 cells/well in proliferation medium (see above). At 20 h post-plating, 5 μM 5-bromo-2deoxyuridine (BrdU, Sigma-Aldrich) was added into the culture medium for 8 hours, after which the cells were fixed with 4% paraformaldehyde for 30 min at room temperature. To detect BrdU incorporation, fixed

cells were pretreated with 1M HCl for 30 min at 37ºC, and then washed with borate buffer, pH 8.5, for 30 min. We then followed our standard immunocytochemistry protocol.

For the differentiation assay, aNPCs were similar treated and plated as in the proliferation assay, but at a density of 50,000 cells/well. At 24 h post-plating, cells were changed into differentiation medium: Neurobasal medium with 1% B27 supplement, 1% Penicillin Streptomycin (Invitrogen), 2 mM L-glutamine(Invitrogen), 5 μM forskolin (Sigma-Aldrich), 1 μM retinoic acid (Sigma-Aldrich). Half of the medium was changed with fresh differentiation medium for four days, followed by fixation with 4% paraformaldehyde for 30 min and standard immunocytochemistry protocol.

Cell cycle analysis

Cells were fixed in 2% paraformaldehyde for 15min at room temperature, and stained with Propidium Iodide (PI) (50μg/ml) in the presence of RNase A (0.1mg/ml) for 40 min at 37ºC. The stained cells were analyzed on a FACS Calibur (BD Biosciences).

Lentivirus preparation

HEK293 cells were triple transfected using the calcium phosphate method with the lentiviral expression plasmid pEF1α-NICD or pEF1α-GFP and packaging vectors (pCAG-VSV-G and pCMV Δ8.91), and were switched to fresh media after 16 hours. The supernatants containing the viral particles were collected 48 hours after transfection and concentrated by ultracentrifuge (SW32 rotor, centrifuge at 25000 rpm, 4ºC for 2.5 hours).

RNA extraction, real-time quantitative RT-PCR and Neural Stem Cell PCR Array

Total RNA was extracted from cultured adult NSCs using TRIzol Reagent (Invitrogen). The qScriptTM cDNA SuperMix kit (Quanta Biosciences) was used for cDNA synthesis. Real-time quantitative PCR was performed on StepOne Plus Real-Time PCR System (Applied Biosystems) using iQ SYBR Green Supermix (Bio-rad). Fold change was calculated with the $2^{-\text{delta Ct}}$ method after normalization to Gapdh.

Primers used are following:

Gapdh: 5'-aatgggaagcttgtcatcaacg-3' (forward), 5'-gaagacaccagtagactccacgacata-3' (reverse).

Dll1: 5'-agcgactgaggtgtaagatg-3' (forward), 5'-aacctggttctcagcagcag-3' (reverse).

Jag1: 5'-atacacgtggccatctctgc-3' (forward), 5'-aaccgcagcaataagtgagc-3' (reverse).

Jag2: 5'-cttccacaggtctgttggtg-3' (forward), 5'-tcctctcacgttctttcctg-3' (reverse).

Notch1: 5'-gaacaacaaggaggagactc-3' (forward), 5'-tccatgtgatccgtgatgtc-3' (reverse).

Notch2: 5'-caggacaataaggaagagac-3' (forward), 5'-tccatgtggtcagtgatgtc-3' (reverse).

Hes1: 5'-gcacttaagaaagatagctcc-3' (forward), 5'-ggtatttccccaacacgctc-3' (reverse).

Hes3: 5'-acactactcacatcagatacg-3' (forward), 5'-agagtccttgcagtgagttc-3' (reverse).

Hes5: 5'-gaaacacagcaaagccttcg-3' (forward), 5'-tgcagggtcaggaactgtac-3' (reverse).

Hey1: 5'-ctttgagaagcagggatctg-3' (forward), 5'-ctccgatagtccatagccag-3' (reverse).

Hey2: 5'-ggtaaaggctactttgatgcc-3' (forward), 5'-aggccttccactgagcttag-3' (reverse).

Heyl: 5'-actgcctttgagaaacaggg-3' (forward), 5'-atcaaagaaccctgtgccac-3' (reverse).

Numb: 5'-gatgccaagaaagctgagac-3' (forward), 5'-catctctgaagatgcagtgc-3' (reverse).

Tuj1: 5'-atctttggtcagagtggtgc-3' (forward), 5'-ggcagtcacaattctcacac-3' (reverse).

NeuroD1: 5'-acggatcaatcttctcttcc-3' (forward), 5'-cgtgaaagatggcattaagc-3' (reverse)

GFAP: 5'-atcggtctaagtttgcagac-3' (forward), 5'-ctccagatcgcaggtcaag-3' (reverse)

Neurogenesis and Neural Stem Cells PCR Array (Qiagen/SABiosciences, PAMM-404A, Version 3.0 system) was performed according to manufacturer's instruction. Data were analyzed using the online software from Qiagen/SABiosciences (http://pcrdataanalysis.sabiosciences.com/pcr/arrayanalysis.php).

Western blot analysis

Cultured adult NPCs were washed with PBS once and then lysed in Laemmli Sample Buffer (Bio-rad) with 0.5% 2-Mercaptoethanol at 95 ºC for 10 minutes. Sonication was used to lyse the cells and shear the genomic DNA, before the samples were subjected to SDS-PAGE. The protein samples were then transferred to Protran BA 85 nitrocellulose membranes (Whatman). The membrane was blocked by 5% dry milk, and incubated with appropriate primary and DyLight dye-conjugated secondary antibodies. The Odyssey Western Detection Methods (LI-COR Biosciences) was used for signal detection. The integrated pixel intensity values for the target protein bands were analyzed with NIH ImageJ software, and then normalized to the intensity of the control β-Actin from the same samples.

Chromatin immunoprecipitation and gene promoter specific real time PCR

Cultured aNPCs were crosslinked with 1% formaldehyde for 15 min. Crosslinking was stopped by adding 1/20 volume of 2.5M glycine. The following chromatin immunoprecipitation procedure was performed as previously described (Li et al., 2011). 20 ng of ChIP DNA and input DNA was used for each quantitative real-time PCR. Real-time quantitative PCR was performed on StepOne Plus Real-Time PCR System (Applied Biosystems) using iQ SYBR Green Supermix (Bio-rad). The ChIP DNA level was normalized to the input DNA level using the 2-delta Ct

method. Relative promoter occupancy was then calculated by setting the level of WT-MeCP2 binding as 1. Primers used in real time PCR are:

Dll1-ChIP: 5'-gtgttgagcatgccatgagc-3' (forward), 5'-ctagctccaagaatcacacc-3' (reverse)

Notch1-ChIP: 5'-tataggcatcaggaggattg-3' (forward), 5'-actcccttctacagaggctg-3' (reverse)

Statistical analysis

No statistical methods were used to predetermine sample sizes, but the samples sizes we used were similar to those generally employed in the field. Data was first tested for normality using the D'Agostino-Pearson omnibus test when necessary. Comparisons between two groups were analyzed by two-tailed paired t-test or unpaired t-test with Welch's correction, depending on the design of the experiment. Multiple comparisons in the same data set were analyzed by one-way ANOVA followed by Tukey's multiple comparisons test. $P < 0.05$ was considered to be statistically significant. Statistical processing was performed using Microsoft Excel and GraphPad Prism Software.

Chapter 4: Phenotype characterization of other *Mecp2* phosphor-mutant mice

Part of this chapter is being prepared for publication.

Summary

MeCP2 can be phosphorylated at multiple sites by diverse extrinsic and intrinsic signals. In order to understand the physiological significance of each of those phosphorylation events, we have generated *Mecp2* phosphor-mutant mice either abolish or mimic phosphorylation at a given amino acid. We have previously shown that loss of S421 phosphorylation leads to enhanced hippocampus-dependent learning and memory and altered adult neurogenesis. Here we describe the phenotypic characterization of the $Mecp2^{S80A}$ and the $Mecp2^{S421E}$ mice. Consistent with the observation that phosphorylations of MeCP2 at S80 and S421 are dynamically regulated in opposite manners, we report here that the loss of S80 phosphorylation results in several phenotypes that are opposite to those caused by the loss of S421 phosphorylation. Moreover, mimicking S421 phosphorylation with the S421E mutation also results in phenotypes that are opposite to those caused by abolishing S421 phosphorylation. These results further confirm the physiological significance of S421 phosphorylation, and highlight the importance to balance the regulation of phosphorylation across multiple sites on MeCP2

Introduction

Rett syndrome, first described by Andreas Rett in 1966 (Rett, 1966), is an autistic spectrum postnatal neurodevelopmental disorder that predominantly affects girls (Hagberg, 1985). It is estimated that one out of every 10000-15000 females develops Rett syndrome, characterized by the loss of acquired language and motor skills, stereotype wringing hand movement, gait ataxia, and social withdraw (Chahrour and Zoghbi, 2007). Mutations in the X-linked *MECP2* gene account for up to 96% of classic Rett syndrome cases (Trappe, et al., 2001). MeCP2, a member of the methyl-CpG binding protein family, is highly expressed in the brain and binds to methylated cytosines broadly across the genome (Nan et al., 1997; Skene et al., 2010).

MeCP2 is dynamically regulated by phosphorylation upon neuronal activity, suggesting MeCP2 may function as an epigenetic regulator that integrates diverse signals from the environment (Chen et al., 2003b; Tao et al., 2009; Zhou et al., 2006). Thus far, more than ten MeCP2 phosphorylation sites have been identified by multiple labs (Ebert et al., 2013; Tao et al., 2009; Zhou et al., 2006), among which S80 and S421 have drawn more attention as the phosphorylations at these two sites are regulated by the same stimulus-neuronal activity in an opposite manner. Specifically, S80 is phosphorylated in resting neurons but dephosphorylated in active neurons, whereas S421 is dephosphorylated in resting neurons but phosphorylated in active neurons (Tao, et al., 2009; Zhou, et al., 2006). Similar to S421, S424 phosphorylation is also induced by neuronal activity (Tao et al., 2009). To elucidate the *in vivo* function of MeCP2 phosphorylation, we generated knockin mice with serine to alanine mutations to abolish MeCP2 phosphorylations. Interestingly, *Mecp2*^{S80A} mice showed decreased locomotor activity, whereas *Mecp2*$^{S421A;S424A}$ mice presented increased locomotor activity, suggesting possible opposing

functions of S80 and S421/S424 phosphorylation *in vivo*(Tao, at al., 2009). Later, comprehensive characterization of the *Mecp2*$^{S421A;S424A}$ mice indicated that loss of MeCP2 S421/S424 phosphorylation leads to enhanced synaptogenesis, LTP, and spatial memory (Li et al., 2011), impaired synaptic homeostasis (Zhong et al., 2012), and altered adult neurogenesis (unpublished data). It is worth noting that *Mecp2*$^{S421A/y}$ mice exhibit increased dendritic complexity and abnormal behavioral responses to novelty (Cohen et al., 2011).

To unequivocally confirm the findings from mice with phospho-abolishing mutations, we have generated knockin mice with serine to glutamic acid mutation mimicking S421 phosphorylation. Initial phenotype characterization revealed impaired contextual fear memory in *Mecp2*$^{S421E/y}$ mice. We also continued the study on S80 phosphorylation and show here that *Mecp2*^{S80A} mice exhibit increased anxiety, impaired hippocampal spatial learning and abnormal adult neurogenesis. Our results added another important piece to the functional spectrum of MeCP2 phosphorylation and further illustrated the importance of MeCP2 phosphorylation for brain development and function.

Results

Initial phenotype characterization reveals impaired contextual fear memory in *Mecp2*$^{S421E/y}$ mice

The *Mecp2*^{S421E} targeting construct was linearized and electroplated into mouse ES cells. Correctly targeted clones were identified by Southern blot analysis and genomic DNA sequencing (data not shown), and then injected into blastocysts to generate chimeric mice. The chimeric mice were crossed with C57/B6 mice to achieve germ-line transmission of the *Mecp2*^{S421E} allele. Genomic DNA sequencing confirms S421E mutation at the endogenous *Mecp2* locus in *Mecp2*$^{S421E/y}$ mice (**Fig. 1a**). In the brain nuclear extracts prepared from *Mecp2*$^{S421E/y}$ mice, MeCP2^{S421E} protein was expressed at a similar level to those in wild type and *Mecp2*$^{S421A;S424A/y}$ mice (**Fig. 1b**). However, MeCP2^{S421E} protein migrated more slowly than WT MeCP2 and MeCP2$^{S421A;S424A}$ during SDS–polyacrylamide gel electrophoresis (SDS-PAGE), mimicking the slow-migrating property of the S421 phosphorylated MeCP2 **(Fig. 1b)**. Furthermore, MeCP2^{S421E} protein was also readily detected by a phospho-S421 specific antibody **(Fig. 1b)**, providing evidence that the S421E mutation in MeCP2 is indeed mimicking S421 phosphorylation.

The *Mecp2*$^{S421E/y}$ mice bred normally, had a normal lifespan, and showed none of the RTT phenotypes observed in the *Mecp2* null mice (data not shown). 6 pairs of *Mecp2*$^{S421E/y}$ mice and their wild type littermates, which had been backcrossed to C57BL/6 background for 2-3 generations, were taken for an initial behavioral phenotype characterization. We first performed

open-field test to examine exploratory activity and anxiety. The *Mecp2*$^{S421E/y}$ mice showed normal amount of exploratory activity, measured by the total distance traveled (**Fig. 2a**), and normal level of anxiety, measured by the percentage of distance mice traveled in the center of the testing box (**Fig. 2b**), as compared to their wild type littermates. We then performed the contextual fear conditioning paradigm, a hippocampus/amygdala function-dependent learning and memory task. The contextual fear memory was measured by the amount of freezing behavior 24 hours after the training. Neither the *Mecp2*$^{S421E/y}$ nor wild type mice showed any baseline freezing to the testing environment (**Fig. 2c**). The *Mecp2*$^{S421E/y}$ mice displayed less freezing than their wild type littermates (**Fig. 2c**), suggesting a constitutive phosphorylation at S421 might actually blocks memory formation. This data, combined with the previous report that *Mecp2*$^{S421A;S424A}$ mice show enhanced contextual fear memory, strongly indicate a important role of MeCP2 S421 phosphorylation in learning and memory. A complete behavioral characterization will be performed on the *Mecp2*$^{S421E/y}$ mice, when the mice are backcrossed to C57BL/6 background for a minimum of 10 generations.

Behavioral abnormality of the *Mecp2*^{S80A} mice

Phosphorylation of MeCP2 at S80 and S421/S424 are dynamically regulated in opposite manners by neuronal activity (Tao et al., 2009). More interestingly, *Mecp2*^{S80A} mice showed decreased locomotor activity, whereas *Mecp2*$^{S421A;S424A}$ mice presented increased locomotor activity(Tao et al., 2009), suggesting that S80 and S421 phosphorylations might indeed play opposing roles in the brain. A comprehensive behavioral characterization of *Mecp2*$^{S421A;S424A}$ mice has been

performed previously (Li et al., 2011), and it becomes necessary to extend the study to the *Mecp2*^{S80A} mice.

Mass spectrometry analysis reveals that ~35% of MeCP2 purified from mouse brain is phosphorylated at S80 and S80 phosphorylation is the most predominant posttranslational modification of MeCP2 at normal condition in our analysis (unpublished data). We hypothesize a significant contribution of S80 phosphorylation to the physiological function of MeCP2. We performed a series of behavioral analyses of *Mecp2*^{S80A} mice, and compare the phenotypes to what have been observed the *Mecp2* deficient mice and the *Mecp2*$^{S421A;S424A}$ mice. As previous report suggested a critical requirement of MeCP2 at 25-30 weeks of age in mice (Cheval et al., 2012), we chose to use 5-6 months old *Mecp2*^{S80A} mice and their littermates control in all the behavioral tests.

To eliminate potential influence of different genetic backgrounds on animal behavior, we had backcrossed the *Mecp2*^{S80A} mice with the C57BL/6 mice for more than 10 generations. The *Mecp2*^{S80A} mice had normal life span, showed normal brain weight and body weight, and exhibited no classic RTT phenotypes (e.g. hindlimb clasping) (data not shown). RTT patients suffer from severe motor impairment, and motor coordination deficit have been observed in several mouse models for RTT. The *Mecp2*^{S80A} mice, however, didn't show any motor coordination dysfunction in rotarod test (**Supplementary Fig. 1a**).

Then, we performed the open-field test to examine the exploratory activity and anxiety. *Mecp2*^{S80A} mice traveled similar total distance as their wild type littermates (**Supplementary Fig. 1b)**, suggesting a normal level of exploratory activity. However, *Mecp2*^{S80A} mice traveled less

percentage of distance in the center of the open field environment than their wild type littermates (**Fig. 3a**), suggesting an increased anxiety level of *Mecp2*^{S80A} mice. Increase anxiety behavior was previously observed in the *Mecp2* deficient mice (Gemelli et al., 2006). To confirm this increased anxiety behavior in *Mecp2*^{S80A} mice, we also examined the mice in another anxiety assay, the light-dark exploration paradigm. The *Mecp2*^{S80A} mice, again, showed an increased anxiety level compared with their wild type littermates, as measured by the times of light-dark transitions mice made and the percentage of time mice spend in the light box (**Fig. 3b-c**).

To determine whether the loss of MeCP2 S80 phosphorylation leads to altered learning and memory, we first perform fear conditioning test. *Mecp2*^{S80A} mice and their wild type littermates were tested using a delayed fear conditioning paradigm, which is designed to test both context and cue-dependent fear memory. Cue-dependent fear memory is dependent on amygdala function, whereas contextual fear memory requires both hippocampus and amygdala functions. The fear conditioning memory was measured by the percentage of freezing time mice spent in the test environment. In the context test, *Mecp2*^{S80A} mice showed no difference in freezing time compared with wild type littermates (**Fig. 3d**). However, *Mecp2*^{S80A} mice froze significantly more than their wild type littermates in the cue test, suggesting an enhanced cue-dependent fear memory (**Fig. 3d**). The combination of results from the context test and the cue test indicate a different requirement of MeCP2 S80 phosphorylation in hippocampus and amygdala for regulating the fear memory.

Finally, to assess hippocampus-dependent spatial learning and memory, we evaluated the *Mecp2*^{S80A} mice in Morris water maze paradigm. *Mecp2*^{S80A} mice and their wild type littermates were trained to locate a hidden platform in a swimming pool with a total of 8 training trials in

four days. As the training continued, *Mecp2*^{S80A} mice did not perform as well as their wild type littermates did, as it took longer time for *Mecp2*^{S80A} mice to find the platform in the last two training trials (**Fig. 3e**). When the platform was removed during the pos-training probe trial, wild type mice showed good spatial memory as they spent more time in the target quadrant than in the other three quadrants (**Fig. 3f**). *Mecp2*^{S80A} mice, however, had difficulty locating the target quadrant and spent equal time in the four quadrants (**Fig. 3f**). Moreover, *Mecp2*^{S80A} mice also crossed the original platform location less frequently than their wild type littermates did (**Fig. 3g**). To rule out the involvement of swimming speed, we measured the swimming velocity of *Mecp2*^{S80A} mice and their wild type littermates during the training, and observed no significant difference between the two genotypes (**Supplementary Fig. 1c)**. To further rule out other possible factors, such as blindness and escape motivation difference, *Mecp2*^{S80A} mice and their wild type littermate were trained in a visible platform version of Morris water maze and the two groups performed equally well finding the platform (**Supplementary Fig. 1d)**. As a summary, this result indicates an impaired spatial learning and memory in *Mecp2*^{S80A} mice.

Thus far, we have observed some opposite phenotypes between *Mecp2*$^{S421A;S424A}$ mice and *Mecp2*^{S80A} mice, including locomotor activity and hippocampus-dependent spatial learning (Li et al., 2011; Tao et al., 2009). To assess the possibility that misregulation of some common target genes might underlie these phenotypes, we examined the mRNA level of *Bdnf* and *Mef2c* in the hippocampus of *Mecp2*^{S80A} mice and their wild type littermates. Both of the genes were misregulated in the hippocampus of *Mecp2*$^{S421A;\ S424A/y}$ mice (Li et al., 2011), and also misexpressed in *MeCP2* null and *MeCP2*^{Tg} mice in opposite manners (Chahrour et al., 2008). However, the mRNA level of *Bdnf* and *Mef2c* is indistinguishable between the *Mecp2*^{S80A} and

wild type mice (**Supplementary Fig. 2a**). The mRNA level of two glutamate receptor genes, *Gria1* and *Gria2*, was also examined. *Mecp2*^{S80A} mice presented subtle, however significantly, reduced level of *Gria2* (**Supplementary Fig. 2a)**.

Previously, in a study using cultured cortical neurons with lentiviruses-mediated expression of wild type MeCP2 or MeCP2^{S80A}, *Igsf4b*, *Rab3d* and *Vamp3* were identified as MeCP2 target genes, and their expressions were upregulated in MeCP2^{S80A} expressing neurons. However, we were not able to validate these changes using mRNA purified from either cultured cortical neurons or the adult brains from the *Mecp2*^{S80A} mice and their wild type littermates (**Supplementary Fig. 2b-c)**.

Altered proliferation and neuronal differentiation in *Mecp2*^{S80A}adult neural progenitor cells

Previously, we reported that MeCP2 S421 phosphorylation is regulated by cell cycle in adult neural progenitor cells (aNPCs). And *Mecp2*$^{S421A;S424A}$aNPCs show decreased proliferation and increased neuronal differentiation *in vitro* and *in vivo* (Chapter 3). Given the contrasting regulation and function of S80 and S421 phosphorylation in neurons, we decided to extend our study of S80 phosphorylation to adult neurogenesis.

We isolated aNPCs from the dentate gyrus of adult wild type and *Mecp2*$^{S80A/y}$ hippocampus. To assess the proliferation of wild type and *Mecp2*$^{S80A/y}$ aNPCs, we pulsed-labeled the cells with BrdU for 8 hours. Quantification of the labeled cells revealed that *Mecp2*$^{S80A/y}$ aNPCs showed larger BrdU incorporation percentage than the WT cells did (**Fig. 4a-b**), suggesting an increased

proliferating potential of *Mecp2*$^{S80A/y}$ aNPCs. Under differentiation condition, both wild type and *Mecp2*$^{S80A/y}$ aNPCs can be differentiated into Tuj1 positive neurons and GFAP positive astrocytes (**Fig. 4c, e**). *Mecp2*$^{S80A/y}$ aNPCs exhibited decreased proportion of cells with Tuj1 immunoreactivity (**Fig. 4c-d**), indicating reduced potential in neural differentiation. In contrast, no difference in astrocyte differentiation was observed between the WT and *Mecp2*$^{S80A/y}$ aNPCs (**Fig. 4e-f**). The reduced neuronal differentiation of *Mecp2*$^{S80A/y}$ aNPCs was further confirmed by RT-qPCR analysis for the expression of *NeuroD1* and *Tuj1* in differentiated WT and *Mecp2*$^{S80A/y}$ aNPCs (**Fig. 4g**). In addition, when aNPCs were isolated from the forebrain of adult WT and the *Mecp2*$^{S80A/y}$ mice, the *Mecp2*$^{S80A/y}$ aNPCs also presented decreased neural differentiation as determined by the percentage of Tuj1 positive cells, *Tuj1* transcription and *NeuroD1* promoter driven luciferase expression (**Supplementary Fig. 3a-c)**. In summary, *Mecp2*$^{S80A/y}$ aNPCs show increased proliferation and reduced neuronal differentiation potential, opposite to what *Mecp2*$^{S421A;S424A/y}$ aNPCs do. The opposite phenotypes in adult neurogenesis in the *Mecp2*$^{S80A/y}$ and *Mecp2*$^{S421A;S424A/y}$ mice, together with previous findings that *MeCP2* null mice exhibited normal aNPC proliferation and differentiation (Smrt et al., 2007), suggest that MeCP2 S80 and S421 phosphorylations play opposite but balanced roles in regulating adult neurogenesis.

Because Notch signaling is down-regulated in *Mecp2*$^{S421A;S424A/y}$ aNPCs, and overexpression of NICD is sufficient to rescue the phenotypes of *Mecp2*$^{S421A;S424A/y}$ aNPCs (Chapter 3). We examined the expression level of major Notch signaling components (including ligands, receptors and target genes) in *Mecp2*$^{S80A/y}$ and wild type aNPCs, but found no significant differences between the two genotypes (**Supplementary Fig. 4a-b)**.

Discussion

This chapter contains the results from several ongoing projects to further investigate the role of MeCP2 phosphorylation in brain development and function. Most of data are from phenotype characterizations of the *Mecp2*$^{S421E/y}$ and *Mecp2*$^{S80A/y}$ mice in behavioral and adult neurogenesis analysis. Detailed cellular and molecular assays will be performed in the future.

Mecp2$^{S421A;S424A/y}$ mice showed enhanced learning and memory in contextual fear conditioning test (Li et al., 2011). While still in a mixed genetic background, *Mecp2*$^{S421E/y}$ mice exhibited learning and memory deficit in the same test. This preliminary result suggests that induction of S421 phosphorylation alone might be sufficient to alter learning and memory function and further raises the question that whether S424 phosphorylation is involved in this process. One possibility is that S424 phosphorylation is not required for normal contextual fear memory. However, it is also possible that S424 phosphorylation is downstream of S421 phosphorylation in the same functional pathway. Actually, the MeCP2 sequence from S421 to S424, when S421 is phosphorylated, matches the consensus phosphorylation site of Casein kinase 1(pS/T-X-X-S/T). The possible crosstalk between S421 and S424 phosphorylation requires further investigation. Comprehensive characterization of the *Mecp2*$^{S421E/y}$ mice at behavioral, cellular, and molecular level will be performed when the mice are backcrossed into pure C57/B6 background. In the meanwhile, *Mecp2*$^{S424A/y}$ and *Mecp2*$^{S424E/y}$ knockin mice should be generated to elucidate the physiological function of S424 phosphorylation.

Mecp2$^{S80A/y}$ didn't show any classic RTT phenotypes. However, the reduced locomotor activity, increased anxiety and impaired spatial learning phenotypes of *Mecp2*$^{S80A/y}$ were also reported in

Mecp2 deficient mice (Gemelli et al., 2006; Moretti et al., 2006), suggesting that S80 phosphorylation is required for some, but not all, aspects of MeCP2 function. Although the *Mecp2*$^{S80A/y}$ and *Mecp2*$^{S421A;S424A/y}$ mice exhibit opposite phenotypes in multiple assays, we failed to detect opposite gene expression changes between the two genotypes by a candidate gene approach. *Gria2,* a gene encoding one of the predominant excitatory neurotransmitter receptors in the brain, is down-regulated in the *Mecp2*$^{S80A/y}$ hippocampus. The functional consequence of reduced *Gria2* expression merits further investigation.

The fact that *Mecp2*$^{S80A/y}$ showed increased anxiety and cue fear memory deficit indicates a malfunction of amygdala, an anatomical region important for the processing of fear memory and emotional reactions. When a good pS80 phospho-specific antibody becomes available, it will be interesting to examine whether S80 phosphorylation is dynamically regulated in the amygdala during and after behavioral training. Gene expression study in the amygdala of *Mecp2*$^{S80A/y}$ mice should be performed to identify the target genes responsible for these phenotypes.

Mecp2$^{S80A/y}$ and *Mecp2*$^{S421A;S424A/y}$ aNPCs showed contrasting phenotypes in proliferation and neuronal differentiation. We propose that MeCP2 phosphorylation function as a regulatory switch on the chromosome accessible to diverse extrinsic and intrinsic stimuli acting through distinct signaling pathways in regulating adult neurogenesis. S80 and S421 phosphorylation plays opposite roles assisting aNPCs to decide to further proliferate or differentiate into neurons. Upon certain stimuli, alteration of a given phosphorylation status will facilitate the adaptive response of adult neurogenesis. MeCP2 S421 phosphorylation is maintained in proliferating aNPCs and regulated by cell cycle. Currently, the upstream trigger for S80 phosphorylation is still unknown. As for the downstream pathways, we provide evidence that S421 phosphorylation

might act through Notch signaling pathway. However, Notch signaling remains unchanged in *Mecp2*$^{S80A/y}$ aNPCs, suggesting the involvement of other signaling pathways.

Figures

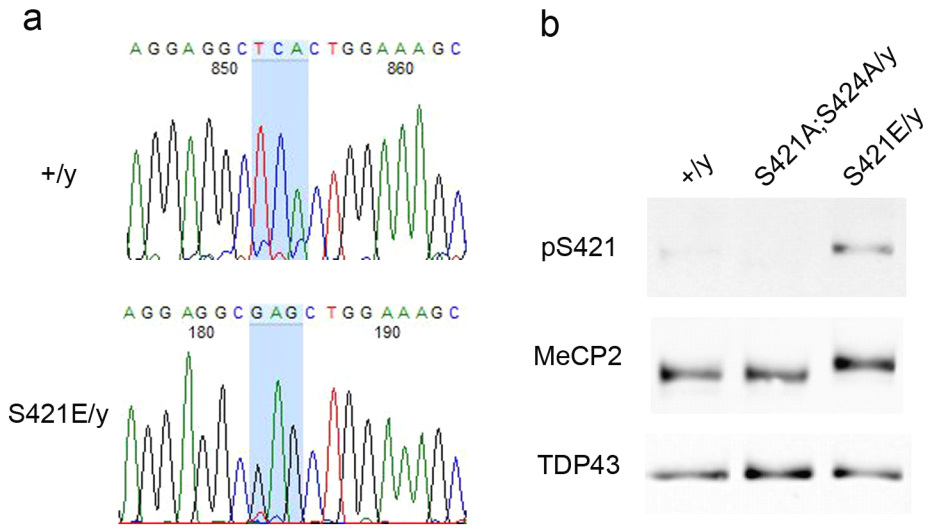

Figure 1: Characterization of *Mecp2*$^{S421E/y}$ mice

(a) Genomic DNA from WT (+/y) and *Mecp2*$^{S421E/y}$ mice was amplified by PCR and sequenced. Sequencing results illustrate the WT sequence TCA (encoding serine) was mutated to GAG (encoding glutamic acid) in *Mecp2*$^{S421E/y}$ mice. **(b)** Western blot analysis of MeCP2 and pS421 in brain nuclear function from +/y, *Mecp2*$^{S421A;S424A/y}$ and *Mecp2*$^{S421E/y}$ mice. A nuclear protein TDP43 was used as a sample loading control.

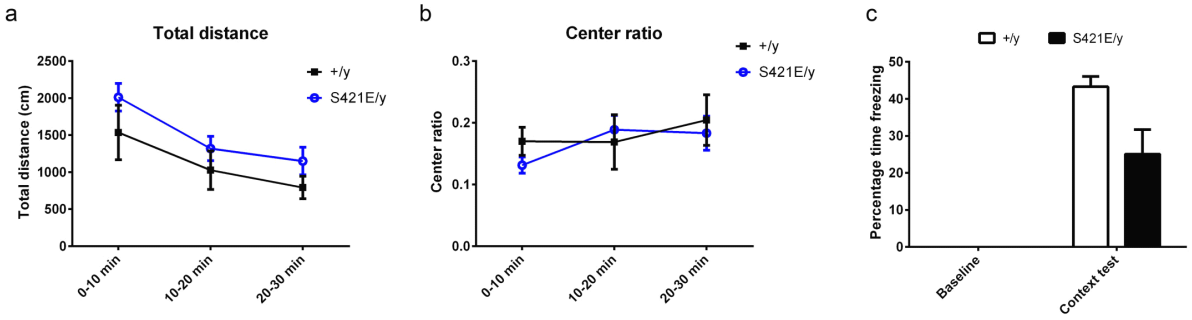

Figure 2: Impaired contextual fear memory in *Mecp2*$^{S421E/y}$ mice

(a) The total distance WT and *Mecp2*$^{S421E/y}$ mice traveled in the open field test. (two-way ANOVA with repeated measures, p=0.24, F (1,10) =1.5. n=6 in each group). **(b)** the percentage distance WT and *Mecp2*$^{S421E/y}$ mice traveled in the center of the open field testing box. (two-way ANOVA with repeated measures, p= 0.75, F (1,10) =0.11. n=6 in each group). **(c)** Percentage time of freezing WT and *Mecp2*$^{S421E/y}$ mice spent during the pre-shock training (baseline) and the context test in contextual fear conditioning paradigm. (unpaired t-test, p=0.050, n=5 for *Mecp2*$^{S421E/y}$ and n=4 for WT) The bar graph shows the mean ± s.e.m

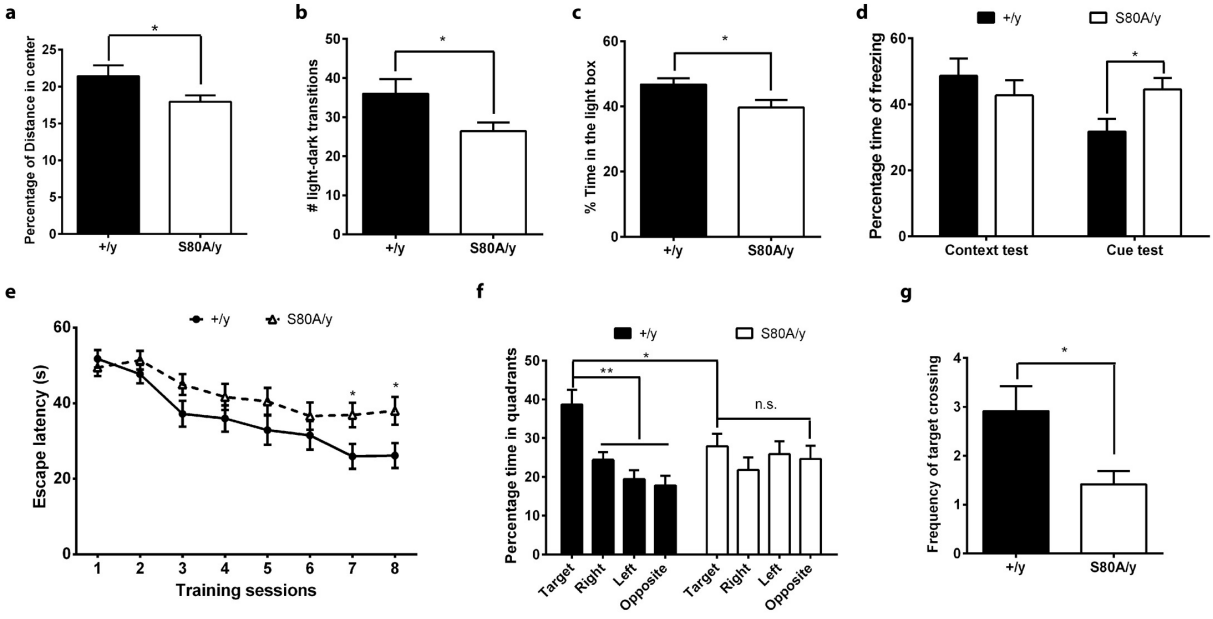

Figure 3: Behavioral abnormality of *Mecp2*^{S80A} mice

(a) The percentage distance WT and *Mecp2*$^{S80A/y}$ mice traveled in the center of the open field testing box. (unpaired t-test, p=0.0495, n=16 in each group) **(b)** The frequency of light-dark transitions WT and *Mecp2*$^{S80A/y}$ mice made in the light-dark exploration test. (unpaired t-test, p=0.0456, n=10 in each group) (c) The percentage of time WT and *Mecp2*$^{S80A/y}$ mice spent in the light box during the light-dark exploration test. (unpaired t-test, p=0.0296, n=10 in each group) **(d)** Percentage time of freezing WT and *Mecp2*$^{S80A/y}$ mice spent during the context test and the cue test in fear conditioning paradigm. (context test: p=0.396; cue test: p=0.0180; unpaired t-test, n=18 for WT and n=19 for *Mecp2*$^{S80A/y}$). **(e)** Escape latency of WT and *Mecp2*$^{S80A/y}$ mice during the Morris water maze training. (two-way ANOVA with Fisher's LSD *post hoc test*, genotype factor: p=0.0591, F(1,45)=3.751; interaction between genotype and training sessions: p=0.109,

F(7,315) =1.697; latency in session 7 WT vs *Mecp2*$^{S80A/y}$: p=0.0165; latency in session 8 WT vs *Mecp2*$^{S80A/y}$: p=0.010; n= 23 for WT and n=24 for *Mecp2*$^{S80A/y}$) **(f)** Percentage of time WT and *Mecp2*$^{S80A/y}$ mice spend in four quadrants during the post-training probe trial of the Morris water maze test (two-way ANOVA with Fisher's LSD *post hoc test*, interaction between genotype and quadrants: p=0.0384, F(3,135)=2.89; WT target quadrant vs other quadrants : p<0.01; *Mecp2*$^{S80A/y}$ target quadrant vs other quadrants: p>0.05; percentage of time in the target quadrant WT vs *Mecp2*$^{S80A/y}$: p=0.0128; n= 23 for WT and n=24 for *Mecp2*$^{S80A/y}$) **(g)** frequency of target crossings WT and *Mecp2*$^{S80A/y}$ mice made during the probe trial. (unpaired t-test, p=0.0145, n= 23 for WT and n=24 for *Mecp2*$^{S80A/y}$). The bar graph shows the mean ± s.e.m * p<0.05 ** p<0.01.

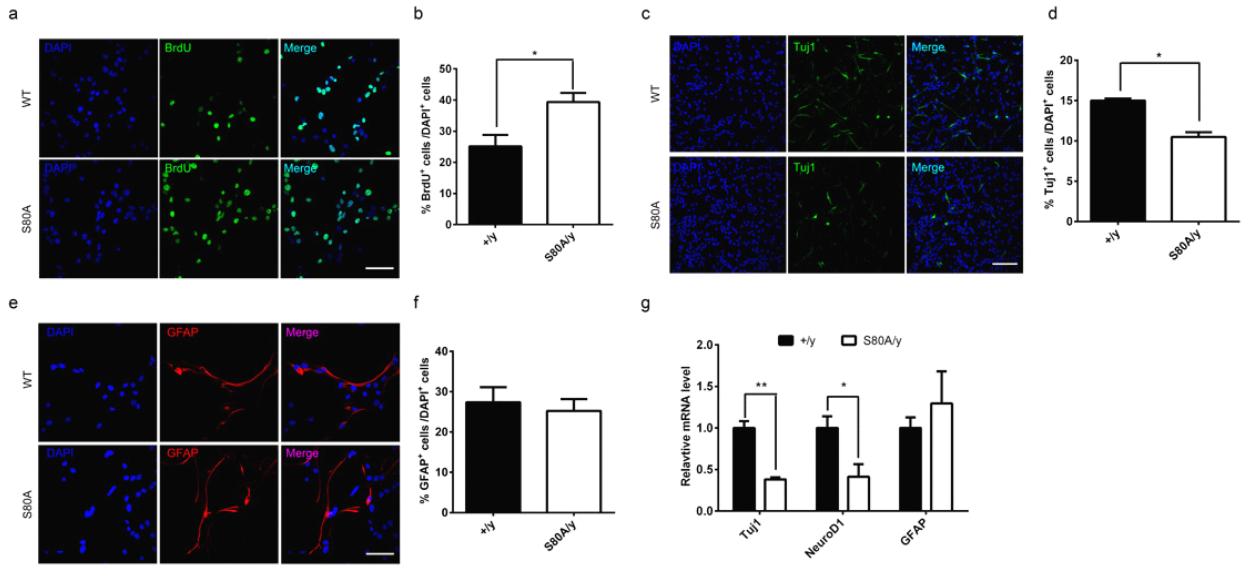

Figure 4: Altered proliferation and neuronal differentiation of *Mecp2*$^{S80A/y}$ aNPCs

(a, b) Representative images and quantification of aNPCs isolated from wild type and *Mecp2*$^{S80A/y}$ adult hippocampus with BrdU pulse labeling, followed by immunocytochemistry analysis (unpaired t-test, p=0.0419, n=3 in each group). **(c,d)** Representative immunocytochemistry images and percentage quantification of Tuj1+ neurons differentiated from WT and *Mecp2*$^{S80A/y}$ aNPCs (unpaired t-test, p=0.0019, n=4 in each group). **(e,f)** Representative immunocytochemistry images and percentage quantification of GFAP+ astrocyte differentiated from WT and *Mecp2*$^{S80A/y}$ aNPCs (unpaired t-test, p=0.677, n=3 in each group).**(g)** Relative mRNA level of neuronal marker (*Tuj1* and *NeuroD1*) and astrocyte marker (*GFAP*) in WT and *Mecp2*$^{S80A/y}$ aNPCs under differentiation condition, assayed by RT-qPCR. (unpaired t-test, *Tuj1* p=0.00196, *NeuroD1* p=0.0468, *GFAP* p=0.509, n=3 in each group) The bar graph shows the mean ± s.e.m * p<0.05 ** p<0.01. Scale bars: 50 μm

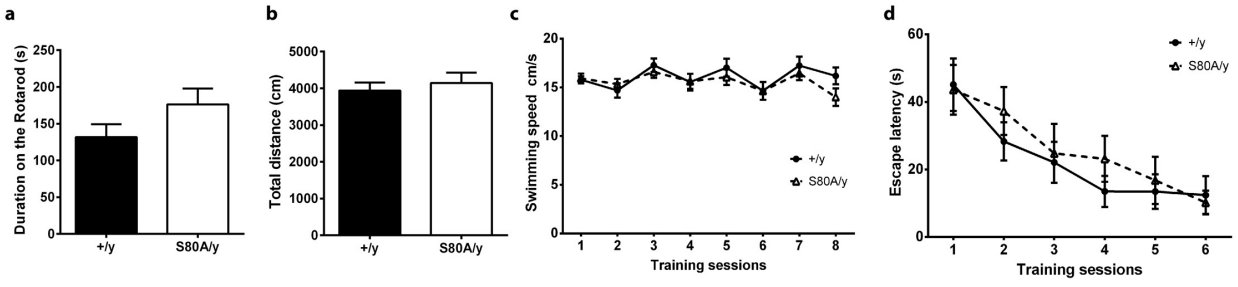

Supplementary Figure 1: Behavioral analysis of the *Mecp2*$^{S80A/y}$ mice

(a) Latency to fall from the rotarod of WT vs *Mecp2*$^{S80A/y}$ mice in a accelerating rotarod test. (unpaired t-test, p=0.119, n=18 for WT and n=19 for *Mecp2*$^{S80A/y}$) **(b)** The total distance WT and *Mecp2*$^{S80A/y}$ mice traveled in the open field test. (unpaired t-test, p=0.570, n=16 for each group) **(c)** The swimming speed of WT and *Mecp2*$^{S80A/y}$ mice during the Morris water maze training. (Two-way ANOVA, p=0.6064, F(1,45)=0.269, n=23 for WT and n=24 for *Mecp2*$^{S80A/y}$) **(d)** Escape latency of WT and *Mecp2*$^{S80A/y}$ mice during the visible platform version of water maze training. (Two-way ANOVA, p=0.6616, F(1,8)=0.2065, n=5 for each genotype) The bar graph shows the mean ± s.e.m

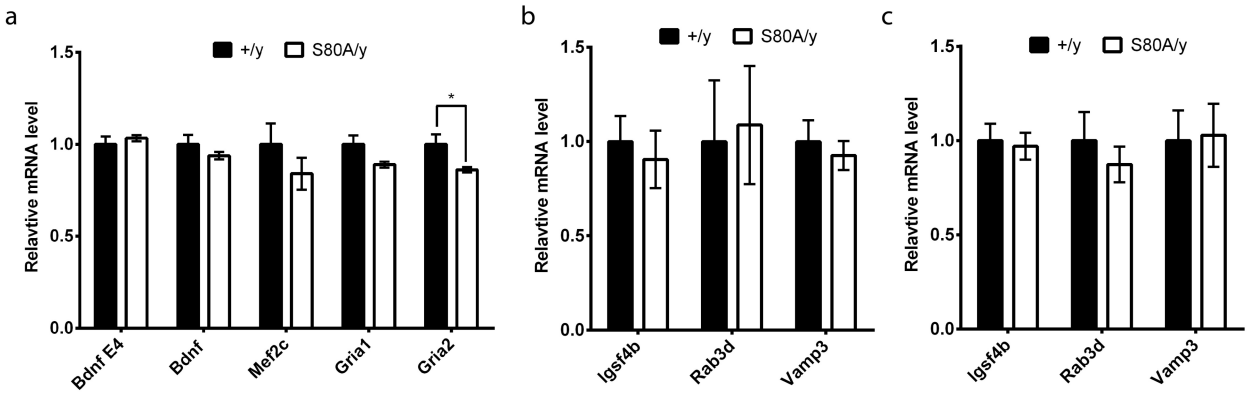

Supplementary Figure 2: Expression level of selected genes in *Mecp2*$^{S80A/y}$ mice

(a) Relative mRNA level of *Bdnf* Exon 4 (E4), *Bdnf*, *Mef2c*, *Gria1* and *Gria2* in WT and *Mecp2*$^{S80A/y}$ hippocampus. (unpaired t-test, p=0.033 for *Gria2*, n=6 in each group) **(b,c)** Relative mRNA level of *Igsf4b*, *Rab3d* and *Vamp3* in cultured cortical neurons (b) or whole brains (c) of WT and *Mecp2*$^{S80A/y}$ mice. The bar graph shows the mean ± s.e.m * $p<0.05$

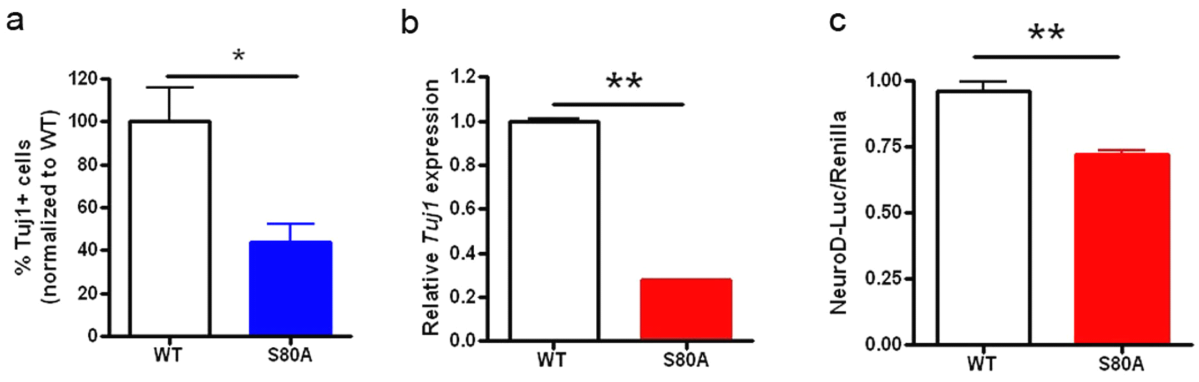

Supplementary Figure 3: Altered neural differentiation of *Mecp2*$^{S80A/y}$ aNPC isolated from forebrain.

aNPCs isolated from the forebrain of WT and *Mecp2*$^{S80A/y}$ mice exhibit reduced neuronal differentiation, assayed by stereology counting of Tuj1+ cells (**a**), RT-qPCR analysis of *Tuj1* RNA level (**b**), and NeuroD1 promoter-driven luciferase reporter level (**c**). The bar graph shows the mean ± s.e.m * $p<0.05$ ** $p<0.01$.

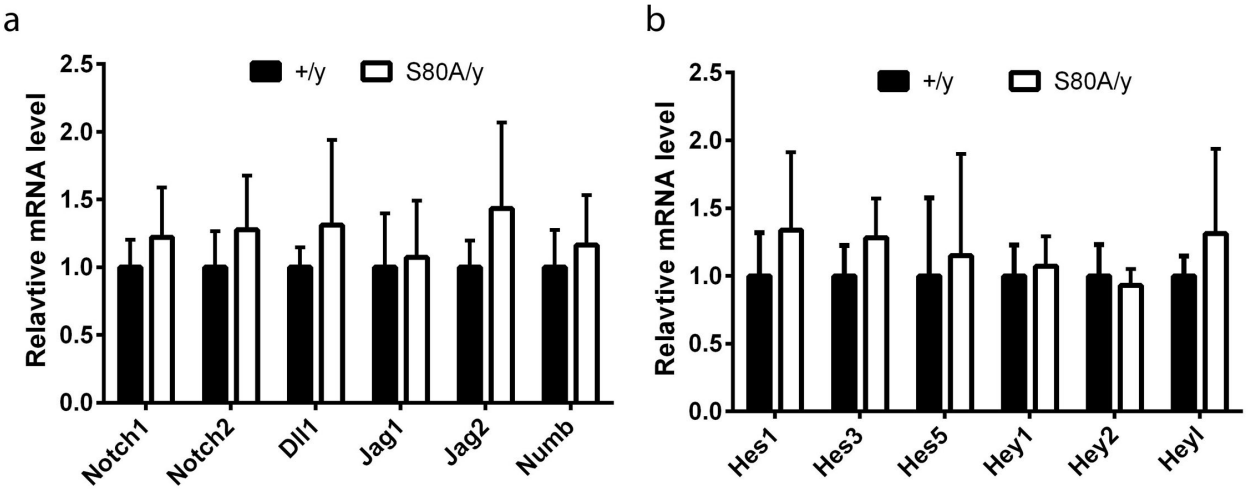

Supplementary Figure 4: Expression level of Notch signaling genes in *Mecp2*$^{S80A/y}$aNPCs

Relative mRNA level of Notch signaling major components **(a)** and target genes **(b)** in WT and *Mecp2*$^{S80A/y}$ aNPCs. The bar graph shows the mean ± s.e.m

Materials and methods

Animals

All the experiments were performed using male mice. *Mecp2*$^{S80A/y}$ mice have been backcrossed to C57BL/6 background for more than 10 generations. *Mecp2*$^{S421E/y}$ mice are in the process of backcrossing to achieve pure genetic background. Mice were housed in 12hr light (6am-6pm)/12 hr dark (6pm-6am) cycle. Mice were housed <5 mice/cage. All protocols were approved by the Institutional Animal Care and Use Committee at University of Wisconsin-Madison.

Antibodies and drugs

The following primary antibodies were used: Anti-MeCP2 (Cell Signaling, 3456), Anti-MeCP2 (Abcam, ab50005), Anti phospho-S421 (custom made by Phospho-solution), anti-β-Actin (Sigma-Aldrich, a5441), anti-TDP43 (Proteintech, cat#:10782-2-AP)

Western blot analysis

Brain nuclear extract lysate was run on 8% SDS-PAGE gel (Bio-rad). The protein samples were then transferred to Protran BA 85 nitrocellulose membranes (Whatman). The membrane was blocked by 5% dry milk, and incubated with appropriate primary and DyLight dye-conjugated secondary antibodies. The Odyssey Western Detection Methods (LI-COR Biosciences) was used for signal detection.

Mouse behavioral tests

All protocols were approved by the Institutional Animal Care and Use Committee at University

of Wisconsin-Madison.

Open field test: Each mouse was placed in the center of a transparent plastic chamber and allowed to explore freely for 30 min. The activity of the mice are automatically detected by the Fusion Node system (Accuscan Instruments). Data collection and analysis were performed using Fusion software. (Accuscan Instruments)

Rotarod test: Mice were placed onto a horizontal rotating rod, with the rotation speed accelerating from 2 rpm to 20 rpm over 5 min. A test lasted from the time the mouse was placed on the rod until it fell off or until 5 min had elapsed.

Light-dark exploration: The testing chamber consists of two unequal compartments: a smaller dark partition painted black and covered by a lid and a larger uncovered compartment with transparent sides. The two parts are connected with a small aperture located in the bottom center. The mice were placed in the center of the light compartment and allowed to explore freely in the testing chamber for 10 min. The duration of time spent in each compartment and the transitions between the two compartments are manually recorded.

Fear conditioning test: In delay training paradigm, mice were placed into a shock chamber and allowed to explore for 2 min. Then, a white noise tone (87 dB) sounded for 30 sec (conditional stimulus or "CS"). During the last 1.5 sec of the tone, mice received a mild footshock (0.5 mA) (unconditioned stimulus or "US"). 2 min later, the same tone-footshock (CS-US) combination was delivered again. 1 min after the end of the second CS-US, mice were returned to their home cages. The context test was performed 22 hr after the training. During the test, mice were placed back into the same training chamber, and monitored by an overhead camera in the

chamber for 5 min. 2 hr after the context test, the cue test was performed, in which colored plexiglass inserts were placed into the training chamber to hide the shock grid and to change the "context" of the chamber. Mice were then placed in the chamber and monitored by the overhead camera for 6 min, during which two CS (spaced the same way as in the training session) were given. In contextual only training paradigm, everything stayed the same except that no tones (CS) were given. Only the context test was administered on the mice trained. All events in the fear conditioning test were programmed and data recorded through the FreezeFrame2 and FreezeView software from (Actimetrics Software, Wilmette, IL, USA).

Morris water maze: Mice were trained to locate a hidden platform (1 cm below the surface of the water) in a circular pool (1.20 m in diameter) of opaque water using distal visual cues. Mice were given 2 blocks of 4 training trials a day for 4 consecutive days. During a training trial, each mouse was released into the pool from 1 of 4 starting positions in a random order. The location of the hidden platform remained constant throughout training. Time to find the platform was measured in each trial. If a mouse did not find the platform within 60 sec, it was gently guided by hand onto the platform and allowed to remain there for 10 sec. After 4 days, the probe test was performed with no platform. Each mouse was allowed to search the platform for 60 sec, while an overhead camera recorded its movement. Time spent searching in each quadrant by a mouse was used to characterize its search behavior. In the visible platform of water maze training, platform position was randomly switched among the four quadrants in each training trial and no probe trial is needed.

Isolation and culture of adult NPCs

NPCs used in this study were isolated from the DG of 6 to 8-week-old male *Mecp2*^{S80A} mice and wild-type (WT) littermate controls based on published methods (Guo et al., 2012). Briefly, DG was microdissected from 400 μm coronal sections of forebrain. After enzymatic digestion using MACS Neural Tissue Dissociation kit (Miltenyi Biotech), DMEM/F-12 (Invitrogen) containing 10% FBS (Invitrogen) were added into each sample for stopping digestion. After filtering through a 70-μm cell strainer (BD Biosciences) and washing with DMEM/F-12, the single-cell suspension was collected and cultured with proliferation medium: Neurobasal medium (Invitrogen) containing 20 ng/ml basic fibroblast growth factor (FGF-2, Waisman Biomanufacturing), 20 ng/ml epidermal growth factor (EGF, Peprotech), B27 supplement (Invitrogen), Penicillin Streptomycin (Invitrogen), and L-glutamine(Invitrogen) in a 5% CO2 incubator at 37 °C. Half of the medium was replaced every two days.

Proliferation and differentiation assays of adult NPCs

Proliferation and differentiation of aNPCs were analyzed using published method (Guo et al., 2011b). Only early passage cells (between passage 4 and 10) and the same passage numbers of wild type and *Mecp2*^{S80A} cells were used for the assay. For each experiment, stereological counting (Stereo Investigator, MBF Bioscience) of immunofluorescence positive cells from duplicated wells were analyzed, and results were averaged as one data point (n = 1). At least 3 independent experiments (n = 3) were performed and used for statistical analyses for each analysis.

In cell proliferation assay, we dissociated aNPCs with 0.05% Trypsin-EDTA (Invitrogen) for no longer than 1 min, stopped the digest with Trypsin inhibitor (Sigma-Aldrich) and finally

plated the cells on poly-L-lysine/laminin-coated cover slips at a density of 100,000 cells/well in proliferation medium (see above). At 20 h post-plating, 5 μM 5-bromo-2deoxyuridine (BrdU, Sigma-Aldrich) was added into the culture medium for 8 hours, after which the cells were fixed with 4% paraformaldehyde for 30 min at room temperature. To detect BrdU incorporation, fixed cells were pretreated with 1M HCl for 30 min at 37ºC, and then washed with borate buffer, pH 8.5, for 30 min. We then followed our standard immunocytochemistry protocol.

For the differentiation assay, aNPCs were similar treated and plated as in the proliferation assay, but at a density of 50,000 cells/well. At 24 h post-plating, cells were changed into differentiation medium: Neurobasal medium with 1% B27 supplement, 1% Penicillin Streptomycin (Invitrogen),2 mM L-glutamine(Invitrogen), 5 μM forskolin (Sigma-Aldrich), 1 μM retinoic acid (Sigma-Aldrich). Half of the medium was changed with fresh differentiation medium for four days, followed by fixation with 4% paraformaldehyde for 30 min and standard immunocytochemistry protocol.

RNA extraction, real-time quantitative RT-PCR

Total RNA from mosue hippocampus was extracted using SV Total RNA Isolation System (Promega). Total RNA from cultured aNSCs was extracted using TRIzol Reagent (Invitrogen). The qScriptTM cDNA SuperMix kit (Quanta Biosciences) was used for cDNA synthesis. Real-time quantitative PCR was performed on StepOne Plus Real-Time PCR System (Applied Biosystems) using iQ SYBR Green Supermix (Bio-rad). Fold change was calculated with the 2ΔCt method after normalization to Gapdh.

Primers used are following:

Gapdh: 5'-aatgggaagcttgtcatcaacg-3' (forward), 5'-gaagacaccagtagactccacgacata-3' (reverse).

Bdnf E4: 5'-cgccatgcaatttccactatcaataatttaac-3’(forward),

5’-ctttttcagtcactacttgtcaaagtaaac-3’(reverse)

Bndf: 5’-gaccatccttttccttactatgg-3’ (forward), 5’-ccattcacgctctccagagtc-3’ (reverse)

Mef2c: 5’-caacaacatatggtactgagtac-3’ (forward), 5’-catgttatgtaggtgctgctgc-3’ (reverse)

Gria1: 5’-agcgagtcgaagcggatgaa -3’, (forward), 5’ -ctctgccattctctccactg -3’ (reverse).

Gria2: 5’ -atgggaaagctgatattgcca -3’ (forward), 5’ -catgatagagattccaaggc- 3’ (reverse),

Igsf4b: 5'-gcagtggtctaaccctgctc-3' (forward), 5'-ttcgcacaggcatagtgaag-3' (reverse),

Vamp3: 5'- ttgaaacaagtgctggcaag-3' (forward), 5'-gagacacaccacacgatgatg-3' (reverse)

Rab3d: 5'- gctatgccgatgactccttc-3' (forward), 5'-agtaggccgtggtgattgtc-3' (reverse)

Dll1: 5'-agcgactgaggtgtaagatg-3' (forward), 5'-aacctggttctcagcagcag-3' (reverse).

Jag1: 5'-atacacgtggccatctctgc-3' (forward), 5'-aaccgcagcaataagtgagc-3' (reverse).

Jag2: 5'-cttccacaggtctgttggtg-3' (forward), 5'-tcctctcacgttctttcctg-3' (reverse).

Notch1: 5'-gaacaacaaggaggagactc-3' (forward), 5'-tccatgtgatccgtgatgtc-3' (reverse).

Notch2: 5'-caggacaataaggaagagac-3' (forward), 5'-tccatgtggtcagtgatgtc-3' (reverse).

Hes1: 5'-gcacttaagaaagatagctcc-3' (forward), 5'-ggtatttccccaacacgctc-3' (reverse).

Hes3: 5'-acactactcacatcagatacg-3' (forward), 5'-agagtccttgcagtgagttc-3' (reverse).

Hes5: 5'-gaaacacagcaaagccttcg-3' (forward), 5'-tgcagggtcaggaactgtac-3' (reverse).

Hey1: 5'-ctttgagaagcagggatctg-3' (forward), 5'-ctccgatagtccatagccag-3' (reverse).

Hey2: 5'-ggtaaaggctactttgatgcc-3' (forward), 5'-aggccttccactgagcttag-3' (reverse).

Heyl: 5'-actgcctttgagaaacaggg-3' (forward), 5'-atcaaagaaccctgtgccac-3' (reverse).

Numb: 5'-gatgccaagaaagctgagac-3' (forward), 5'-catctctgaagatgcagtgc-3' (reverse).

Tuj1: 5'-atctttggtcagagtggtgc-3' (forward), 5'-ggcagtcacaattctcacac-3' (reverse).

NeuroD1: 5'-acggatcaatcttctcttcc-3' (forward), 5'-cgtgaaagatggcattaagc-3' (reverse)

GFAP: 5'-atcggtctaagtttgcagac-3' (forward), 5'-ctccagatcgcaggtcaag-3' (reverse)

Chapter 5: Conclusions and future directions

The yin and yang of MeCP2 phosphorylation

Right after the discovery that phosphorylation of MeCP2 at S80 and S421/S424 is dynamically regulated in opposite manners by neuronal activity, a "yin-yang" model was proposed that phosphorylations at S80 and S421/S424 serve as balancing forces in modulating MeCP2 function (Chao and Zoghbi, 2009; Tao et al., 2009). Over the past several years, we performed a series of studies to investigate the *in vivo* function of MeCP2 phosphorylation, and provided evidence that loss of S80 phosphorylation and loss of S421/S424 phosphorylations in mice lead to opposite phenotypes, including locomotor activity, hippocampus-dependent spatial learning, and adult neurogenesis (Li et al., 2011; Tao et al., 2009). Molecularly, abolishing S421/S424 phosphorylation results in stronger MeCP2 chromatin occupation at certain gene promoters (*Bdnf, Mef2c, Bmp4, Grm1*) with corresponding alterations of gene expression (Li et al., 2011). And previous work using cortical neuron system eliminating S80 phosphorylation results in reduced association of MeCP2 at specific gene promoters (*Rab3d*, *Vamp3* and *Igsf4b*) and increased expression of those genes (Tao et al., 2009). Thus, S80 and S421/S424 phosphorylations may serve as regulatory switches on the chromosome accessible to diverse extrinsic and intrinsic stimuli, fine-tuning MeCP2 function during brain development and function.

A number of experiments should be performed in the future to further elucidate the function of MeCP2 phosphorylation and refine the "yin-yang" model. First, comprehensive behavioral analysis of mice with phospho-mimicking mutations (S80E, S421E/S424E) will help

unequivocally confirm the *in vivo* functions of MeCP2 phosphorylation identified from mice with phospho-abolishing mutations (S80A, S421A;S424A). Second, gene expression profiling (RNA-seq) and chromatin occupation profiling (ChIP-seq) can be performed to identify misregulated target genes in mutant mice at the genome-wide level. Extra care of experimental design is required for these assays, as critical phenotype-related alterations in gene expression might occur only in specific brain regions or specific type of neurons, some of which might be even dependent on certain stimuli. Finally, it will be interesting to mutate both S80 and S421/S424 on the same allele (S80A;S421A ;S424A and S80E;S421E;S424E) and investigate the biological consequence of losing or gaining both S80 and S421/S424 phosphorylations.

MeCP2 phosphorylation and Rett syndrome

Mutations in S80, S421 and S424 have not been found in any patient with classic RTT syndrome, suggesting that the loss or gain of such phosphorylations do not lead to a complete loss of MeCP2 function. This is consistent with the evidence from *Mecp2*$^{S80A/y}$ and *Mecp2*$^{S421A;S424A/y}$ mice that S80, S421 and S424 phosphorylations are only required for certain aspects of MeCP2 function, such as learning and memory, and anxiety. Milder *MECP2* mutations have been identified in patients with mild mental retardation, learning disabilities, and autism spectrum disorders (Chahrour and Zoghbi, 2007). It will be interesting to examine whether any of these mutations involve misregulation of MeCP2 phosphorylation.

On the other hand, MeCP2 phosphorylation might be a target for RTT syndrome drug screening. *Mecp2*$^{S421A;S424A/y}$ mice share considerable phenotypes with the MeCP2 gain of

function model *Mecp2*^{Tg} mice. *Mecp2*$^{S80A/y}$ mice, however, recapitulates several loss of function phenotypes of *Mecp2* deficient mice. Taken together, the evidence from these mouse models suggest that manipulation of MeCP2 phosphorylation state could dramatically influence some, if not all, of MeCP2 function. In RTT patients with MECP2 missense mutations, S80 and S421/S424 sites are preserved. It is possible that the MeCP2 function in these patients can be at least partially revived by promoting S80 phosphorylation and preventing S421/S424 phosphorylation. Thus, the specific kinases and phosphatases that are responsible for MeCP2 phosphorylation regulation, once identified, could be potential targets for drug screening.

A functional "code" for modifications of MeCP2

Recent work from the Bird and Greenberg groups demonstrated that MeCP2 protein is almost as abundant as histone octamers in the mouse brain and MeCP2 is globally distributed across the entire mouse genome in a pattern similar to that of histone H3 (Cohen et al., 2011; Skene et al., 2010). Another histone-like feature of MeCP2 is that it is dynamically regulated by posttranslational modifications.

Mass spectrometry analysis of MeCP2 purified from mouse brain revealed 7 amino acids that could be phosphorylated, including by S80, S399, T148/S149, S164, S229, S421, and S424 (Tao et al., 2009). Recently, 3 additional phosphorylation sites (S86, S274 and T308) were identified by phosphotryptic mapping (Ebert et al., 2013). Among these, phosphorylations on S80, S399 occur in neurons at basal level, and phosphorylations on other sites are induced by neuronal activity. We also showed the dynamics of S421 phosphorylation in cell cycle in adult neural

progenitor cells. As far as other post-translational modifications, acetylations on R92 and K135 have been consistently detected by mass spectrometry in our lab (unpublished data); O-GlcNAc glycosylation, SUMOylation and ubiquitylation of MeCP2 have been also reported (Gonzales et al., 2012; Miyake and Nagai, 2007; Rexach et al., 2010).

Post-translational modifications increase the functional diversity of proteins, as covalent addition of functional group may regulate activity, localization and interaction with other cellular molecules. Thus, post-translational modifications of MeCP2 could be employed to fine-tune MeCP2 function in response to distinct stimuli. Different from the well-studied “histone code”, the functional spectrum of MeCP2 modifications is largely unknown. Phosphorylation of T308 blocks the interaction of the repressor domain of MECP2 with the nuclear receptor co-repressor (NCoR) complex (Ebert et al., 2013). We and others provide evidence that loss of S421/S424 or S80 phosphorylation leads to altered chromatin occupation of MeCP2 (Li et al., 2011; Tao et al., 2009). A recent study also suggests that phosphorylations at S229 and S80 influences the interactions of MeCP2 with the chromatin factors HP1 and SMC3 and the cofactors Sin3A and YB-1(Gonzales et al., 2012). Additional biochemistry and genetics studies should to be performed to address the functional significance of these post-translational modifications and their possible involvement in Rett syndrome.

Appendix: MeCP2 S421 phosphorylation in neuronal cell lines

Results

Previously, we reported the presence of MeCP2 S421 phosphorylation in adult neural progenitor cells (aNPCs), and provide evidence that S421 phosphorylation is regulated by cell cycle in a cycling-dependent kinase (CDK)-dependent manner (Chapter 3). And the loss of S421 phosphorylation in *Mecp2*$^{S421A;S424A}$ aNPCs results in decreased proliferation and increased neuronal differentiation, raising up the possibility that S421 phosphorylation may serve as a general regulator of proliferation and differentiation in proliferating cells. To test this hypothesis, we first extend S421 phosphorylation study to two neuronal cell lines: Neuro-2a and HT22.

Under normal growth condition, S421 phosphorylation was almost undetectable in Neuro-2a and HT-22 cells, but was readily induced by synchronizing the cells into G2/M phase with nocodazole (**Figure a, b**). High potassium, which induces depolarization and the ensuing S421 phosphorylation in neurons (Chen et al., 2003b; Zhou et al., 2006), failed to induce S421 phosphorylation in Neuro-2a cells (**Figure c**). This result is consistent with previous findings that proliferating cells and postmotitic neurons utilize distinct mechanisms for S421 phosphorylation.

Applying roscovitine, a CDK inhibitor, to pre-synchronized HT22 cells effectively blocks nocodazole-induced S421 phosphorylation (**Figure d**), suggesting a common pathway for S421 phosphorylation induction in aNPCs and neuronal cell lines. We noticed the existence of two slow-migrating MeCP2 species in nocodazole treated Neuro-2a cells from Western blot (**Figure a,c**), and the S421 phosphorylated MeCP2 co-localize with the top species, suggesting the presence of additional unknown posttranslational modifications of MeCP2 in the bottom species.

Discussion

We provide evidence that MeCP2 S421 phosphorylation is regulated by cell cycle in a CDK-dependent manner in Neuro-2a and HT22 cells. Neuro-2a and HT22 cells are easy to maintain and transfect, which makes them good tools for studying the mechanisms of S421 phosphorylation in proliferating cells. siRNA or shRNA library screening can be used to identify the kinases and phosphatase responsible for S421 phosphorylation and dephosphorylation. With the new technique of high-efficiency genetic modifying of mammalian cells (Cho et al., 2013; Mali et al., 2013), phospho-abolishing (S to A) and phospho-mimicking (S to E) mutations can be introduced to these cell lines to investigate the cell-autonomous function of S421 phosphorylation for cell proliferation and differentiation.

Figure

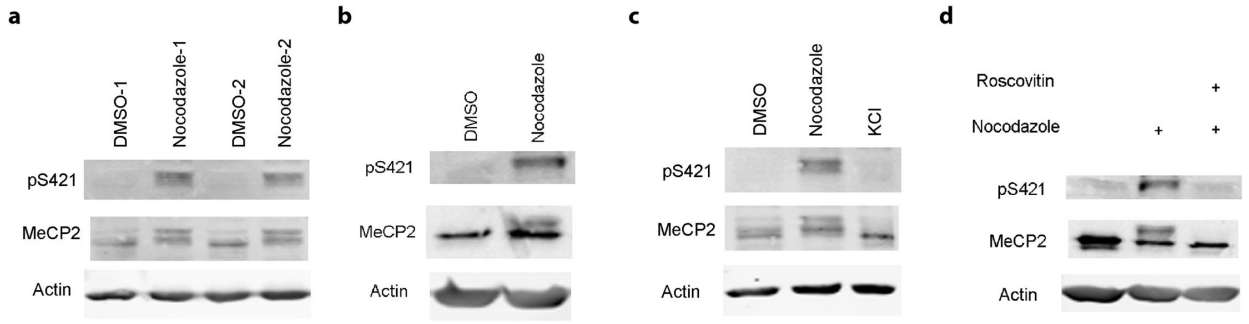

(a) Western blot analysis of MeCP2 Ser421 phosphorylation in Neuro-2a cells treated with DMSO or nocodazole (150ng/ml) for 24hr. **(b)** Western blot analysis of MeCP2 Ser421 phosphorylation in HT22 cells treated with DMSO or nocodazole (150ng/ml) for 24hr. **(c)** Western blot analysis of MeCP2 Ser421 phosphorylation in Neuro-2a cells treated with DMSO or nocodazole (150ng/ml) for 24hr and KCl for 3hr. **(d)** Western blot analysis of MeCP2 Ser421 phosphorylation in HT22 cells under conditions: 1) DMSO, 2) 36 hours of nocodazole treatment, 3) 24 hours of roscovitine (25 μM) treatment after pre-synchronization of the cells by nocodazole for 12 hours.

Materials and methods

cell culture

Neuro-2a and HT22 cells are cultured in DMEM (Invitrogen) with 10% FBS (Invitrogen). Neuro-2a cells are from ACTT, and HT22 cells are kindly provided by Dr. John Svaren's lab as a gift.

Antibodies and drugs

he following primary antibodies were used: Anti-MeCP2 (Cell Signaling, 3456), Anti-MeCP2 (Abcam, ab50005), Anti phospho-S421 (custom made by Phospho-solutions) DyLight 680/800 conjugated secondary antibodies (Thermo Fisher Scientific) were used for Western blot.

The following drugs were used: nocodazole (Sigma-Aldrich), roscovitine (Calbiochem)

Western blot analysis

Cell lysate was run on 8% SDS-PAGE gel (Bio-rad). The protein samples were then transferred to Protran BA 85 nitrocellulose membranes (Whatman). The membrane was blocked by 5% dry milk, and incubated with appropriate primary and DyLight dye-conjugated secondary antibodies. The Odyssey Western Detection Methods (LI-COR Biosciences) was used for signal detection.

References

Ables, J.L., Decarolis, N.A., Johnson, M.A., Rivera, P.D., Gao, Z., Cooper, D.C., Radtke, F., Hsieh, J., and Eisch, A.J. (2010). Notch1 is required for maintenance of the reservoir of adult hippocampal stem cells. The Journal of neuroscience : the official journal of the Society for Neuroscience *30*, 10484-10492.

Adachi, M., Autry, A.E., Covington, H.E., 3rd, and Monteggia, L.M. (2009). MeCP2-mediated transcription repression in the basolateral amygdala may underlie heightened anxiety in a mouse model of Rett syndrome. The Journal of neuroscience : the official journal of the Society for Neuroscience *29*, 4218-4227.

Aid, T., Kazantseva, A., Piirsoo, M., Palm, K., and Timmusk, T. (2007). Mouse and rat BDNF gene structure and expression revisited. Journal of neuroscience research *85*, 525-535.

Alvarez-Buylla, A., and Lim, D.A. (2004). For the long run: maintaining germinal niches in the adult brain. Neuron *41*, 683-686.

Amir, R.E., Van den Veyver, I.B., Wan, M., Tran, C.Q., Francke, U., and Zoghbi, H.Y. (1999). Rett syndrome is caused by mutations in X-linked MECP2, encoding methyl-CpG-binding protein 2. Nature genetics *23*, 185-188.

Arita, K., Isogai, S., Oda, T., Unoki, M., Sugita, K., Sekiyama, N., Kuwata, K., Hamamoto, R., Tochio, H., Sato, M.*, et al.* (2012). Recognition of modification status on a histone H3 tail by linked histone reader modules of the epigenetic regulator UHRF1. Proceedings of the National Academy of Sciences of the United States of America *109*, 12950-12955.

Artavanis-Tsakonas, S., Rand, M.D., and Lake, R.J. (1999). Notch signaling: cell fate control and signal integration in development. Science *284*, 770-776.

Asaka, Y., Jugloff, D.G., Zhang, L., Eubanks, J.H., and Fitzsimonds, R.M. (2006). Hippocampal synaptic plasticity is impaired in the Mecp2-null mouse model of Rett syndrome. Neurobiology of disease *21*, 217-227.

Baker, S.A., Chen, L., Wilkins, A.D., Yu, P., Lichtarge, O., and Zoghbi, H.Y. (2013). An AT-hook domain in MeCP2 determines the clinical course of Rett syndrome and related disorders. Cell *152*, 984-996.

Ballas, N., Lioy, D.T., Grunseich, C., and Mandel, G. (2009). Non-cell autonomous influence of MeCP2-deficient glia on neuronal dendritic morphology. Nature neuroscience *12*, 311-317.

Barreto, G., Schafer, A., Marhold, J., Stach, D., Swaminathan, S.K., Handa, V., Doderlein, G., Maltry, N., Wu, W., Lyko, F.*, et al.* (2007). Gadd45a promotes epigenetic gene activation by repair-mediated DNA demethylation. Nature *445*, 671-675.

Bath, K.G., Akins, M.R., and Lee, F.S. (2012). BDNF control of adult SVZ neurogenesis. Developmental psychobiology *54*, 578-589.

Bird, A.P., and Wolffe, A.P. (1999). Methylation-induced repression--belts, braces, and chromatin. Cell *99*, 451-454.

Bonaguidi, M.A., Wheeler, M.A., Shapiro, J.S., Stadel, R.P., Sun, G.J., Ming, G.L., and Song, H. (2011). In vivo clonal analysis reveals self-renewing and multipotent adult neural stem cell characteristics. Cell *145*, 1142-1155.

Bracaglia, G., Conca, B., Bergo, A., Rusconi, L., Zhou, Z., Greenberg, M.E., Landsberger, N., Soddu, S., and Kilstrup-Nielsen, C. (2009). Methyl-CpG-binding protein 2 is phosphorylated by homeodomain-interacting protein kinase 2 and contributes to apoptosis. EMBO reports *10*, 1327-1333.

Bray, S., and Bernard, F. (2010). Notch targets and their regulation. Current topics in developmental biology *92*, 253-275.

Budden, S.S., Dorsey, H.C., and Steiner, R.D. (2005). Clinical profile of a male with Rett syndrome. Brain & development *27 Suppl 1*, S69-S71.

Carney, R.M., Wolpert, C.M., Ravan, S.A., Shahbazian, M., Ashley-Koch, A., Cuccaro, M.L., Vance, J.M., and Pericak-Vance, M.A. (2003). Identification of MeCP2 mutations in a series of females with autistic disorder. Pediatric neurology *28*, 205-211.

Chahrour, M., Jung, S.Y., Shaw, C., Zhou, X., Wong, S.T., Qin, J., and Zoghbi, H.Y. (2008). MeCP2, a key contributor to neurological disease, activates and represses transcription. Science *320*, 1224-1229.

Chahrour, M., and Zoghbi, H.Y. (2007). The story of Rett syndrome: from clinic to neurobiology. Neuron *56*, 422-437.

Chang, Q., Khare, G., Dani, V., Nelson, S., and Jaenisch, R. (2006). The disease progression of Mecp2 mutant mice is affected by the level of BDNF expression. Neuron *49*, 341-348.

Chao, H.T., Chen, H., Samaco, R.C., Xue, M., Chahrour, M., Yoo, J., Neul, J.L., Gong, S., Lu, H.C., Heintz, N.*, et al.* (2010). Dysfunction in GABA signalling mediates autism-like stereotypies and Rett syndrome phenotypes. Nature *468*, 263-269.

Chao, H.T., and Zoghbi, H.Y. (2009). The yin and yang of MeCP2 phosphorylation. Proceedings of the National Academy of Sciences of the United States of America *106*, 4577-4578.

Chao, H.T., Zoghbi, H.Y., and Rosenmund, C. (2007). MeCP2 controls excitatory synaptic strength by regulating glutamatergic synapse number. Neuron *56*, 58-65.

Chen, R.Z., Akbarian, S., Tudor, M., and Jaenisch, R. (2001). Deficiency of methyl-CpG binding

protein-2 in CNS neurons results in a Rett-like phenotype in mice. Nature genetics *27*, 327-331.

Chen, T., Ueda, Y., Dodge, J.E., Wang, Z., and Li, E. (2003a). Establishment and maintenance of genomic methylation patterns in mouse embryonic stem cells by Dnmt3a and Dnmt3b. Molecular and cellular biology *23*, 5594-5605.

Chen, W.G., Chang, Q., Lin, Y., Meissner, A., West, A.E., Griffith, E.C., Jaenisch, R., and Greenberg, M.E. (2003b). Derepression of BDNF transcription involves calcium-dependent phosphorylation of MeCP2. Science *302*, 885-889.

Cheval, H., Guy, J., Merusi, C., De Sousa, D., Selfridge, J., and Bird, A. (2012). Postnatal inactivation reveals enhanced requirement for MeCP2 at distinct age windows. Human molecular genetics *21*, 3806-3814.

Cho, S.W., Kim, S., Kim, J.M., and Kim, J.S. (2013). Targeted genome engineering in human cells with the Cas9 RNA-guided endonuclease. Nature biotechnology *31*, 230-232.

Cohen, S., Gabel, H.W., Hemberg, M., Hutchinson, A.N., Sadacca, L.A., Ebert, D.H., Harmin, D.A., Greenberg, R.S., Verdine, V.K., Zhou, Z.*, et al.* (2011). Genome-Wide Activity-Dependent MeCP2 Phosphorylation Regulates Nervous System Development and Function. Neuron *72*, 72-85.

Collins, A.L., Levenson, J.M., Vilaythong, A.P., Richman, R., Armstrong, D.L., Noebels, J.L., David Sweatt, J., and Zoghbi, H.Y. (2004). Mild overexpression of MeCP2 causes a progressive neurological disorder in mice. Human molecular genetics *13*, 2679-2689.

Deaton, A.M., and Bird, A. (2011). CpG islands and the regulation of transcription. Genes & development *25*, 1010-1022.

Defossez, P.A., and Stancheva, I. (2011). Biological functions of methyl-CpG-binding proteins. Progress in molecular biology and translational science *101*, 377-398.

Deng, J.V., Rodriguiz, R.M., Hutchinson, A.N., Kim, I.H., Wetsel, W.C., and West, A.E. (2010a). MeCP2 in the nucleus accumbens contributes to neural and behavioral responses to psychostimulants. Nature neuroscience *13*, 1128-1136.

Deng, W., Aimone, J.B., and Gage, F.H. (2010b). New neurons and new memories: how does adult hippocampal neurogenesis affect learning and memory? Nature reviews Neuroscience *11*, 339-350.

Derecki, N.C., Cronk, J.C., Lu, Z., Xu, E., Abbott, S.B., Guyenet, P.G., and Kipnis, J. (2012). Wild-type microglia arrest pathology in a mouse model of Rett syndrome. Nature *484*, 105-109.

Ebert, D.H., Gabel, H.W., Robinson, N.D., Kastan, N.R., Hu, L.S., Cohen, S., Navarro, A.J., Lyst, M.J., Ekiert, R., Bird, A.P.*, et al.* (2013). Activity-dependent phosphorylation of MeCP2 threonine 308 regulates interaction with NCoR. Nature *499*, 341-345.

Encinas, J.M., and Enikolopov, G. (2008). Identifying and quantitating neural stem and progenitor cells in the adult brain. Methods in cell biology *85*, 243-272.

Eriksson, P.S., Perfilieva, E., Bjork-Eriksson, T., Alborn, A.M., Nordborg, C., Peterson, D.A., and Gage, F.H. (1998). Neurogenesis in the adult human hippocampus. Nature medicine *4*, 1313-1317.

Faigle, R., and Song, H. (2013). Signaling mechanisms regulating adult neural stem cells and neurogenesis. Biochimica et biophysica acta *1830*, 2435-2448.

Feng, J., Chang, H., Li, E., and Fan, G. (2005). Dynamic expression of de novo DNA methyltransferases Dnmt3a and Dnmt3b in the central nervous system. Journal of neuroscience research *79*, 734-746.

Feng, J., Zhou, Y., Campbell, S.L., Le, T., Li, E., Sweatt, J.D., Silva, A.J., and Fan, G. (2010a). Dnmt1 and Dnmt3a maintain DNA methylation and regulate synaptic function in adult forebrain neurons. Nature neuroscience *13*, 423-430.

Feng, S., Jacobsen, S.E., and Reik, W. (2010b). Epigenetic reprogramming in plant and animal development. Science *330*, 622-627.

Frankland, P.W., Bontempi, B., Talton, L.E., Kaczmarek, L., and Silva, A.J. (2004). The involvement of the anterior cingulate cortex in remote contextual fear memory. Science *304*, 881-883.

Friez, M.J., Jones, J.R., Clarkson, K., Lubs, H., Abuelo, D., Bier, J.A., Pai, S., Simensen, R., Williams, C., Giampietro, P.F*., et al.* (2006). Recurrent infections, hypotonia, and mental retardation caused by duplication of MECP2 and adjacent region in Xq28. Pediatrics *118*, e1687-1695.

Fyffe, S.L., Neul, J.L., Samaco, R.C., Chao, H.T., Ben-Shachar, S., Moretti, P., McGill, B.E., Goulding, E.H., Sullivan, E., Tecott, L.H*., et al.* (2008). Deletion of Mecp2 in Sim1-expressing neurons reveals a critical role for MeCP2 in feeding behavior, aggression, and the response to stress. Neuron *59*, 947-958.

Gage, F.H. (2000). Mammalian neural stem cells. Science *287*, 1433-1438.

Ge, S., Yang, C.H., Hsu, K.S., Ming, G.L., and Song, H. (2007). A critical period for enhanced synaptic plasticity in newly generated neurons of the adult brain. Neuron *54*, 559-566.

Gemelli, T., Berton, O., Nelson, E.D., Perrotti, L.I., Jaenisch, R., and Monteggia, L.M. (2006). Postnatal loss of methyl-CpG binding protein 2 in the forebrain is sufficient to mediate behavioral aspects of Rett syndrome in mice. Biological psychiatry *59*, 468-476.

Giacometti, E., Luikenhuis, S., Beard, C., and Jaenisch, R. (2007). Partial rescue of MeCP2 deficiency by postnatal activation of MeCP2. Proceedings of the National Academy of Sciences

of the United States of America *104*, 1931-1936.

Goffin, D., Allen, M., Zhang, L., Amorim, M., Wang, I.T., Reyes, A.R., Mercado-Berton, A., Ong, C., Cohen, S., Hu, L.*, et al.* (2012). Rett syndrome mutation MeCP2 T158A disrupts DNA binding, protein stability and ERP responses. Nature neuroscience *15*, 274-283.

Goldberg, A.D., Allis, C.D., and Bernstein, E. (2007). Epigenetics: a landscape takes shape. Cell *128*, 635-638.

Gonzales, M.L., Adams, S., Dunaway, K.W., and LaSalle, J.M. (2012). Phosphorylation of distinct sites in MeCP2 modifies cofactor associations and the dynamics of transcriptional regulation. Molecular and cellular biology *32*, 2894-2903.

Griffith, J.S., and Mahler, H.R. (1969). DNA ticketing theory of memory. Nature *223*, 580-582.

Grosso, S., Brogna, A., Bazzotti, S., Renieri, A., Morgese, G., and Balestri, P. (2007). Seizures and electroencephalographic findings in CDKL5 mutations: case report and review. Brain & development *29*, 239-242.

Guo, J.U., Ma, D.K., Mo, H., Ball, M.P., Jang, M.H., Bonaguidi, M.A., Balazer, J.A., Eaves, H.L., Xie, B., Ford, E.*, et al.* (2011a). Neuronal activity modifies the DNA methylation landscape in the adult brain. Nature neuroscience *14*, 1345-1351.

Guo, W., Patzlaff, N.E., Jobe, E.M., and Zhao, X. (2012). Isolation of multipotent neural stem or progenitor cells from both the dentate gyrus and subventricular zone of a single adult mouse. Nature protocols *7*, 2005-2012.

Guo, W., Zhang, L., Christopher, D.M., Teng, Z.Q., Fausett, S.R., Liu, C., George, O.L., Klingensmith, J., Jin, P., and Zhao, X. (2011b). RNA-binding protein FXR2 regulates adult hippocampal neurogenesis by reducing Noggin expression. Neuron *70*, 924-938.

Guy, J., Cheval, H., Selfridge, J., and Bird, A. (2011). The role of MeCP2 in the brain. Annual review of cell and developmental biology *27*, 631-652.

Guy, J., Gan, J., Selfridge, J., Cobb, S., and Bird, A. (2007). Reversal of neurological defects in a mouse model of Rett syndrome. Science *315*, 1143-1147.

Guy, J., Hendrich, B., Holmes, M., Martin, J.E., and Bird, A. (2001). A mouse Mecp2-null mutation causes neurological symptoms that mimic Rett syndrome. Nature genetics *27*, 322-326.

Hagberg, B. (1985). Rett's syndrome: prevalence and impact on progressive severe mental retardation in girls. Acta paediatrica Scandinavica *74*, 405-408.

Hagberg, B., Aicardi, J., Dias, K., and Ramos, O. (1983). A progressive syndrome of autism, dementia, ataxia, and loss of purposeful hand use in girls: Rett's syndrome: report of 35 cases. Annals of neurology *14*, 471-479.

Hansen, R.S., Wijmenga, C., Luo, P., Stanek, A.M., Canfield, T.K., Weemaes, C.M., and Gartler, S.M. (1999). The DNMT3B DNA methyltransferase gene is mutated in the ICF immunodeficiency syndrome. Proceedings of the National Academy of Sciences of the United States of America *96*, 14412-14417.

Hendrich, B., and Bird, A. (1998). Identification and characterization of a family of mammalian methyl-CpG binding proteins. Molecular and cellular biology *18*, 6538-6547.

Hendrich, B., and Tweedie, S. (2003). The methyl-CpG binding domain and the evolving role of DNA methylation in animals. Trends in genetics : TIG *19*, 269-277.

Ho, K.L., McNae, I.W., Schmiedeberg, L., Klose, R.J., Bird, A.P., and Walkinshaw, M.D. (2008). MeCP2 binding to DNA depends upon hydration at methyl-CpG. Molecular cell *29*, 525-531.

Jaenisch, R., and Bird, A. (2003). Epigenetic regulation of gene expression: how the genome integrates intrinsic and environmental signals. Nat Genet *33 Suppl*, 245-254.

Johnson, R.A., Lam, M., Punzo, A.M., Li, H., Lin, B.R., Ye, K., Mitchell, G.S., and Chang, Q. (2012). 7,8-dihydroxyflavone exhibits therapeutic efficacy in a mouse model of Rett syndrome. Journal of applied physiology *112*, 704-710.

Jones, P.L., Veenstra, G.J., Wade, P.A., Vermaak, D., Kass, S.U., Landsberger, N., Strouboulis, J., and Wolffe, A.P. (1998). Methylated DNA and MeCP2 recruit histone deacetylase to repress transcription. Nature genetics *19*, 187-191.

Jung, B.P., Jugloff, D.G., Zhang, G., Logan, R., Brown, S., and Eubanks, J.H. (2003). The expression of methyl CpG binding factor MeCP2 correlates with cellular differentiation in the developing rat brain and in cultured cells. Journal of neurobiology *55*, 86-96.

Kafri, T., Ariel, M., Brandeis, M., Shemer, R., Urven, L., McCarrey, J., Cedar, H., and Razin, A. (1992). Developmental pattern of gene-specific DNA methylation in the mouse embryo and germ line. Genes & development *6*, 705-714.

Klauck, S.M., Lindsay, S., Beyer, K.S., Splitt, M., Burn, J., and Poustka, A. (2002). A mutation hot spot for nonspecific X-linked mental retardation in the MECP2 gene causes the PPM-X syndrome. American journal of human genetics *70*, 1034-1037.

Kleefstra, T., Yntema, H.G., Oudakker, A.R., Romein, T., Sistermans, E., Nillessen, W., van Bokhoven, H., de Vries, B.B., and Hamel, B.C. (2002). De novo MECP2 frameshift mutation in a boy with moderate mental retardation, obesity and gynaecomastia. Clinical genetics *61*, 359-362.

Kohyama, J., Kojima, T., Takatsuka, E., Yamashita, T., Namiki, J., Hsieh, J., Gage, F.H., Namihira, M., Okano, H., Sawamoto, K.*, et al.* (2008). Epigenetic regulation of neural cell differentiation plasticity in the adult mammalian brain. Proceedings of the National Academy of Sciences of the United States of America *105*, 18012-18017.

Kouzarides, T. (2007). Chromatin modifications and their function. Cell *128*, 693-705.

Kriaucionis, S., and Bird, A. (2004). The major form of MeCP2 has a novel N-terminus generated by alternative splicing. Nucleic acids research *32*, 1818-1823.

Kuhn, H.G., Dickinson-Anson, H., and Gage, F.H. (1996). Neurogenesis in the dentate gyrus of the adult rat: age-related decrease of neuronal progenitor proliferation. The Journal of neuroscience : the official journal of the Society for Neuroscience *16*, 2027-2033.

Kumar, A., Kamboj, S., Malone, B.M., Kudo, S., Twiss, J.L., Czymmek, K.J., LaSalle, J.M., and Schanen, N.C. (2008). Analysis of protein domains and Rett syndrome mutations indicate that multiple regions influence chromatin-binding dynamics of the chromatin-associated protein MECP2 in vivo. Journal of cell science *121*, 1128-1137.

Laget, S., Joulie, M., Le Masson, F., Sasai, N., Christians, E., Pradhan, S., Roberts, R.J., and Defossez, P.A. (2010). The human proteins MBD5 and MBD6 associate with heterochromatin but they do not bind methylated DNA. PloS one *5*, e11982.

Lazarini, F., and Lledo, P.M. (2011). Is adult neurogenesis essential for olfaction? Trends in neurosciences *34*, 20-30.

Levenson, J.M., Roth, T.L., Lubin, F.D., Miller, C.A., Huang, I.C., Desai, P., Malone, L.M., and Sweatt, J.D. (2006). Evidence that DNA (cytosine-5) methyltransferase regulates synaptic plasticity in the hippocampus. The Journal of biological chemistry *281*, 15763-15773.

Lewis, J.D., Meehan, R.R., Henzel, W.J., Maurer-Fogy, I., Jeppesen, P., Klein, F., and Bird, A. (1992). Purification, sequence, and cellular localization of a novel chromosomal protein that binds to methylated DNA. Cell *69*, 905-914.

Li, E., Bestor, T.H., and Jaenisch, R. (1992). Targeted mutation of the DNA methyltransferase gene results in embryonic lethality. Cell *69*, 915-926.

Li, H., Zhong, X., Chau, K.F., Williams, E.C., and Chang, Q. (2011). Loss of activity-induced phosphorylation of MeCP2 enhances synaptogenesis, LTP and spatial memory. Nature neuroscience *14*, 1001-1008.

Li, X., Barkho, B.Z., Luo, Y., Smrt, R.D., Santistevan, N.J., Liu, C., Kuwabara, T., Gage, F.H., and Zhao, X. (2008). Epigenetic regulation of the stem cell mitogen Fgf-2 by Mbd1 in adult neural stem/progenitor cells. The Journal of biological chemistry *283*, 27644-27652.

Lim, D.A., Tramontin, A.D., Trevejo, J.M., Herrera, D.G., Garcia-Verdugo, J.M., and Alvarez-Buylla, A. (2000). Noggin antagonizes BMP signaling to create a niche for adult neurogenesis. Neuron *28*, 713-726.

Lioy, D.T., Garg, S.K., Monaghan, C.E., Raber, J., Foust, K.D., Kaspar, B.K., Hirrlinger, P.G., Kirchhoff, F., Bissonnette, J.M., Ballas, N.*, et al.* (2011). A role for glia in the progression of

Rett's syndrome. Nature *475*, 497-500.

Liu, C., Teng, Z.Q., Santistevan, N.J., Szulwach, K.E., Guo, W., Jin, P., and Zhao, X. (2010). Epigenetic regulation of miR-184 by MBD1 governs neural stem cell proliferation and differentiation. Cell stem cell *6*, 433-444.

Lois, C., and Alvarez-Buylla, A. (1994). Long-distance neuronal migration in the adult mammalian brain. Science *264*, 1145-1148.

Louvi, A., and Artavanis-Tsakonas, S. (2006). Notch signalling in vertebrate neural development. Nature reviews Neuroscience *7*, 93-102.

Lubin, F.D., Roth, T.L., and Sweatt, J.D. (2008). Epigenetic regulation of BDNF gene transcription in the consolidation of fear memory. The Journal of neuroscience : the official journal of the Society for Neuroscience *28*, 10576-10586.

Luikenhuis, S., Giacometti, E., Beard, C.F., and Jaenisch, R. (2004). Expression of MeCP2 in postmitotic neurons rescues Rett syndrome in mice. Proceedings of the National Academy of Sciences of the United States of America *101*, 6033-6038.

Lyst, M.J., Ekiert, R., Ebert, D.H., Merusi, C., Nowak, J., Selfridge, J., Guy, J., Kastan, N.R., Robinson, N.D., de Lima Alves, F*., et al.* (2013). Rett syndrome mutations abolish the interaction of MeCP2 with the NCoR/SMRT co-repressor. Nature neuroscience *16*, 898-902.

Ma, D.K., Jang, M.H., Guo, J.U., Kitabatake, Y., Chang, M.L., Pow-Anpongkul, N., Flavell, R.A., Lu, B., Ming, G.L., and Song, H. (2009). Neuronal activity-induced Gadd45b promotes epigenetic DNA demethylation and adult neurogenesis. Science *323*, 1074-1077.

Maezawa, I., and Jin, L.W. (2010). Rett syndrome microglia damage dendrites and synapses by the elevated release of glutamate. The Journal of neuroscience : the official journal of the Society for Neuroscience *30*, 5346-5356.

Mali, P., Yang, L., Esvelt, K.M., Aach, J., Guell, M., DiCarlo, J.E., Norville, J.E., and Church, G.M. (2013). RNA-guided human genome engineering via Cas9. Science *339*, 823-826.

Mao, L.M., Horton, E., Guo, M.L., Xue, B., Jin, D.Z., Fibuch, E.E., and Wang, J.Q. (2011). Cocaine increases phosphorylation of MeCP2 in the rat striatum in vivo: a differential role of NMDA receptors. Neurochemistry international *59*, 610-617.

Martinowich, K., Hattori, D., Wu, H., Fouse, S., He, F., Hu, Y., Fan, G., and Sun, Y.E. (2003). DNA methylation-related chromatin remodeling in activity-dependent BDNF gene regulation. Science *302*, 890-893.

Meehan, R.R., Lewis, J.D., McKay, S., Kleiner, E.L., and Bird, A.P. (1989). Identification of a mammalian protein that binds specifically to DNA containing methylated CpGs. Cell *58*, 499-507.

Miller, C.A., Gavin, C.F., White, J.A., Parrish, R.R., Honasoge, A., Yancey, C.R., Rivera, I.M., Rubio, M.D., Rumbaugh, G., and Sweatt, J.D. (2010). Cortical DNA methylation maintains remote memory. Nature neuroscience *13*, 664-666.

Miller, C.A., and Sweatt, J.D. (2007). Covalent modification of DNA regulates memory formation. Neuron *53*, 857-869.

Misteli, T., Gunjan, A., Hock, R., Bustin, M., and Brown, D.T. (2000). Dynamic binding of histone H1 to chromatin in living cells. Nature *408*, 877-881.

Miyake, K., and Nagai, K. (2007). Phosphorylation of methyl-CpG binding protein 2 (MeCP2) regulates the intracellular localization during neuronal cell differentiation. Neurochemistry international *50*, 264-270.

Mnatzakanian, G.N., Lohi, H., Munteanu, I., Alfred, S.E., Yamada, T., MacLeod, P.J., Jones, J.R., Scherer, S.W., Schanen, N.C., Friez, M.J*., et al.* (2004). A previously unidentified MECP2 open reading frame defines a new protein isoform relevant to Rett syndrome. Nature genetics *36*, 339-341.

Monk, M., Boubelik, M., and Lehnert, S. (1987). Temporal and regional changes in DNA methylation in the embryonic, extraembryonic and germ cell lineages during mouse embryo development. Development *99*, 371-382.

Moretti, P., Levenson, J.M., Battaglia, F., Atkinson, R., Teague, R., Antalffy, B., Armstrong, D., Arancio, O., Sweatt, J.D., and Zoghbi, H.Y. (2006). Learning and memory and synaptic plasticity are impaired in a mouse model of Rett syndrome. The Journal of neuroscience : the official journal of the Society for Neuroscience *26*, 319-327.

Mullaney, B.C., Johnston, M.V., and Blue, M.E. (2004). Developmental expression of methyl-CpG binding protein 2 is dynamically regulated in the rodent brain. Neuroscience *123*, 939-949.

Murgatroyd, C., Patchev, A.V., Wu, Y., Micale, V., Bockmuhl, Y., Fischer, D., Holsboer, F., Wotjak, C.T., Almeida, O.F., and Spengler, D. (2009). Dynamic DNA methylation programs persistent adverse effects of early-life stress. Nature neuroscience *12*, 1559-1566.

Na, E.S., Nelson, E.D., Adachi, M., Autry, A.E., Mahgoub, M.A., Kavalali, E.T., and Monteggia, L.M. (2012). A mouse model for MeCP2 duplication syndrome: MeCP2 overexpression impairs learning and memory and synaptic transmission. The Journal of neuroscience : the official journal of the Society for Neuroscience *32*, 3109-3117.

Nan, X., Campoy, F.J., and Bird, A. (1997). MeCP2 is a transcriptional repressor with abundant binding sites in genomic chromatin. Cell *88*, 471-481.

Nan, X., Meehan, R.R., and Bird, A. (1993). Dissection of the methyl-CpG binding domain from the chromosomal protein MeCP2. Nucleic acids research *21*, 4886-4892.

Nan, X., Ng, H.H., Johnson, C.A., Laherty, C.D., Turner, B.M., Eisenman, R.N., and Bird, A. (1998). Transcriptional repression by the methyl-CpG-binding protein MeCP2 involves a histone deacetylase complex. Nature *393*, 386-389.

Neul, J.L., Kaufmann, W.E., Glaze, D.G., Christodoulou, J., Clarke, A.J., Bahi-Buisson, N., Leonard, H., Bailey, M.E., Schanen, N.C., Zappella, M*., et al.* (2010). Rett syndrome: revised diagnostic criteria and nomenclature. Annals of neurology *68*, 944-950.

Ohki, I., Shimotake, N., Fujita, N., Jee, J., Ikegami, T., Nakao, M., and Shirakawa, M. (2001). Solution structure of the methyl-CpG binding domain of human MBD1 in complex with methylated DNA. Cell *105*, 487-497.

Okano, H., Hirano, T., and Balaban, E. (2000). Learning and memory. Proceedings of the National Academy of Sciences of the United States of America *97*, 12403-12404.

Okano, M., Bell, D.W., Haber, D.A., and Li, E. (1999). DNA methyltransferases Dnmt3a and Dnmt3b are essential for de novo methylation and mammalian development. Cell *99*, 247-257.

Pelka, G.J., Watson, C.M., Christodoulou, J., and Tam, P.P. (2005). Distinct expression profiles of Mecp2 transcripts with different lengths of 3'UTR in the brain and visceral organs during mouse development. Genomics *85*, 441-452.

Ramocki, M.B., Tavyev, Y.J., and Peters, S.U. (2010). The MECP2 duplication syndrome. American journal of medical genetics Part A *152A*, 1079-1088.

Rett, A. (1966). [On a unusual brain atrophy syndrome in hyperammonemia in childhood]. Wiener medizinische Wochenschrift *116*, 723-726.

Rexach, J.E., Rogers, C.J., Yu, S.H., Tao, J., Sun, Y.E., and Hsieh-Wilson, L.C. (2010). Quantification of O-glycosylation stoichiometry and dynamics using resolvable mass tags. Nature chemical biology *6*, 645-651.

Roth, T.L., Lubin, F.D., Funk, A.J., and Sweatt, J.D. (2009). Lasting epigenetic influence of early-life adversity on the BDNF gene. Biological psychiatry *65*, 760-769.

Samaco, R.C., Mandel-Brehm, C., Chao, H.T., Ward, C.S., Fyffe-Maricich, S.L., Ren, J., Hyland, K., Thaller, C., Maricich, S.M., Humphreys, P*., et al.* (2009). Loss of MeCP2 in aminergic neurons causes cell-autonomous defects in neurotransmitter synthesis and specific behavioral abnormalities. Proceedings of the National Academy of Sciences of the United States of America *106*, 21966-21971.

Samaco, R.C., Mandel-Brehm, C., McGraw, C.M., Shaw, C.A., McGill, B.E., and Zoghbi, H.Y. (2012). Crh and Oprm1 mediate anxiety-related behavior and social approach in a mouse model of MECP2 duplication syndrome. Nature genetics *44*, 206-211.

Schmid, D.A., Yang, T., Ogier, M., Adams, I., Mirakhur, Y., Wang, Q., Massa, S.M., Longo, F.M.,

and Katz, D.M. (2012). A TrkB small molecule partial agonist rescues TrkB phosphorylation deficits and improves respiratory function in a mouse model of Rett syndrome. The Journal of neuroscience : the official journal of the Society for Neuroscience *32*, 1803-1810.

Schmidt-Hieber, C., Jonas, P., and Bischofberger, J. (2004). Enhanced synaptic plasticity in newly generated granule cells of the adult hippocampus. Nature *429*, 184-187.

Shahbazian, M., Young, J., Yuva-Paylor, L., Spencer, C., Antalffy, B., Noebels, J., Armstrong, D., Paylor, R., and Zoghbi, H. (2002). Mice with truncated MeCP2 recapitulate many Rett syndrome features and display hyperacetylation of histone H3. Neuron *35*, 243-254.

Shors, T.J., Miesegaes, G., Beylin, A., Zhao, M., Rydel, T., and Gould, E. (2001). Neurogenesis in the adult is involved in the formation of trace memories. Nature *410*, 372-376.

Skene, P.J., Illingworth, R.S., Webb, S., Kerr, A.R., James, K.D., Turner, D.J., Andrews, R., and Bird, A.P. (2010). Neuronal MeCP2 is expressed at near histone-octamer levels and globally alters the chromatin state. Molecular cell *37*, 457-468.

Smeets, E., Terhal, P., Casaer, P., Peters, A., Midro, A., Schollen, E., van Roozendaal, K., Moog, U., Matthijs, G., Herbergs, J.*, et al.* (2005). Rett syndrome in females with CTS hot spot deletions: a disorder profile. American journal of medical genetics Part A *132A*, 117-120.

Smith, Z.D., and Meissner, A. (2013). DNA methylation: roles in mammalian development. Nature reviews Genetics *14*, 204-220.

Smrt, R.D., Eaves-Egenes, J., Barkho, B.Z., Santistevan, N.J., Zhao, C., Aimone, J.B., Gage, F.H., and Zhao, X. (2007). Mecp2 deficiency leads to delayed maturation and altered gene expression in hippocampal neurons. Neurobiology of disease *27*, 77-89.

Snyder, J.S., Kee, N., and Wojtowicz, J.M. (2001). Effects of adult neurogenesis on synaptic plasticity in the rat dentate gyrus. Journal of neurophysiology *85*, 2423-2431.

Szulwach, K.E., Li, X., Smrt, R.D., Li, Y., Luo, Y., Lin, L., Santistevan, N.J., Li, W., Zhao, X., and Jin, P. (2010). Cross talk between microRNA and epigenetic regulation in adult neurogenesis. The Journal of cell biology *189*, 127-141.

Szyf, M., Bozovic, V., and Tanigawa, G. (1991). Growth regulation of mouse DNA methyltransferase gene expression. The Journal of biological chemistry *266*, 10027-10030.

Tao, J., Hu, K., Chang, Q., Wu, H., Sherman, N.E., Martinowich, K., Klose, R.J., Schanen, C., Jaenisch, R., Wang, W.*, et al.* (2009). Phosphorylation of MeCP2 at Serine 80 regulates its chromatin association and neurological function. Proceedings of the National Academy of Sciences of the United States of America *106*, 4882-4887.

Tawa, R., Ono, T., Kurishita, A., Okada, S., and Hirose, S. (1990). Changes of DNA methylation level during pre- and postnatal periods in mice. Differentiation; research in biological diversity

45, 44-48.

Trappe, R., Laccone, F., Cobilanschi, J., Meins, M., Huppke, P., Hanefeld, F., and Engel, W. (2001). MECP2 mutations in sporadic cases of Rett syndrome are almost exclusively of paternal origin. American journal of human genetics *68*, 1093-1101.

Tudor, M., Akbarian, S., Chen, R.Z., and Jaenisch, R. (2002). Transcriptional profiling of a mouse model for Rett syndrome reveals subtle transcriptional changes in the brain. Proceedings of the National Academy of Sciences of the United States of America *99*, 15536-15541.

Waddington, C.H. (1942). Endeavour, Vol 1.

Wan, M., Lee, S.S., Zhang, X., Houwink-Manville, I., Song, H.R., Amir, R.E., Budden, S., Naidu, S., Pereira, J.L., Lo, I.F*., et al.* (1999). Rett syndrome and beyond: recurrent spontaneous and familial MECP2 mutations at CpG hotspots. American journal of human genetics *65*, 1520-1529.

Waterhouse, E.G., An, J.J., Orefice, L.L., Baydyuk, M., Liao, G.Y., Zheng, K., Lu, B., and Xu, B. (2012). BDNF promotes differentiation and maturation of adult-born neurons through GABAergic transmission. The Journal of neuroscience : the official journal of the Society for Neuroscience *32*, 14318-14330.

Weaver, I.C., Cervoni, N., Champagne, F.A., D'Alessio, A.C., Sharma, S., Seckl, J.R., Dymov, S., Szyf, M., and Meaney, M.J. (2004). Epigenetic programming by maternal behavior. Nature neuroscience *7*, 847-854.

Weber, M., Hellmann, I., Stadler, M.B., Ramos, L., Paabo, S., Rebhan, M., and Schubeler, D. (2007). Distribution, silencing potential and evolutionary impact of promoter DNA methylation in the human genome. Nature genetics *39*, 457-466.

Wu, H., Coskun, V., Tao, J., Xie, W., Ge, W., Yoshikawa, K., Li, E., Zhang, Y., and Sun, Y.E. (2010). Dnmt3a-dependent nonpromoter DNA methylation facilitates transcription of neurogenic genes. Science *329*, 444-448.

Yasui, D.H., Peddada, S., Bieda, M.C., Vallero, R.O., Hogart, A., Nagarajan, R.P., Thatcher, K.N., Farnham, P.J., and Lasalle, J.M. (2007). Integrated epigenomic analyses of neuronal MeCP2 reveal a role for long-range interaction with active genes. Proceedings of the National Academy of Sciences of the United States of America *104*, 19416-19421.

Young, J.I., Hong, E.P., Castle, J.C., Crespo-Barreto, J., Bowman, A.B., Rose, M.F., Kang, D., Richman, R., Johnson, J.M., Berget, S*., et al.* (2005). Regulation of RNA splicing by the methylation-dependent transcriptional repressor methyl-CpG binding protein 2. Proceedings of the National Academy of Sciences of the United States of America *102*, 17551-17558.

Zappella, M., Meloni, I., Longo, I., Hayek, G., and Renieri, A. (2001). Preserved speech variants of the Rett syndrome: molecular and clinical analysis. American journal of medical genetics *104*, 14-22.

Zhao, X., Ueba, T., Christie, B.R., Barkho, B., McConnell, M.J., Nakashima, K., Lein, E.S., Eadie, B.D., Willhoite, A.R., Muotri, A.R.*, et al.* (2003). Mice lacking methyl-CpG binding protein 1 have deficits in adult neurogenesis and hippocampal function. Proceedings of the National Academy of Sciences of the United States of America *100*, 6777-6782.

Zhong, X., Li, H., and Chang, Q. (2012). MeCP2 phosphorylation is required for modulating synaptic scaling through mGluR5. The Journal of neuroscience : the official journal of the Society for Neuroscience *32*, 12841-12847.

Zhou, Z., Hong, E.J., Cohen, S., Zhao, W.N., Ho, H.Y., Schmidt, L., Chen, W.G., Lin, Y., Savner, E., Griffith, E.C.*, et al.* (2006). Brain-specific phosphorylation of MeCP2 regulates activity-dependent Bdnf transcription, dendritic growth, and spine maturation. Neuron *52*, 255-269.